Lawrence Berkeley Laboratory
UNIVERSITY OF CALIFORNIA

EARTH SCIENCES DIVISION

Inversion of Static Displacement of the Earth's Surface

D.W. Vasco
(Ph.D. Thesis)

August 1986

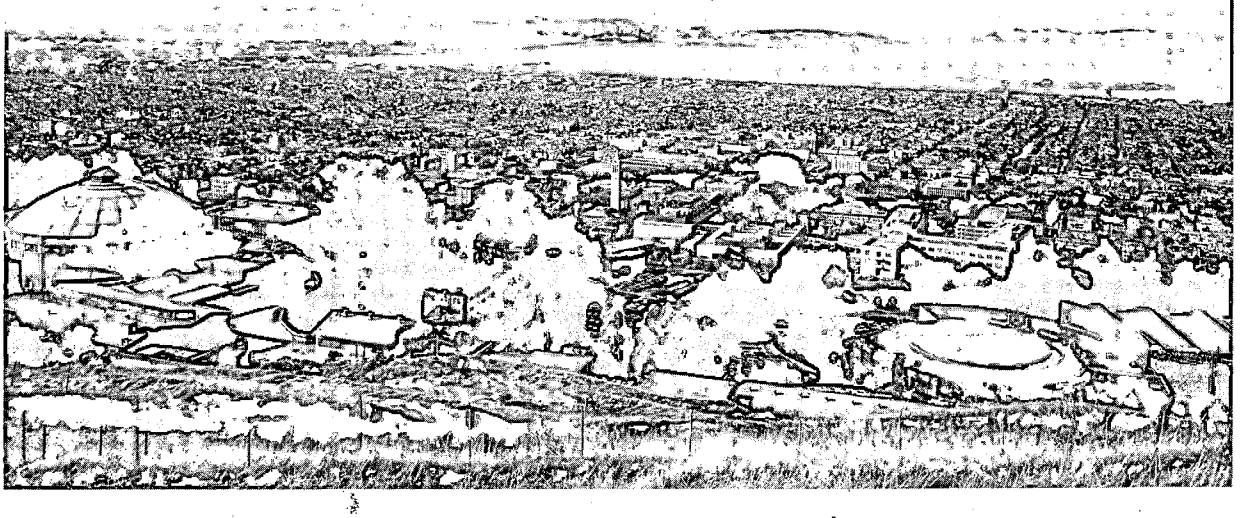

Prepared for the U.S. Department of Energy under Contract Number DE-AC03-76SF00098.

DISCLAIMER

LBL-21814

Inversion of Static Displacement of the Earth's Surface

D.W. Vasco
(Ph.D. Thesis)

Lawrence Berkeley Laboratory
University of California
Berkeley, California 94720

August 1986

Supported by the U.S. Department of Energy under Contract Number DE-AC03-76SF00098.

Inversion of Static Displacement of the Earth's Surface

Donald Wyman Vasco

Abstract

A method is presented which uses observations of surface displacement to place constraints on the components of the strain tensor at depth. Using a volume integral form of Volterra'a integral and a series expansion method, the problem is discretized. An extremal inverse approach is described allowing the calculation of bounds on model parameters from bounds on the data. Methods of placing bounds on generalized moments of the perturbing body are developed, and techniques of handling errors in the data are discussed.

A special case, the use of uplift measurements to bound fractional volume change in the subsurface, is developed. The connection between extremal bound techniques and the method of ideal bodies is explored. As an application, uplift data from 1982, 1983 and 1985, are used to constrain the depth and horizontal extent of any possible magma intrusion at depth. It was found that, in order to satisfy the 1982, 1983 and 1985 uplift data, volume expansion was required above depths of 11, 9 and 8 kilometers respectively. Furthermore, bounds on fractional volume change of individual blocks were calculated.

Finally, a method is developed which determines multiple solutions to non-linear inverse problems. An extension of Newton's method for non-linear optimization, the algorithm projects through solutions and searches for additional ones. The technique is applied to finding best fitting polyhedral volume source for a given displacement anomaly. This method has applications in many areas of geophysics.

This dissertation is dedicated to

Dianne May Vasco, my mother,

for her strength and courage.

Acknowledgements

During the past five years I have encountered many fine people. Primarily I wish to thank my advisor, Dr. Lane Johnson, for his extreme helpfulness and attention. His dedication to geophysics and enthusiasm for new ideas brightened the end of many a long day.

Dr. Thomas McEvilly's humor and critical examination of ideas brought a sense of excitement to aspects of geophysics in which I was involved. Dr. Shimon Coen, a friend as well as a teacher, helped many ideas in this dissertation spring to life. In a similar vain Dr. Peter Weidelt deserves mention. The busy afternoons and late nights were bearable only because of the humour and peculiarly slanted outlook of my fellow graduate students at CCS.

I must thank my mother and father for all their support on the way to and through graduate school. I am also grateful to my brother Dan who lead the way. Finally, I wish to thank Robin Berman and Katherine Bettis who made the difference.

Table of Contents

Chapter 1

Introduction

Inversion of surface displacement

Surface deformation is one of the most direct indications of tectonic movements. As such it contains information on the source mechanisms responsible for the motions. Hence inversion techniques, to estimate the source model parameters from deformation, would be useful. Approaches to this problem have been tried, yet the field is somewhat undeveloped. The principal techniques consists of assuming a source type and shape and fitting model parameters by trial and error or in a least squares sense. This dissertation will explore an alternative method for inverting surface displacements for subsurface source mechanisms.

The calculation of surface deformation of a semi-infinite elastic body due to a strain nuclei has been solved by many authors (Sezawa 1929, Whipple 1936). The basis for the calculations rests on the work of Volterra on dislocations in an elastic whole space (Volterra 1907). The displacements $u_m(\vec{x})$ are related to a dislocation distribution, $\Delta u_k(\vec{\xi})$, on an internal surface Σ by the integral

$$u_m(\vec{x}) = \int\int_{\Sigma} \Delta u_k(\vec{\xi})\, W^m{}_{kl}(\vec{x},\vec{\xi})\upsilon_l \, d\Sigma \tag{1.1}$$

where $\vec{x}=(x_1,x_2,x_3)$ is any point in the half space other than points on the dislocation surface itself and $\vec{\xi}=(\xi_1,\xi_2,\xi_3)$ is a point on the dislocation surface, Σ. $W^m{}_{kl}(\vec{x},\vec{\xi})$ is the Green function relating the dislocation $\Delta u_k(\vec{\xi})$ to the surface displacement component $u_m(\vec{x})$. υ_l is the l-th component of the normal to the surface Σ. The inverse problem consists of determining information on $\Delta u_k(\vec{\xi})$ from measurements of $u_m(\vec{x})$.

Previous Studies

Most previous inversions of the Volterra integral assumed a source model, such as a fault with constant slip or an expanding volume. But this is an a priori assumption which may introduce model errors. For example, consider the early work of Savage and Hastie (1969) who, " Attempt to find a simple dislocation model which best fits observed surface displacement..." Their dislocation model is uniform slip over a surface of unknown width, length, depth, dip and slip. The description of the inversion procedure is somewhat vague. Essentially the authors select a dislocation model, " roughly consistent with the observed deformation. Then a least-squares procedure is used to optimize this model by selecting the best value for the parameters." They investigate other models by varying the parameters.

The paper by Canitez and Tokoz (1972) also attempted to explain surface deformation resulting from faulting. Slip along a plane was the proposed mechanism. They assumed a fault of given strike and dip and fixed dimension. The fault plane was gridded and the effect of the dislocation for each grid element on each station was calculated by evaluating the Volterra integral numerically. Questions of uniqueness and goodness of fit were never addressed or only qualitatively analyzed in these early studies.

In the early 1970s the influence of Backus and Gilbert's papers (1967,1968) were felt. One of the first applications to the inversion of static deformation data was that of Alewine and Jordan (1973). They studied the fault motion associated with the 1971 San Fernando earthquake. A three dimensional fault model was constructed, constrained to " ...conform to other observed geophysical properties of the fault, such as the hypocentral fault plane solution of the main shock, the slip vectors of the aftershocks, the pattern of aftershock activity, and the observed surface faulting." They then utilized the expressions for the displacements in an elastic half-space due to an inclined rectangular fault given by Manshina and Smylie (1971). The geodetic measurements provided the vertical and lateral displacement data. The fault surface was discretized and slip on each element was assumed to be constant. The result was a linear system of equations which was solved by the stochastic inversion method described by Franklin (1970) and later by Jordan and

Franklin (1971). A similar approach was taken by McCowen, Glover and Alexander (1977). These authors use a two-dimensional finite element model to generate a one-dimensional slip model for a planar fault dipping at 45°. Weighted least-squares with a trade-off correction is used to determine node point displacements on the fault surface.

Jovanovich (1975) formally linearized the problem about some initial fault model and then attempted to solve for small perturbations of the fault parameters. An iterative algorithm was used to determine a solution. The iteration was stabilized by the stipulation that the norm of the perturbation vector was also minimized. Essentially this was Marquart's method for non-linear minimization. Matsu'ura (1977) published a similar method which instead relied on Lanczos' decomposition of the linearized problem and the deletion of small eigenvalues (Wiggins 1972).

An alternative method to study fault displacement was proposed by Langbein (1981). The technique relied on the linearization about a fault model. The fault plane was discretized and linear programing determined bounds on properties of the fault slip. Errors in the data were also accounted for in the inversion.

A new and interesting inversion method has been developed by Ikeda (unpublished Masters thesis). Essentially the technique downward continues the surface displacement field to any specified depth above the source. The inversion was restricted in that the continuation could not proceed past the source. Also, instabilities arose due to the presence of errors. Unlike the previous methods, no assumptions were made about the nature of the source.

Essentially, there seem to be four approaches to the inversion of surface displacement: model fitting using least squares on a linearized problem, Marquart iteration for the non-linear problem, downward continuation and maximal inversion for bounds on model properties for the linearized problem. Each method has advantages and disadvantages and the methods may be complementary. The first two suffer from a dependence on an initial model. The latter suffers from error instability. In this dissertation an alternative method is proposed. The idea is related to the maximal inversion of Langbein (1981). However, volume change and faulting may be considered simultaneously and linearization about an initial model is not required.

Dissertation summary

It has been mentioned that past methods of inverting surface displacement relied on assumptions of the source. Assumptions about the source type lead to a non-linear problem in terms of the source parameters. A number of methods have been proposed along these lines. These methods then used a variation of Newton's method to find a solution iteratively. This introduced a dependence on the initial model and the possibility of finding a local minimum. In Chapter 2 an alternative method is suggested. The strain distribution in the region of interest is expanded in a set of basis functions. The resulting inverse problem for the strain components at depth then is linear. A least squares approach may be taken for the linear problem. Because the problem will often be highly under-determined an extremal inversion method is suggested. A special case is studied in Chapter 3, the inversion of surface displacement due to volume expansion at depth. A number of examples are presented and the versatility of the method demonstrated. Chapter 4 applies the inversion method of the previous chapter to three years of vertical displacement data gathered at Long Valley caldera during 1982, 1983 and 1985. Depth bounds are derived as are upper bounds on any fractional volume change at depth.

Finally, in Chapter 5 an extension is suggested to the standard Newton-type of iterative linearization method. This path-following algorithm projects past local extrema to find other adjacent extrema. While not a complete global search method, it can help assess the non-uniqueness present due to non-linearity. It is applied to determine the best fitting polygonal volume source giving rise to a set of vertical surface displacement measurements.

Chapter 2

Constraints on Strain at Depth

Introduction

As mentioned in the introduction, many methods have been proposed for the determination of fault slip from surface displacement observations. Unfortunately, all but one of these methods rely on local linearization about some assumed fault geometry. The technique which did not make this assumption, Ikeda's downward continuation, is unstable for depths greater than the source depth. The purpose of this chapter is to present a stable way to invert surface displacement for deformation at depth without assuming an initial source model. This will be done by examining the problem in terms of the displacement gradient distribution at depth instead of in terms of fault slip. This distribution can also be viewed in terms of the distribution of the tensor components of strain at depth. The distribution is discretized using a series expansion method and a linear inverse problem presented without local linearization. This problem may be solved by a least squares algorithm. Unfortunately, for each term of the series expansion, nine unknowns are involved, resulting in many parameters for a reasonable order of expansion. For most problems this results in a highly under-determined inverse problem. Because of this, an extremal inversion solution in proposed for the linear inverse problem.

The Static Earth Displacement Problem

As stated before, the only evidence of displacements at depth, such as those caused by faulting or the expansion of magma bodies, is often their surface expression. Hence inferences about these internal movements must be made solely from surface displacement measurements. The displacements $u_m(\vec{x})$ are related to a dislocation distribution, $\Delta u_k(\vec{\xi})$, on an internal surface Σ by

the Volterra integral

$$u_m(\vec{x}) = \int\int_{\Sigma} \Delta u_k(\vec{\xi}) W^m{}_{kl}(\vec{x},\vec{\xi}) \upsilon_l \, d\Sigma \tag{2.1}$$

where $\vec{x}=(x_1,x_2,x_3)$ is any point in the half space other than the dislocation surface itself and $\vec{\xi}=(\xi_1,\xi_2,\xi_3)$ is a point on the dislocation surface. $W^m{}_{kl}(\vec{x},\vec{\xi})$ is the Green function relating the dislocation $\Delta u_k(\vec{\xi})$ to the surface displacement component $u_m(\vec{x})$. υ_l is the l-th component of the normal to the surface Σ. Unless the shape of the perturbing body (a fault surface or an expanding volume) is known, the problem is highly nonlinear (Jovanovich 1975). Assumptions of source shape must be made and a linearization must be introduced to bring the problem into the realm of linear inverse problems. Further, the linearized problem must be discretized in order to have a well determined solution. Dieterich and Decker (1975) have illustrated the ambiguity caused by variations in source shape. Considering a variety of volume sources fitting the same vertical uplift data, these authors note that source depths varied by a factor of 3.5. Hence estimates of depths to source bodies must be viewed with caution.

For displacements due to a strain at depth one may convert the Volterra integral (2.1) into the form necessary for the application of series expansion techniques. Using the divergence theorem on (2.1),

$$u_m(\vec{x}) = \int\int\int_V \left\{ \Delta u_k(\vec{\xi}) W^m{}_{kl}(\vec{x},\vec{\xi}) \right\}_{,l} dV(\vec{\xi})$$

Differentiating,

$$u_m(\vec{x}) = \int\int\int_V \left\{ \Delta u_{k,l}(\vec{\xi}) W^m{}_{kl}(\vec{x},\vec{\xi}) + \Delta u_k(\vec{\xi}) W^m{}_{kl,l}(\vec{x},\vec{\xi}) \right\} dV(\vec{\xi}) \tag{2.2}$$

One may consider $W^m{}_{kl}(\vec{x},\vec{\xi})$ to be the kl-th component of the stress tensor at the point $\vec{x}$ due to a unit body force in the m direction at the point $\vec{\xi}$ (Maruyama 1964). Hence it satisfies the equation of equilibrium

$$W^m{}_{kl,l}(\vec{x},\vec{\xi}) + \delta^m{}_k \delta(\vec{x}-\vec{\xi}) = 0$$

Using the above equation in the volume integral, the second term on the right side becomes

$$-\int\int\int_V \Delta u_k(\vec{\xi})\delta^m{}_k\,\delta(\vec{x}-\vec{\xi})dV(\xi) = \Delta u_m(\vec{x})$$

But there is no dislocation discontinuity at the surface so $\Delta u_m(\vec{x})$ vanishes. Hence,

$$u_m(\vec{x}) = \int\int\int_V \Delta u_{k,l}(\vec{\xi})W^m{}_{kl}(\vec{x},\vec{\xi})dV(\vec{\xi}). \tag{2.3}$$

The problem in terms of the displacement gradient

Begin with the Voltera integral in the form given in equation (2.3),

$$u_m(\vec{x}) = \int\int\int \Delta u_{k,l}(\vec{\xi})W^m{}_{kl}(\vec{x},\vec{\xi})dV.$$

For a dislocation distributed in space $\Delta u_{k,l}(\vec{\xi})$ can be thought of as the gradient of each component of the displacement vector at $\vec{\xi}$. This can, in turn, lead to the tensor components of small strain e_{kl},

$$e_{11} = \frac{\partial \Delta u_1}{\partial \xi_1}$$

$$e_{22} = \frac{\partial \Delta u_2}{\partial \xi_2}$$

$$e_{33} = \frac{\partial \Delta u_3}{\partial \xi_3}$$

$$e_{12} = \frac{1}{2}\left(\frac{\partial \Delta u_1}{\partial \xi_2} + \frac{\partial \Delta u_2}{\partial \xi_1}\right)$$

$$e_{13} = \frac{1}{2}\left(\frac{\partial \Delta u_1}{\partial \xi_3} + \frac{\partial \Delta u_3}{\partial \xi_1}\right)$$

$$e_{23} = \frac{1}{2}\left(\frac{\partial \Delta u_2}{\partial \xi_3} + \frac{\partial \Delta u_3}{\partial \xi_2}\right)$$

The e_{kl} are symmetric in k and l. Therefore there are only six independent e_{kl} while there are nine independent $\frac{\partial \Delta u_k}{\partial \xi_l}$. The remaining three degrees of freedom are the rotations about the three independent axes. Total slip in the *kth* direction over some interval in the direction of the *lth* axis can be determined by integration over this interval.

Discretization of the model

This section linearizes the inverse problem through a discretization of the displacement gradient distribution. This is done by the series expansion method. First, a set of N orthonormal basis functions $\beta_j(\vec{\xi})$, $j=1,...,N$ is introduced. The model space is now restricted to those model perturbations $\Delta u_{k,l}(\vec{\xi})$ which may be described as a linear combination of the N basis functions,

$$\Delta u_{k,l}(\vec{\xi}) = \sum_{j=1}^{N} b_j{}^{kl}\,\beta_j(\vec{\xi}).$$

The problem becomes one of determining the coefficients of the expansion $b_j{}^{kl}$ such that the model is compatible with the data. Rewriting the equation (2.3) using the series expansion given above and suppressing the summation convention,

$$u_m(\vec{x}) = \iiint \sum_{j=1}^{N}\sum_{k=1}^{3}\sum_{l=1}^{3} b_j{}^{kl}\,\beta_j(\vec{\xi})\,W^m{}_{kl}(\vec{x},\vec{\xi})\,dV.$$

Defining

$$G_j{}^{klm}(\vec{x}) = \iiint \beta_j(\vec{\xi})\,W^m{}_{kl}(\vec{x},\vec{\xi})\,dV$$

results in

$$u_m(\vec{x}) = \sum_{j=1}^{N}\sum_{k=1}^{3}\sum_{l=1}^{3} b_j{}^{kl}\,G_j{}^{klm}(\vec{x}).$$

Rewriting the triple sum as a single sum from 1 to $9\times N$,

$$u_m(\vec{x}) = \sum_{I=1}^{9\times N} b^I\,G^I{}_m \tag{2.4}$$

or, in matrix form,

$$\mathbf{u} = \mathbf{G}\mathbf{b}$$

a set of linear equations for the $9\times N$ unknown parameters $b_j{}^{kl}$. A commonly used set of basis functions are the rectangular constant basis functions,

$$\beta_j(\vec{\xi}) = \begin{cases} 1, & \vec{\xi}\ in\ R_j \\ 0, & \vec{\xi}\ not\ in\ R_j \end{cases}. \tag{2.5}$$

where R_j is the j-th rectangle or pixel. For such basis functions $G_j{}^{klm}(\vec{x})$ is the average of $W^m{}_{kl}(\vec{x},\vec{\xi})$ over R_j. $b_j{}^{kl}$ is the average displacement gradient perturbation of cell j.

The resulting linear system of equations (2.4) may be solved by any of the methods commonly used in geophysics. For example, the generalized inverse presented in Wiggins (1972) may be used, as may the stochastic inverse of Franklin (1970) or the general method of Tarantola and Valette (1982). However, because most problems are likely to be highly under-determined, it might be preferable to compute extremal bounds on properties of the strain model. This approach is discussed in the next section.

Extremal Inversion

As mentioned above, non-uniqueness may lead to a search for bounds on model properties of interest (Parker, 1975; Sabatier, 1977a,b; Safon et al., 1977; Oldenburg, 1983). These bounds may be used to characterize the range of possible solutions. Specifically, consider model properties which are linear functionals of the model perturbations,

$$A = \int\int\int_V \sum_{k=1}^{3}\sum_{l=1}^{3} \alpha^{kl}(\vec{\xi})\Delta u_{k,l}(\vec{\xi})dV. \tag{2.6}$$

Note that the integration is over the total volume V of the region of interest. Using the series expansion of $\Delta u_{k,l}(\vec{\xi})$,

$$\begin{aligned} A &= \int\int\int_V \sum_{j=1}^{N}\sum_{k=1}^{3}\sum_{l=1}^{3} \alpha^{kl}(\vec{\xi}) b_j{}^{kl}\beta_j(\vec{\xi})dV \\ &= \sum_{j=1}^{N}\sum_{k=1}^{3}\sum_{l=1}^{3} b_j{}^{kl}\int_V \alpha^{kl}(\vec{\xi})\beta_j(\vec{\xi})dV. \end{aligned} \tag{2.7}$$

Define

$$a_j{}^{kl} = \int\int\int_V \alpha^{kl}(\vec{\xi})\beta_j(\vec{\xi})dV.$$

Then the linear functional becomes

$$A = \sum_{i=1}^{9\times N} a^I b^I. \tag{2.8}$$

Or, in matrix notation,

$$A = \mathbf{a}^t \mathbf{b}$$

Note that for the rectangular constant basis functions given in equation (2.5),

$$a_j{}^{kl} = \int\int\int_{R_j} \alpha^{kl}(\vec{\xi}) dV \tag{2.9}$$

the integral of $\alpha^{kl}(\vec{\xi})$ over the j th pixel. Many useful properties of the model can be put in the form shown in equation (2.9). For example, bounds on the total volume change giving rise to a set of observations can be determined by the choice

$$\alpha^{kl}(\vec{\xi}) = 1.0 \qquad (kl) = (11),(22),(33)$$

otherwise

$$\alpha^{kl}(\vec{\xi}) = 0.0$$

Then $a_j{}^{kl}$ becomes

$$a_j{}^{kl} = \int\int\int_V \beta_j(\vec{\xi}) dV \qquad (kl) = (11),(22),(33).$$

For the rectangular constant functions this is just the volume of the pixel $\Delta x\, \Delta y\, \Delta z$ for the pixels for which (kl) is a term for the volume expansion. Similarly, bounds can be placed on any n-th order moment of the strain model about the point in space, ξ_0,

$$\alpha^{kl}(\vec{\xi}) = |\, \xi - \xi_0 \,|^n . \tag{2.10}$$

Higher order moments $n = 2, 3$ represent compactness and skewness of the solution about ξ_0.

Another choice of $\alpha^{kl}(\vec{\xi})$ is

$$\alpha^{kl}(\vec{\xi}) = \begin{cases} 1, & \xi \text{ in } U \\ 0, & \xi \text{ not in } U \end{cases} \tag{2.11}$$

resulting in

$$a_j{}^{kl} = \int_U \beta_j(\vec{\xi}) dV, \tag{2.12}$$

where U is a subregion of V; ie. some collection of pixels R_i . This is a useful choice of $\alpha^{kl}(\vec{\xi})$

and some examples of its use will be given later. For now, note that by letting U be a specified pixel R_i this $\alpha^{kl}(\vec{\xi})$ can be used to place bounds on the possible strain anomaly within the i-th pixel for the $(kl)th$ component of the displacement gradient anomaly.

Having shown some useful properties of the strain model which may be bounded, a method to compute these bounds is needed. Finding the minimum or maximum of $\mathbf{a}^t\mathbf{b}$ is a linear optimization problem. However, the problem is constrained by the requirement that any model satisfy the observations,

$$\mathbf{Gb} = \mathbf{u}.$$

In addition, an inequality constraint may be required,

$$\mathbf{Cb} \leq \mathbf{h}.$$

For example the fractional volume change in the region may be required to be non-negative. Therefore the formal problem of extremal inversion can be stated as

$$\begin{aligned} &\textit{minimize} \quad \mathbf{a}^t\mathbf{b} \\ &\textit{subject} \\ &\mathbf{u} = \mathbf{Gb} \\ &\mathbf{Cb} \leq \mathbf{h} \end{aligned} \tag{2.13}$$

Note that minimization and maximization problems are equivalent. One is obtained from the other by a sign change in $\mathbf{a}$.

Linear optimization problems subject to linear equality and inequality constraints, such as presented in equation (2.13), are easily solved using linear programming techniques (Hadley 1962). The simplex method, the standard solution algorithm (Dantzig 1963) is very efficient and can solve problems of the order of thousands of variables and thousands of constraints. Recently, a new method was proposed (Karmarkar 1985) which can solve large linear programming problems even faster than the simplex algorithm. Its use awaits further development.

Conclusions

It has been shown how the problem of determining the deformation at depth from surface displacements may be discretized through an expansion of the displacement gradient distribution into orthonormal basis functions. The resulting problem may be solved by a least squares inverse method or by extremal inversion. The advantage of the above approach is that no source need be assumed. In some cases it may be more correct to treat a fault zone as a region of shear rather than slip over an infinitesimal plane. Unfortunately, the choice of basis functions and the number of basis functions to use remains unspecified. The number of basis functions to use will depend on the scale of the anomaly and on the station spacing. The type of basis functions will depend on the properties to be bounded or determined. Useful basis functions include the rectangular basis functions and the Fourier basis functions.

In the next chapter rectangular basis functions are used to place bounds properties of any model of fractional volume change giving rise to a set of displacement measurements. This is a special case of the volume integral form of the Volterra integral (2.3) when $k = l$. It will be seen in that chapter that the problem is mathematically identical to the gravitational problem.

Chapter 3

Extremal Inversion of Static Earth Displacement due to Volume Expansion

Introduction

This chapter extends the method of ideal bodies (Parker 1974) and the method of positivity constraints (Sabatier 1977) to the problem of static earth displacement due to volume expansion at depth. Using these extremal inversion techniques one may estimate bounds on various model properties such as the greatest depth to a perturbing volume source. There are important reasons for producing these estimates; surface displacement, like gravity, cannot in general be inverted to yield a unique source. Even when a body force is specified, the source shape is still not uniquely determined. With such non-uniqueness present it is desirable to derive, if possible, some properties common to all possible sources. Fortunately, methods exist in the field of mathematical optimization (Luenberger 1969) by which one may derive extreme models which satisfy the data. Parker (1974) and Sabatier (1977a,b) have developed parallel methods in geophysics to extract bounds from potential field anomalies. Given the non-uniqueness of the data it is perhaps best to search for properties which must be satisfied by every model fitting the data. The method of ideal bodies (Parker 1974) and the method of positivity constraints (Sabatier 1977a) are able to produce unique extremal bounds on various model parameters. It has been shown by Sabatier (1977b) that the ideal body is a bound on a particular moment. The method of positivity constraints applied to discretized problems results in a formulation of the inverse problem as a search for the set of extremal solutions. Through the addition of a functional to be optimized over the model space, one may derive interesting bounds such as a greatest lower bound on the fractional volume change or a least upper bound on the depth of a body. Each of these methods is developed below

within the context of the static earth displacement problem. The presentation follows a somewhat historical order with the method of ideal bodies followed by the method of positivity constraints.

The Ideal Body Theorem

As noted by Parker (1972), when there are few data available for an inverse problem an appropriate approach is to use the observations to bound various functionals of the model parameters. One must give up the idea of determining the structure causing the anomaly and instead search for inequalities which the model must satisfy. It cannot be expressed any better than Parker's statement "...inadequate data cannot give us a detailed model, but they can be used to rule out certain classes of structure that otherwise might appear admissible." After this realization that bounds on functionals are appropriate one is left with the question " Which of the infinitely many functionals should I bound?" One class of functionals can be eliminated at the outset, namely linear functionals. Backus (1970) has shown that when the data are linear functionals of the model parameters there are no upper or lower bounds on any other linear functionals of the model. An exception occurs when the functional is a linear combination of the data functionals. Excepting all linear functionals one is still left with a plethora of nonlinear functionals. Because the norm of a model space is an important concept one might consider a bound on the norm defined over the model space. However, there are many possible norms. As a beginning one might consider some of the rather standard norms for the model space namely L^1, L^2 and L^∞. These are special cases of the general L^p norm defined by

$$L^p(\Delta\theta(\vec{r})) = \| \Delta\theta(\vec{r}) \|_p = \left(\frac{1}{V} \int\int\int_V | \Delta\theta(\vec{r}) |^p \, dV \right)^{\frac{1}{p}} \tag{3.1}$$

$\Delta\theta(\vec{r})$ denotes a scalar model property such as density or fractional volume change which varies over the volume V. Keeping in mind that we are seeking to place bounds on model parameters, the L^∞ norm has a particularly significant physical property. For as p approaches infinity, $\| \Delta\theta(\vec{r}) \|_p$ approaches the maximum of $| \Delta\theta(\vec{r}) |$ on V.

It is the L^∞ norm which gives rise to Parker's (1975) ideal body theorem. This theorem follows from an attempt to minimize the L^∞ norm over the space of all possible solutions. This is a problem of the constrained minimization of

$$L^\infty(\Delta\theta(\vec{r})) = \lim_{p\to\infty} \| \, |\Delta\theta(\vec{r})| \, \|_p = \lim_{p\to\infty}\left(\frac{1}{V}\int\int\int_V |\Delta\theta(\vec{r})|^p \, dV\right)^{\frac{1}{p}}$$

The constraints are that the model fit the data and that $\Delta\theta(\vec{r})$ be of one sign. The extremum produced by this minimization is a least upper bound of $\Delta\theta(\vec{r})$. The result is very general and may be used in many applications provided that the property of interest is related to N observations by a linear equation of the form,

$$u_i = \int\int\int_V \Delta\theta(\vec{r}) K_i(\vec{r}) dV, \qquad i = 1,2,3,....,N. \tag{3.2}$$

Here u_i are the observations, $K_i(\vec{r})$ are the kernels relating the the model values to the observations. They are independent of $\Delta\theta(\vec{r})$ in this linear problem. Parker (1975) showed that certain parameters may be found describing "a body of least $\Delta\theta(\vec{r})$ that fits the original data set." It was proved that a sufficient condition for the existence of a positive lower bound on the largest value of $\Delta\theta(\vec{r})$ is the existence of constants

$$\theta, \alpha_i \qquad i = 1,2,3,....,N$$

such that the function

$$\Delta\theta(\vec{r}) = \begin{cases} \theta \\ 0 \end{cases} \; where \; \begin{matrix} \sum \alpha_i K_i(\vec{r}) > 0 \\ \sum \alpha_i K_i(\vec{r}) \leq 0 \end{matrix}$$

satisfies the equation (3.2) given above. This condition arises from the constrained minimization mentioned above. θ is the positive lower bound on the maximum $\Delta\theta(\vec{r})$, and the α_i's are Lagrange multipliers which are necessary because of the constraint that the model fit the data. It was further shown that the volumes V_+ and V_- in which the above linear combination of the kernels $K_i(\vec{r})$ is positive or negative respectively are uniquely determined under the condition that the set of points where

$$F(\vec{r}) = \sum \alpha_i K_i(\vec{r}) = 0$$

has zero volume.

Lastly it should be noted that the problem of finding a lower bound on the largest value of $|\Delta\theta(\vec{r})|$ subject to the constraints of equation (3.2) has a geometrical interpretation (Huestis 1982). By an application of the Fenchel Duality Theorem (Luenberger 1969) Huestis shows that the problem is equivalent to the discovery of a particular hyperplane tangent to a convex set in an N dimensional space.

Ideal Bodies for Volume Expansion in an Elastic Earth

For a displacement due to a purely dilatational source one may convert the integral (2.3) into the form necessary for the application of Parker's theorem. Considering only a volume dilatational source i.e. kl = 11, 22, 33 and vertical (m = 3) deformation observed at the surface,

$$u_3(\vec{x}) = \int\int\int_V \Delta u_{k,k}(\vec{\xi}) W^3{}_{kk}(\vec{x},\vec{\xi}) dV(\vec{\xi}) \tag{3.3}$$

where

$$\Delta u_{k,k}(\vec{\xi}) = \Delta e_{kk}(\vec{\xi})$$

For a fluid source volume undergoing a transformational strain Δe_{ij}

$$\Delta e_{11} = \Delta e_{22} = \Delta e_{33} = \frac{\Delta\theta}{3}$$

where $\Delta\theta$ represents the fractional volume change which is defined by $\frac{\Delta V}{V_0}$. ΔV denotes the change in volume and V_0 is the initial volume of the fluid body. Defining

$$K_i(\vec{\xi}) = \frac{1}{3} W^3{}_{kk}(\vec{x}^i,\vec{\xi})$$

equation (3.3) becomes

$$u_3(\vec{x}^i) = \int\int\int_V \Delta\theta(\vec{\xi}) K_i(\vec{\xi}) dV(\xi). \tag{3.4}$$

This is of the form necessary for the use of Parker's theorem. The kernel $K_i(\vec{\xi})$ appearing in equation (3.4) has been derived by an extension of Maruyama's (1964) study of the response of a

homogenous half space to point forces and couples. For the two dimensional problem, the anomalous body infinitely long in one direction, the kernel is,

$$K_i(\vec{\xi}) = \frac{2}{3\pi}(\nu+1)\frac{\xi_3}{S^2} \tag{3.5}$$

where ν is Poisson's ratio for the half space. ξ_3 is the vertical coordinate of the source point and

$$S = |\vec{x}^i - \vec{\xi}| = \sqrt{(x^i{}_1 - \xi_1)^2 + \xi_3^2}$$

for $\vec{x}^i = (x^i{}_1, x^i{}_2, 0)$ a vector giving the location of station i. For the full three dimensional treatment we have

$$K_i(\vec{\xi}) = \frac{1}{3\pi}(\nu+1)\frac{\xi_3}{S^3} \tag{3.6}$$

where

$$S = \sqrt{(x^i{}_1 - \xi_1)^2 + (x^i{}_2 - \xi_2)^2 + \xi_3^2}.$$

In addition to vertical displacements one may consider radial movements. In the three dimensional problem the kernel is given by

$$K_i(\vec{\xi}) = \frac{1}{3\pi}(\nu+1)\frac{((x^i{}_1-\xi_1)^2 + (x^i{}_2\xi_2)^2)^{\frac{1}{2}}}{S^3} \tag{3.6a}$$

Here S is defined as above and the origin of the coordinate system is chosen at the point of no radial displacement.

In the examples considered below only vertical displacement is inverted. Note that the functional forms of the kernels (3.5) and (3.6) are equivalent to Parker's kernels for the two and three dimensional gravity problem. Hence the two extremal inverse problems are formally equivalent. Jovanovich et al. (1974) have derived expressions for the kernels when the halfspace is layered. They also present approximations which enable the rapid evaluation of these expressions. These expressions allow one to account for overlying structure in the inversion.

N Datum and Two Datum Ideal Bodies

For N observations at points $\vec{x}_i$ Parker's theorem states that the equation

$$F(\vec{\xi}) = \sum \alpha_i K_i(\vec{\xi}) = 0 \tag{3.7}$$

defines a surface separating V_+ and V_-, which is a surface bounding the anomalous body. This general equation is very difficult to solve and analytical attempts to do so quickly give way to numerical methods. Given the development of the method of positivity constraints which is described below, the ideal body method for N > 2 data is not so useful. For N = 2 data however the ideal body method provides a quick way to produce bounds on the fractional volume change (depth) given bounds on the depth (fractional volume change). Therefore in what follows we consider only the case N = 2, i.e. measurements at two stations. Readers interested in the case N > 2 should consult Parker (1975).

As noted by Parker(1974), the substitution of the three dimensional kernel equation (3.6) into equation (3.7) for the two datum case results in the equation

$$\alpha_1 \frac{\hat{z}\cdot(\vec{x}^1-\vec{\xi})}{|\vec{x}^1-\vec{\xi}|^3} + \alpha_2 \frac{\hat{z}\cdot(\vec{x}^2-\vec{\xi})}{|\vec{x}^2-\vec{\xi}|^3} = 0$$

In this equation $\hat{z}$ is a vertical unit vector, $\vec{\xi}$ denotes the vector from the origin to a point, say s, on the surface. This equation is satisfied when

$$\hat{z}\cdot(\vec{x}^1-\vec{\xi}) = \hat{z}\cdot(\vec{x}^2-\vec{\xi}) = 0$$

and also when

$$|\vec{x}^1-\vec{\xi}| = \beta\,|\vec{x}^2-\vec{\xi}|$$

$\beta = -\left(\frac{\alpha_1}{\alpha_2}\right)^{\frac{1}{3}} \neq 1$, a constant. This is because $\hat{z}\cdot(\vec{x}^1-\vec{\xi}) = \hat{z}\cdot(\vec{x}^2-\vec{\xi})$ when both $\vec{x}^1-\vec{\xi}$ and $\vec{x}^2-\vec{\xi}$ extend from points on the free surface to some point s on the anomalous body's surface. These two equations define a hemispherical body of radius $\beta\frac{|\vec{x}^1-\vec{x}^2|}{|1-\beta^2|}$ with center at $\frac{(\vec{x}^1-\beta^2\vec{x}^2)}{(1-\beta^2)}$. The first of these two equations says that this hemisphere is truncated by a plane at or parallel to

the surface. In the two dimensional problem the bodies are infinitely long cylinders. The axial cross sections of various two dimensional bodies are shown in Figure 3.1. In Figure 3.2 the vertical displacements associated with these volume sources is presented. In Figure 3.3 the three dimensional hemispherical ideal bodies appear.

Having derived the ideal bodies and the uplifts associated with them, one may now attack the inverse problem of determining the greatest lower bound on the fractional volume change or a least upper bound on the depth. These are complementary problems in that to find one extremum the other property must be bounded. For example, to bound the depth one must place a lower bound on the fractional volume change. One calculates u_1 and u_2, the uplift at stations $\vec{x}^1$ and $\vec{x}^2$, for all β in the interval (0,1) and (1,∞) keeping the fractional volume change $\Delta\theta$ and the station spacing D fixed. As β varies a curve will be traced out relating the ratio $\frac{u_2}{u_1}$ and a fractional volume change normalized by $\frac{D}{u_1}$. Such curves are shown in Figures 3.4 and 3.5 for the two and three dimensional cases, respectively. From these curves one may determine a greatest lower bound on the fractional volume change or conversely estimate a least upper bound on the depth. In absence of any estimates one may take the most pessimistic estimate possible: an infinite fractional volume change or a zero depth.

When three or more measurements are considered the calculations become difficult. In such a case the most expedient course is to consider various pairs of anomaly measurements. The pair which gives an extremum in $\Delta\theta$ or D is then used. Unfortunately this is not quite as good an estimate as the full N datum treatment (Parker 1975).

The Inclusion of Errors

In the presence of errors the extremums derived may be incorrect. At the cost of loosening the bound this may be remedied however. Consider N data u_i each with a standard deviation σ_i. As the 'true' measurement must lie within the interval $[u_i - 2\sigma_i, u_i + 2\sigma_i]$ with about 95% confidence one may consider these bounds in deriving an extremal estimate. For example, in the

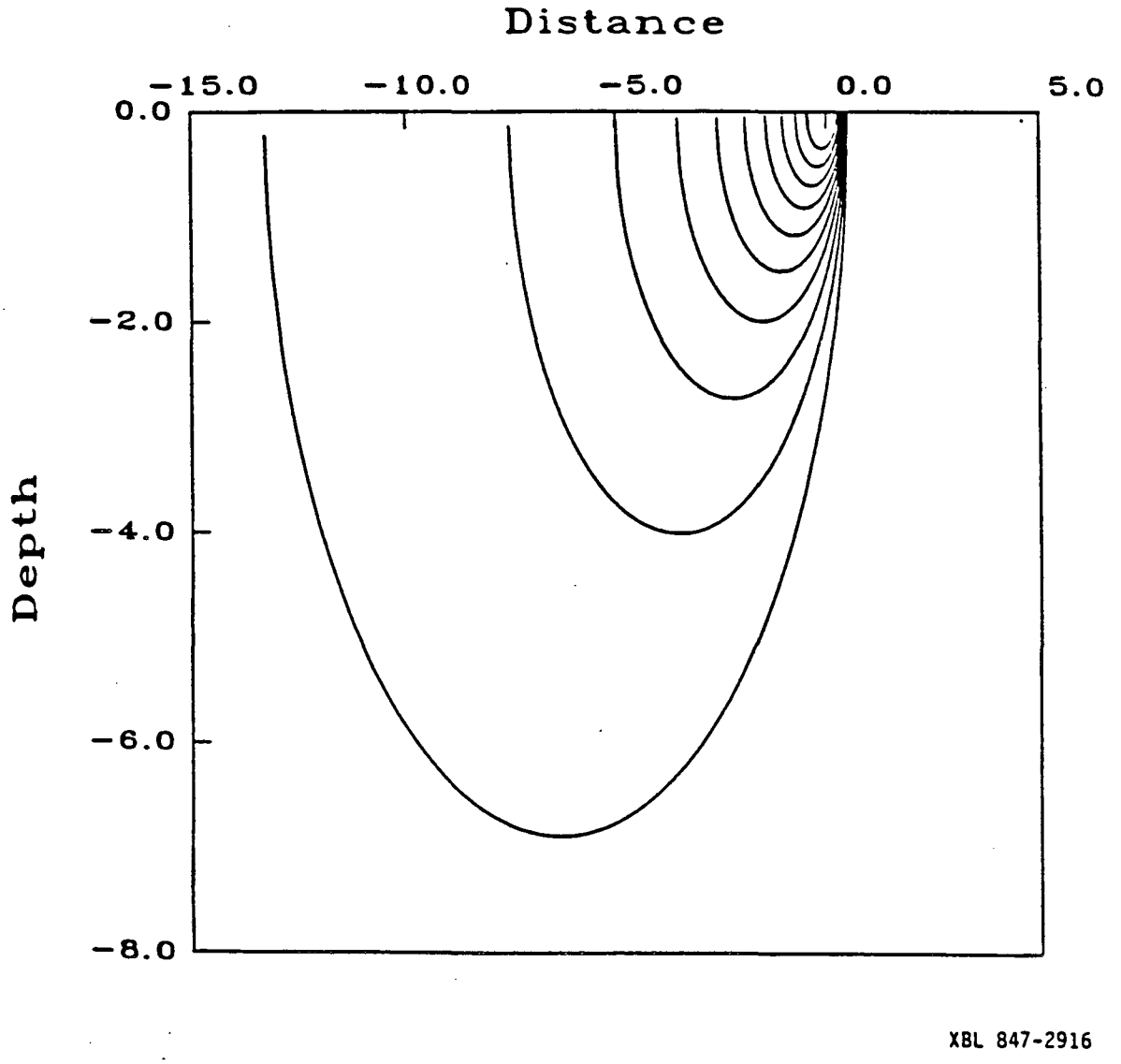

Figure 3.1 The ideal body forms for the 2-D two datum problem. The shape and size changes as the parameter β varies from 0.1 (smallest body) to 0.95 (largest body) in ten increments. All distances have been scaled relative to the station spacing D. Stations $\mathbf{x}^1$ and $\mathbf{x}^2$ are at distances of 0 and 1 respectively.

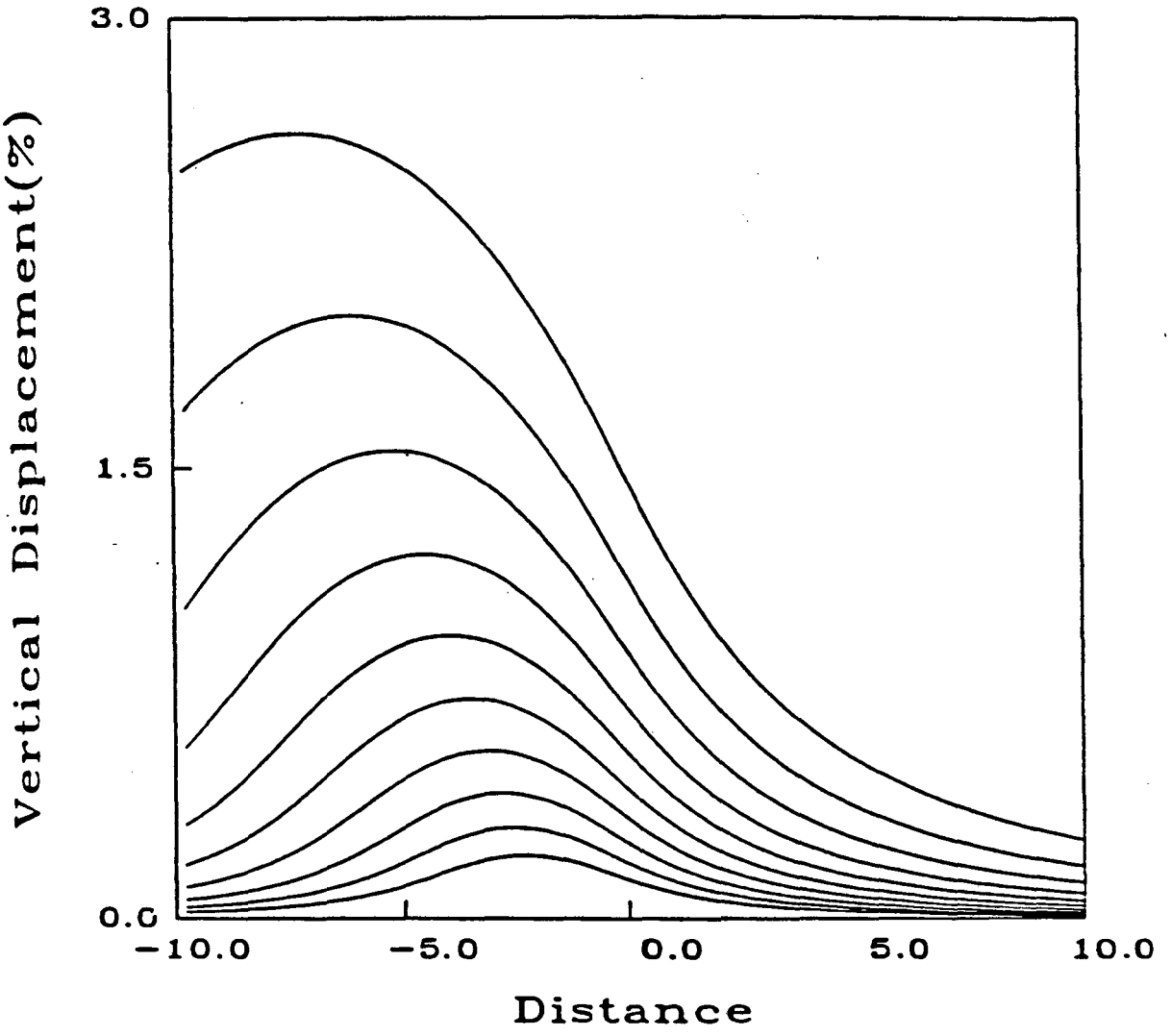

Figure 3.2 Uplift associated with ten 2-D two datum ideal bodies characterized by $0.7 \leq \beta \leq 0.9$. The bodies have all undergone a 1 per cent volume change and lie at a depth of two station spacings. All distances are in units of station spacing.

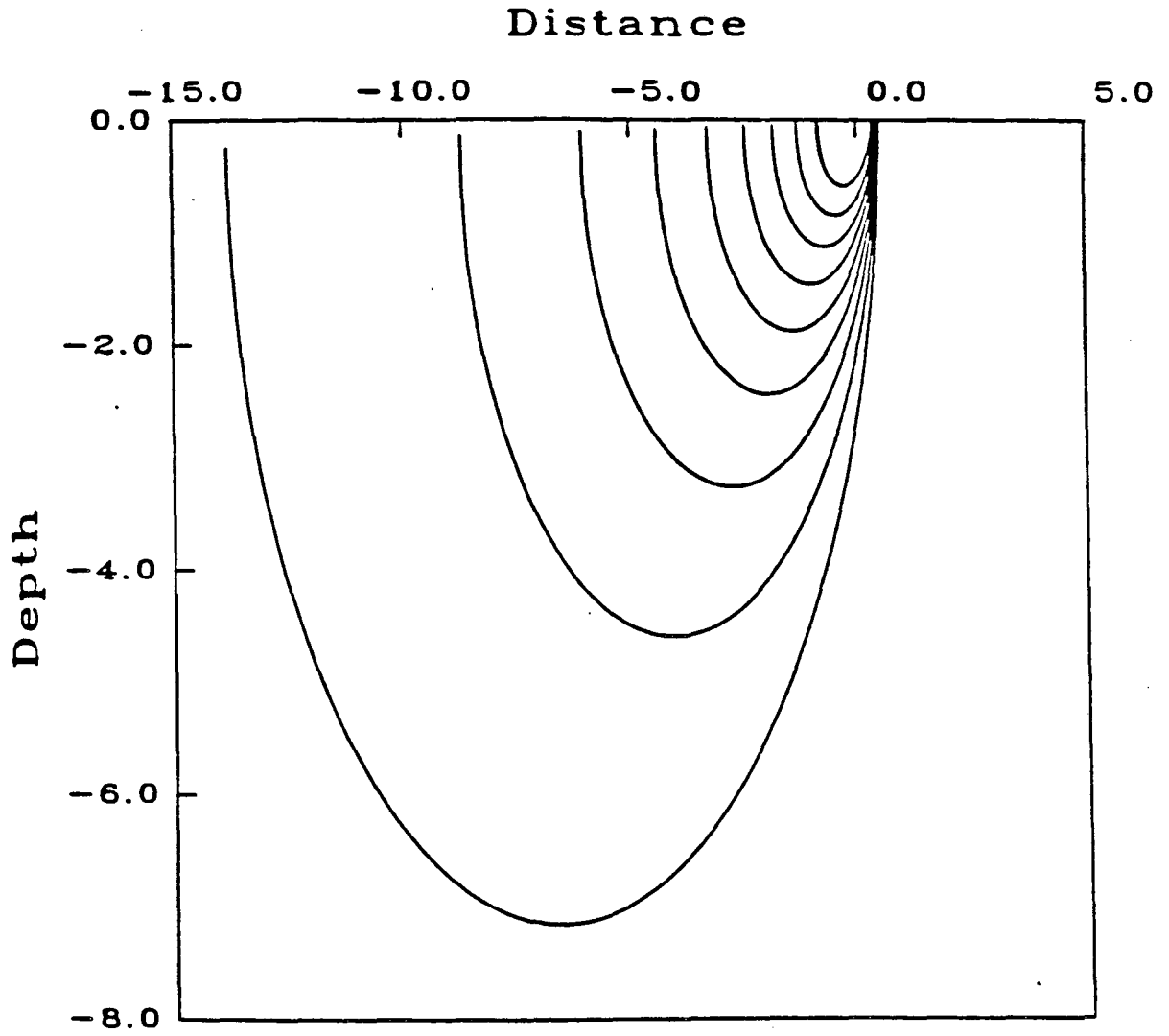

Figure 3.3 3-D two datum ideal bodies corresponding to β varying from 0.1 (smallest) to 0.9 (largest) in nine steps. The 3-D bodies are radially symmetric. Shown here is an (r, z) cross-section. The stations are located as in Figure 1.

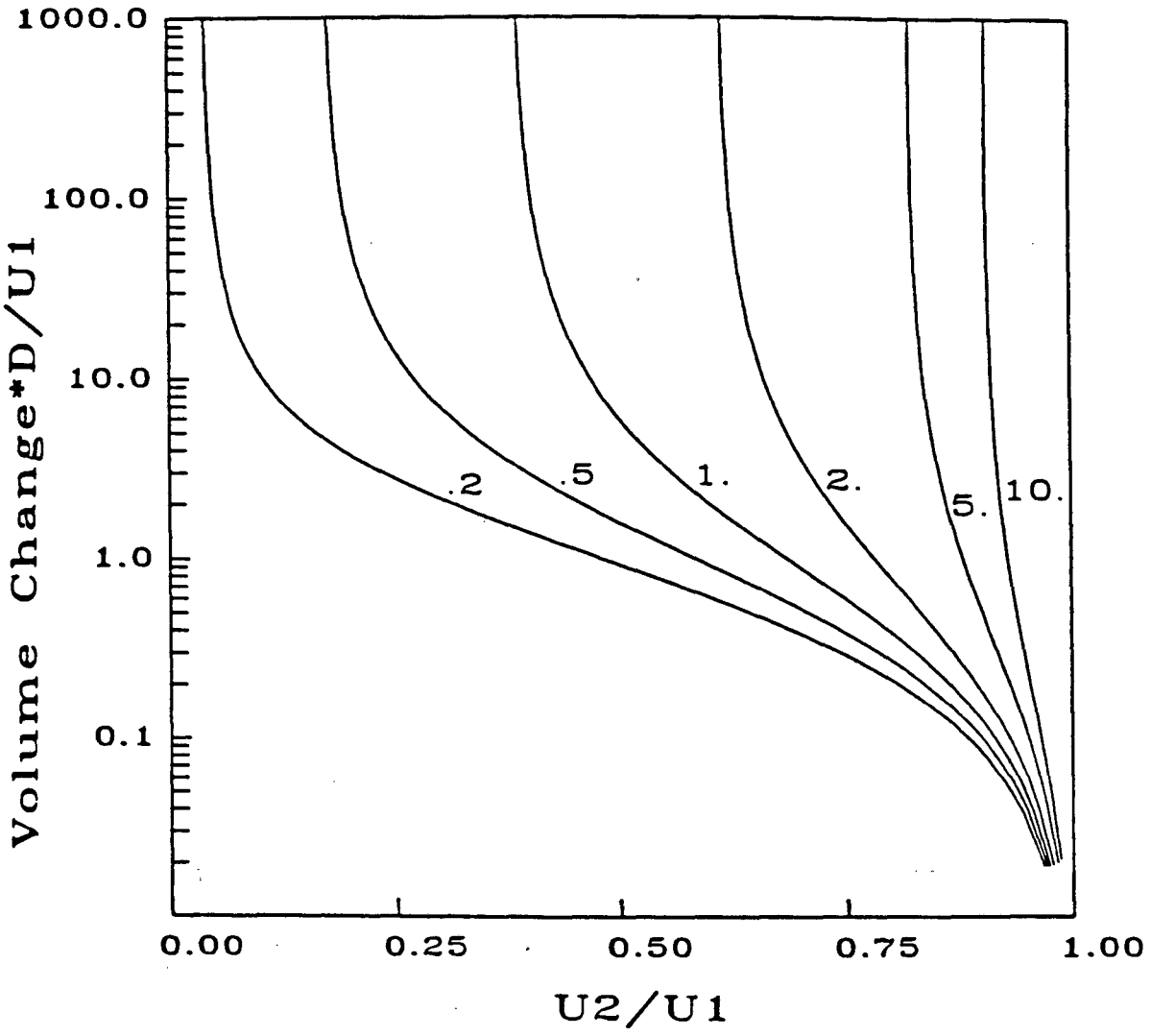

XBL 847-2918

Figure 3.4 Fractional volume change bounds as a function of the ratio of the uplifts u_1 at $\mathbf{x}^1$ and u_2 at $\mathbf{x}^2$ for depths of burial given by labels on the curves. There bounds have been derived for the 2-D two datum problem and a Poisson's ratio of 0.25. When the fractional volume change is known these curves may be used to derive a depth bound. All distances are relative to the station spacing D.

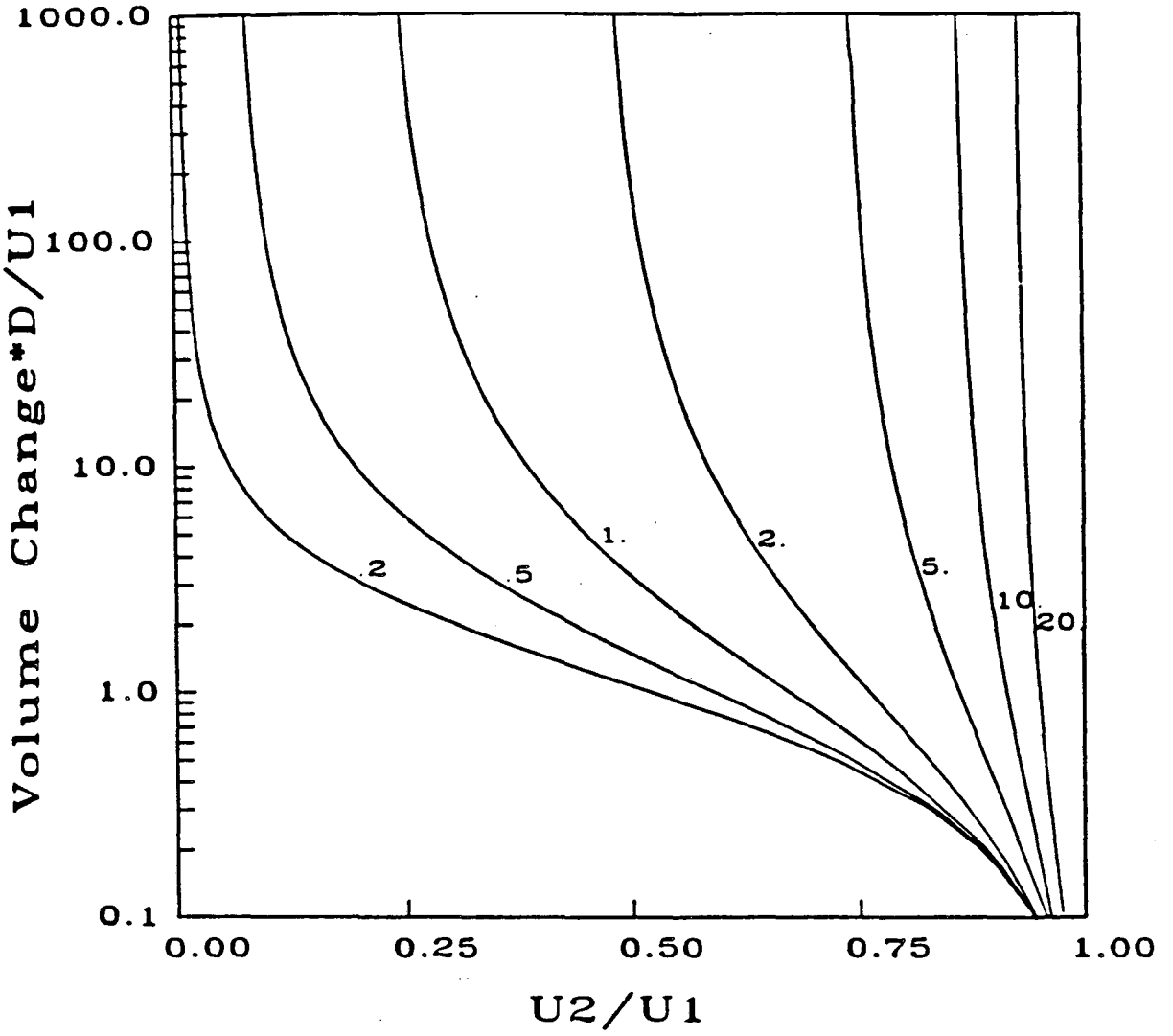

Figure 3.5 Similar to Figure 4 for the 3-D two datum case.

two datum case there are the possible pairs $[u_1 + 2\sigma_1, u_2 + 2\sigma_2]$, $[u_1 + 2\sigma_1, u_2 - 2\sigma_2]$,$[u_1 - 2\sigma_1, u_2 + 2\sigma_2]$ and $[u_1 - 2\sigma_1, u_2 - 2\sigma_2]$. The pair which gives the most pessimistic extremum (the deepest least upper bound on depth, etc.) should be used as a matter of caution.

The Method of Positivity Constraints

As noted by Sabatier (1977b), the ideal body problem may be framed in the following manner. Given a set of piecewise continuous kernels $\{K_i(\vec{r})\}$ and a set of measurements $\{m_i\}$, find non-negative, piecewise continuous functions $\Delta\theta(\vec{r})$ and $\Phi(\vec{r})$ such that the model satisfies the data

$$m_i = \int_V \Delta\theta(\vec{r}) K_i(\vec{r}) dV \qquad i = 1,2,3,.....,M \tag{3.8}$$

and the sum α ,

$$\alpha = \Delta\theta(\vec{r}) + \Phi(\vec{r})$$

is a minimum. Because $\Phi(\vec{r})$ is always a non-negative function the above sum will always exceed or equal $\Delta\theta(\vec{r})$, i.e. it is a supremum of $\Delta\theta(\vec{r})$. Hence minimizing α will produce

$$\min_{all\ solutions} \left[sup_{\vec{r}} \Delta\theta(\vec{r}) \right]$$

which resembles Parker's ideal body. Note that non-negativity is a nonlinear constraint. This approach introduces new degrees of freedom not present in Parker's original formulation. Strictly speaking in Parker's approach the model parameter $\Delta\theta(\vec{r})$ is a binary variable, taking only two values: zero and θ. Therefore one should treat the problem as an integer programming problem. Unfortunately the solution of integer programs is not well developed (Garfinkel and Nemhauser, 1972). The advantage of the linear programming formulation of the ideal body problem is that it puts it within a large class of well-studied optimization problems. Also it is easy to generalize the above technique to produce other useful bounds such as bounds on moments or on the position of the center of mass. This generalization was proposed by Sabatier (1977a) and used by him to find all possible solutions of linear inverse problems with positivity constraints. It was also used in the study of the inverse gravity problem (Safon et al. 1977).

Practical use of the algorithm relies on a discretization of the problem. In the next chapter a general method for discretizing the fractional volume change distribution will be given. In what follows the volume V is simply partitioned into domains ω_n on which $\Delta\theta(\vec{r})$ and $K_i(\vec{r})$ are considered constant. The extremal solution depends on the partition chosen. It is affected by both the size of each element in the partition as well as the extent of the total region considered. However, in the limit as the size approaches (but does not equal) zero there is a point at which a finer subdivision does not introduce any new information. Each new cell has the same fractional volume change as it had before. This is known as the saturation of the analysis (Sabatier 1977a). Sabatier has suggested this as a criteria for choosing the partitioning. Safon et al. (1977) however advocate that some other physical considerations such as station spacing be used to partition the problem. They note the difficulty of reaching the saturation point and the likelihood of oscillatory solutions with such a partition. The extent of the volume which if modeled depends for the most part on the scale of the anomaly. One encompasses the total anomaly as much as possible.

A generalization of the above, in discrete form, is to determine the extremum of

$$A = \sum_{n=1}^{N} \alpha_n \Delta\theta_n \tag{3.9}$$

under the constraints,

$$\sum_{n=1}^{N} k_{i,n} \Delta\theta_n = m_i \quad i = 1,2,3,.....,M \tag{3.10}$$

$$\Delta\theta_n \geq 0 \quad n = 1,2,3,.....,N \tag{3.11}$$

where

$$k_{i,n} = \int_{\omega_n} K_i(\vec{r}) dV$$

$K_i(\vec{r})$ is given by equation (3.5) for the two dimensional vertical displacement problem and equation (3.6) for the three dimensional vertical displacement problem. In the three dimensional radial displacement problem the kernel is given by (6a). One may also invert the combined radial and vertical displacement. If it is necessary to include layering effects the kernels presented in Jovanovich et al. (1974) must be used. The above formulation may be solved by the well known

simplex algorithm. In terms of the static displacement problem, equation (3.10) requires that the model satisfy the displacement data while equation (3.11) requires that each component of the model vector be non-negative. The later requirement is met for a fluid body undergoing pure expansion. The first requirement , the minimization of A, is very general and various choices of α_n can produce interesting bounds (Safon et al 1977), such as Parker's ideal body for a discrete problem.

In Figure 3.6 are examples of ideal bodies computed through the solution of a discretized version of equation (3.8). The bodies were computed for the two datum problem (M = 2). The resemblance to the two dimensional ideal bodies (Figure 3.1) is striking considering the possible variation in $\Delta\theta(\vec{r})$. This shows that for two data points the ideal body method and the positivity constraint method give qualitatively similar results.

Other values of the coefficients α_n will introduce other bounds or extremal solutions. For example, a bound on the m th order moment about $\vec{r}_0$,

$$V_m^{\vec{r}_0} = \int_V (r - r_0)^m \Delta\theta(r)\, dV \approx \sum_{n=1}^{N} (r_n - r_0)^m \Delta\theta_n \Delta V_n$$

will be produced by the choice

$$\alpha_n = (r_n - r_0)^m \Delta V_n .$$

The zeroth order moment produces bounds on the total volume change

$$V_0 = \int_V \Delta\theta(\vec{r})\, dV = \sum_{n=1}^{N} \Delta\theta_n \Delta V_n .$$

In Figure 3.7 is a two dimensional volume source model. The body has undergone a .05 volume change within a half space characterized by $\nu = .25$. Shown in Figure 3.8 are distributions, for the ten datum problem, corresponding to the minimum and maximum volume changes which might give rise to the anomaly caused by the model. The minimum and maximum volume changes of .038 and .065 respectively bracket the true value.

From the zeroth and first order moments one may estimate the "center of mass" of the body,

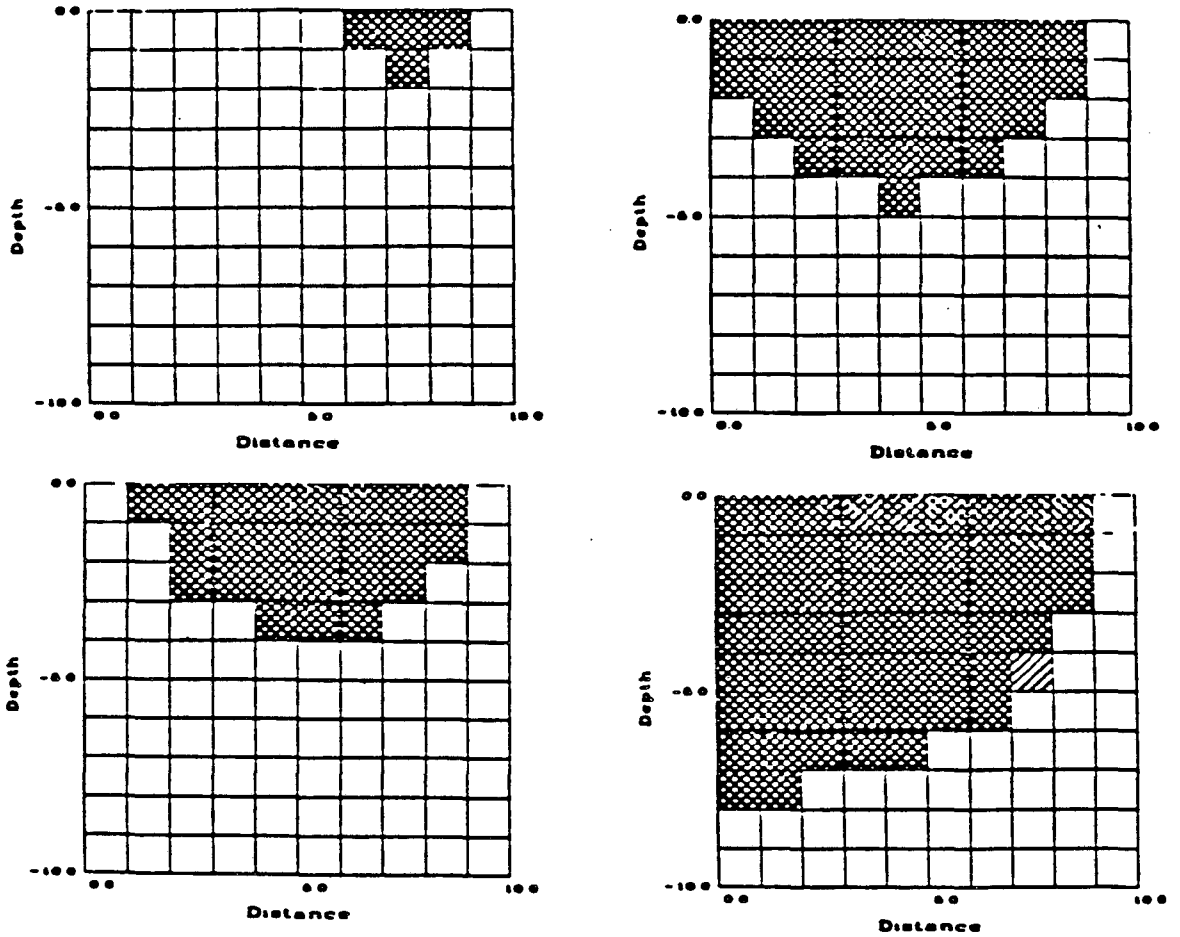

XBL 847-2914

Figure 3.8 Two datum 2-D ideal bodies derived using the linear programming method of Sabatier (1977a,b). These four bodies correspond to uplift ratios of 0.16 (upper left) 0.18 (lower left), 0.21 (upper right), and 0.15 (lower right). The two stations are at 8.5 and 9.5. The double hatchured pattern denotes a fractional volume change in the upper two-thirds of the total range of fractional volume changes. Blank areas denote regions with no fractional volume change.

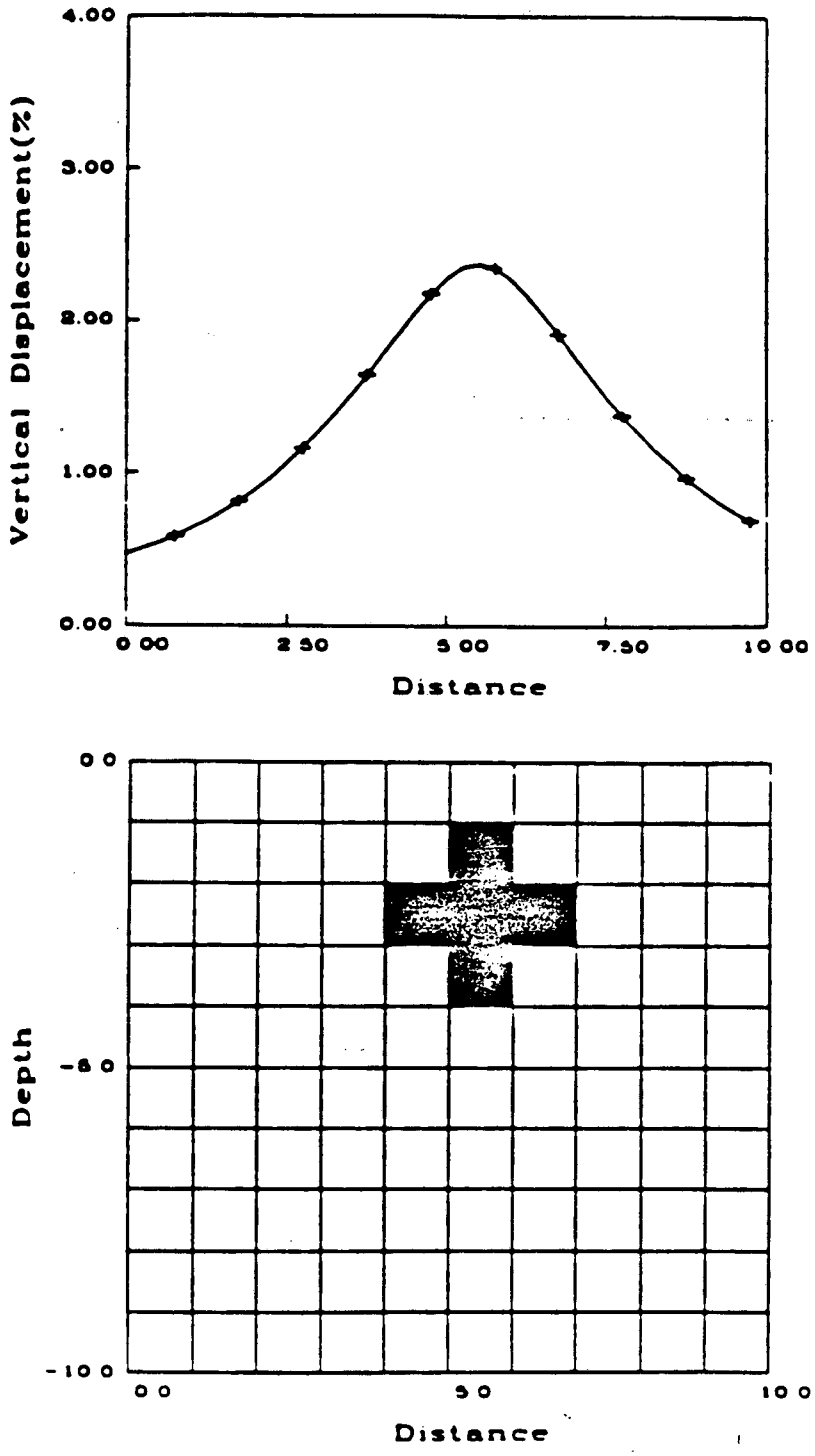

Figure 3.7 2-D volume source model used in subsequent calculations. A 1 per cent fractional volume change within the black region gives rise to the anomaly shown above it. The anomaly is sampled at 10 stations. The samples are denoted by crosses. The model lies in an elastic half-space which has a Poisson's ratio of 0.25.

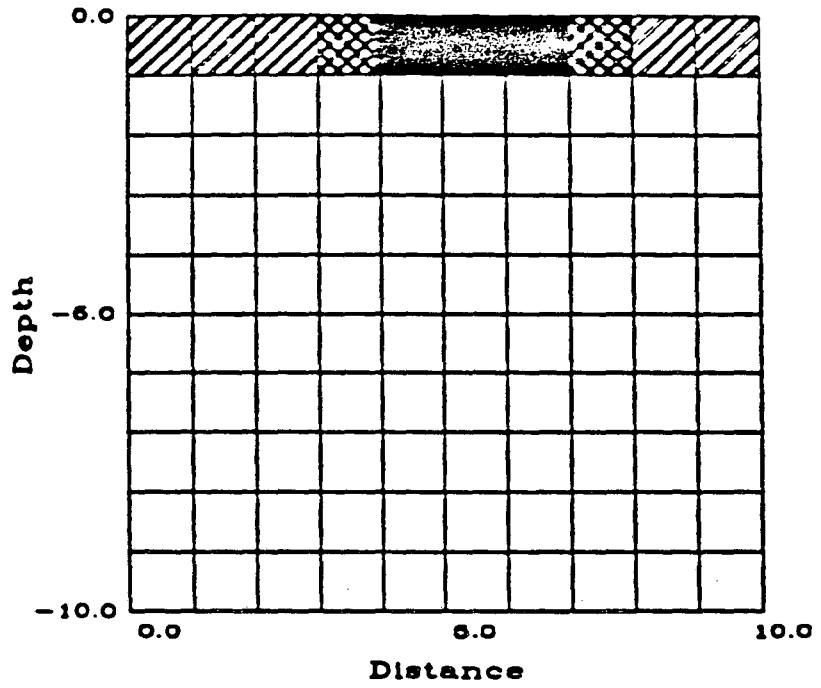

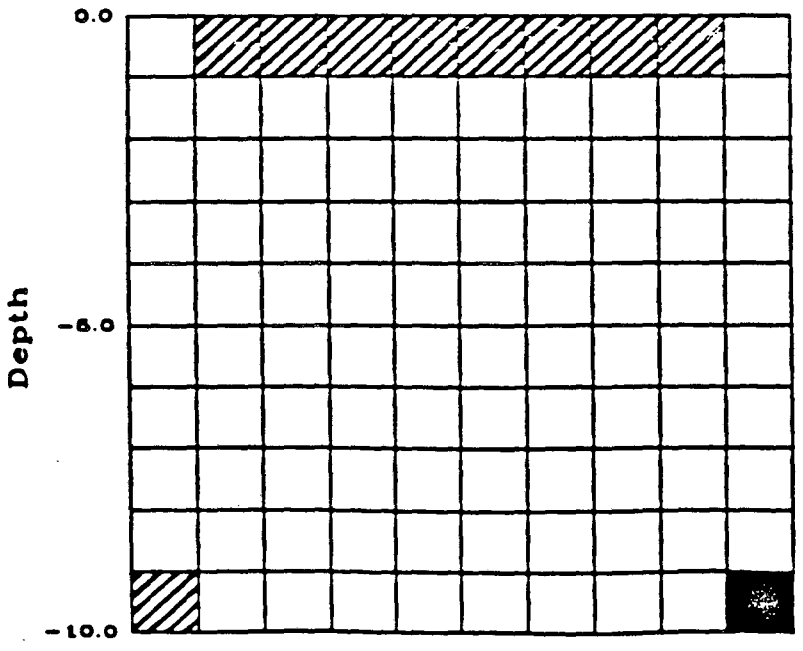

Figure 3.8 Minimum (upper figure) and maximum (lower figure) total volume change distributions which would give rise to an anomaly such as that caused by the model. The range of fractional volume change occurring in the region was divided into four regions: the upper one third (black), the middle third (double hatchure), the lower third (single hatchure) and zero (blank). The minimum total volume change is 0.038. The maximum is 0.065.

$$\vec{x} = \frac{V_1^{\vec{x}}}{V_0}$$

$$\vec{y} = \frac{V_1^{\vec{y}}}{V_0}$$

$$\vec{z} = \frac{V_1^{\vec{z}}}{V_0}$$

Higher order moment bounds about the center of mass then give estimates of the compactness and symmetry of the perturbing body.

Other bounds on the extent of the source may be deduced through the minimization of the volume change above a certain depth z_0,

$$\Delta V_z = \int_0^z \int_{y_{min}}^{y_{max}} \int_{x_{min}}^{x_{max}} \Delta\theta(\vec{r})\,dx\,dy\,dz$$

or the volume change to one side of a vertical plane, for instance the plane perpendicular to the x axis,

$$\Delta V_x = \int_{x_{min}}^{x} \int_{y_{min}}^{y_{max}} \int_{z_{min}}^{z_{max}} \Delta\theta(\vec{r})\,dx\,dy\,dz$$

These are examples of generalized moments where $\alpha(\vec{r})$ is defined such that for a given region U of domain V,

$$\alpha(\vec{r}) = \begin{cases} 1 & \omega_n \ in \ U \\ 0 & \omega_n \ not \ in \ U \end{cases}$$

If the lower bound of such moments equals zero there exists at least one solution which has no volume change within the region of integration. If there is no such vanishing solution then a volume change must have occurred within the specified region of integration. By varying the boundary one may bound the region of volume change in two or three dimensions. Consider the body shown in Figure 3.7 and the corresponding ten measurements of uplift produced by a 1 % volume change within this body. Figure 3.9 shows horizontal and vertical bounds derived from the anomaly produced by this two dimensional volume change. These figures delineate a region with horizontal coordinates between 5 and 6 km and extending in depth from 2 km to infinity.

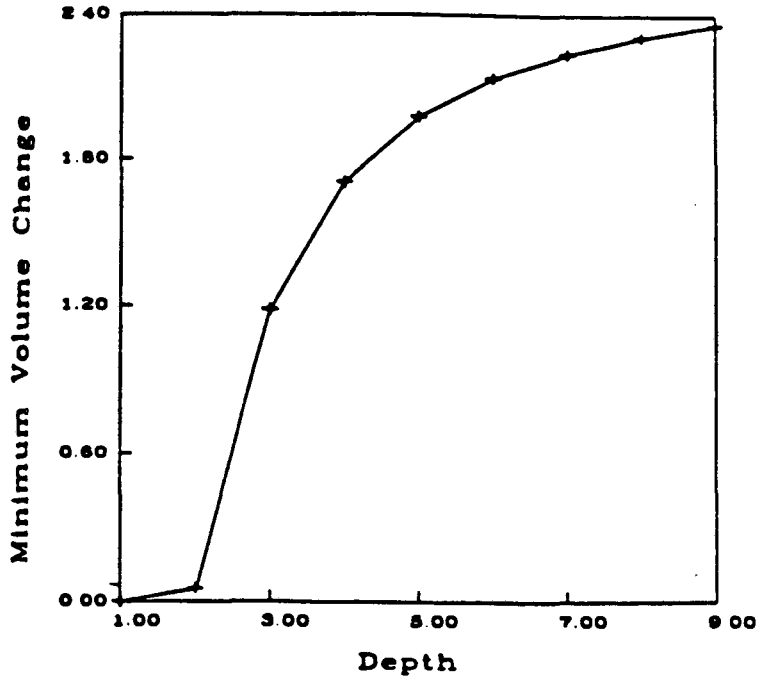

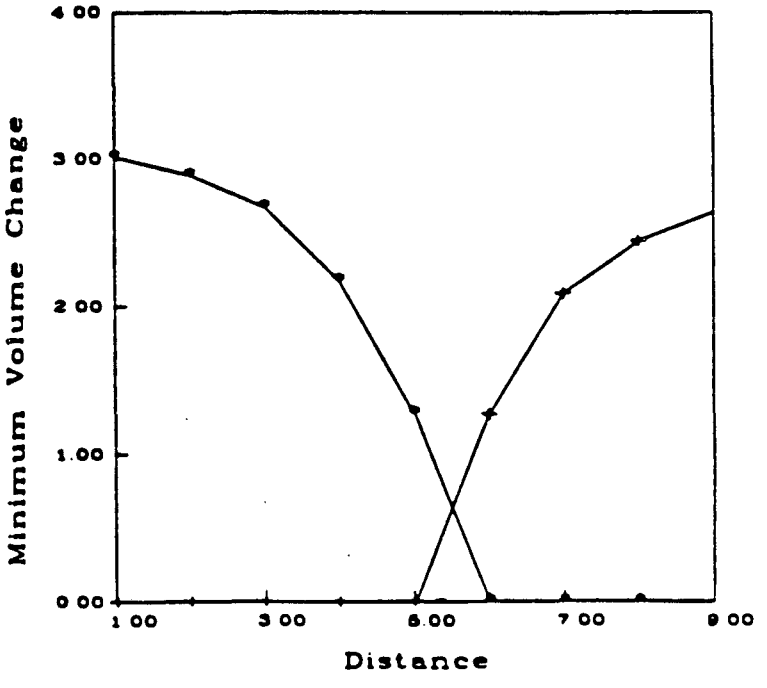

XBL 847-2912

Figure 3.9 Horizontal and vertical bounds derived from the data. The upper figure shows the minimum volume change which must occur above the given depth. The lower figure displays the minimum volume change which must occur to the right of the points * and to the left of the points +.

The anomalous body corresponding to any solution must extend beyond the bounds of this region. Thus this illustrates a property which is common to all possible sources of the anomaly.

By decreasing the size of the region U in equation (2.11) until it encompasses just a single pixel allows the placement of upper and lower bounds on fractional volume change at depth. Because of the highly under-determined nature of the problem the lower bounds are uniformly zero. The upper bounds on each pixel are shown in Figure 3.10. Shown in Figure 3.11 are the upper bounds when the region is discretized in a twenty by twenty grid. It is seen that bounds smear out under the increase of unknowns. Further, the bounds on the pixels increase in value.

Generalization: Nonpositive Bounds

The fact that the fractional volume change $\Delta\theta(\vec{r})$ is allowed to vary over the region considered allows one to account for more than one initial volume undergoing pure volume expansion. Another possibility is for material to withdraw from one region to a remote region. Such movement implies negative fractional volume changes, violating the positivity constraint. It is possible to modify the formulation such that the fractional volume change is bounded, possibly by a negative bound (Hadley 1962; Safon et al. 1977),

$$\Delta\theta_{\min} \leq \Delta\theta_n \leq \Delta\theta_{\max}.$$

Then one must consider the transformed variables

$$\delta\theta_n^{\min} = \Delta\theta_n - \Delta\theta_{\min}$$

$$\delta\theta_n^{\max} = \Delta\theta_{\max} - \Delta\theta_n$$

and the problem

$$\sum_{n=1}^{N} k_{i,n}\,\delta\theta_n^{\min} = m_i - \sum_{n=1}^{N} k_{i,n}\,\Delta\theta_{\min}$$

$$\delta\theta_n^{\min} + \delta\theta_n^{\max} = \Delta\theta_{\max} - \Delta\theta_{\min}$$

$$\delta\theta_n^{\max} \geq 0 \quad \delta\theta_n^{\min} \geq 0$$

However, if the region of negative volume change is sufficiently far removed one need only

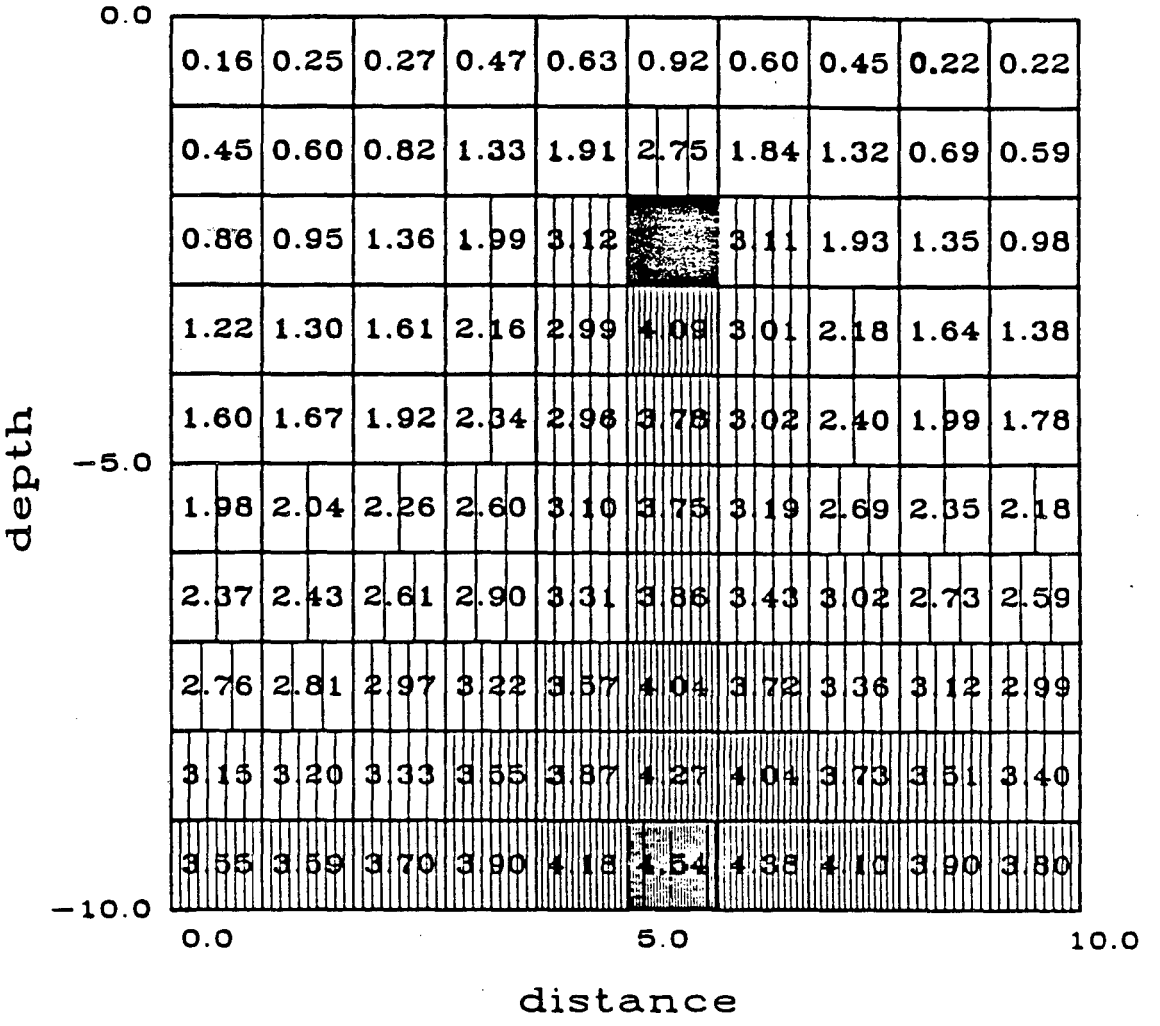

Figure 3.10 Upper bounds on the individual blocks or pixels.

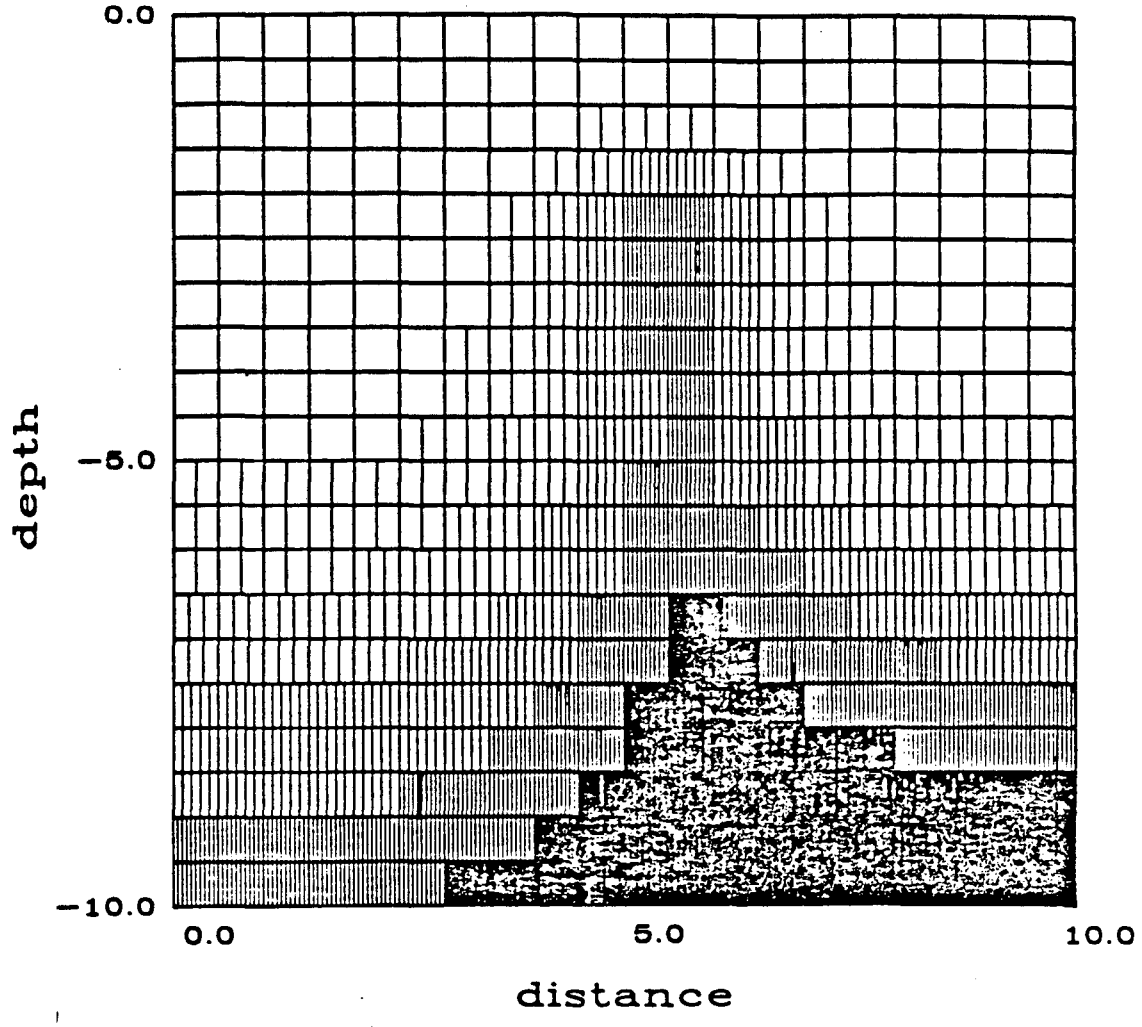

Figure 3.11 Similar to Figure 10 but the region is now discretized by a twenty by twenty grid.

consider pure expansion ($\Delta\theta_n \geq 0$).

Errors in the Data

In formulating the extremal inversion problem as a linear programming problem it is possible to account for errors explicitly in the data (Safon et al., 1977; Oldenburg, 1983). There are three possible approaches to the treatment of errors.

In the first case, instead of requiring that the data satisfy the equality constraints of equation (3.10) exactly, the solution may be required to fit the data to within a prescribed bound. The extremal inversion problem becomes, in matrix form,

$$\textit{minimize } \mathbf{a}^t \Delta\theta$$

$$\textit{with}$$

$$\mathbf{m}-\boldsymbol{\eta} \leq \mathbf{K}\Delta\boldsymbol{\theta} \leq \mathbf{m}+\boldsymbol{\eta}. \tag{3.12}$$

Also, the inequality constraints

$$\mathbf{C}\Delta\boldsymbol{\theta} \leq \mathbf{h}$$

may be present. This is a more realistic formulation in that real data contain measurement errors. These equations allow a formal mapping of error bounds on the data to bounds on model properties. Data errors result in an under-determined problem with positivity constraints. This becomes clear when equation (3.12) is transformed into a system of equalities. Introducing a non-negative variable to each inequality transforms it to an equality. For N two-sided inequalities $2N$ additional variables are required.

Unfortunately, the data bounds presented above are rigid and do not allow for large spurious errors. In fact, for data containing additive gaussian noise with zero mean and standard deviation σ_j, the probability that all N data lie within the bounds $\pm\sigma_j$ is $(.65)^N$ (Oldenburg, 1983). For large N this becomes very small. If the bounds are widened significantly to allow for outlying values than the possible misfit for each data point may become unacceptably large.

These difficulties suggest constraining some measure of total error. One that has been suggested by several authors is the l_1 norm of the normalized errors. This is the second procedure for including errors in linear programming. To accomplish this the data constraints are written in the form of the following equality,

$$\frac{m_i}{\sigma_i} = \sum_{j=1}^{M} \frac{K_{ij}}{\sigma_i} \Delta\theta_j + \gamma_i$$

where σ_i is the assigned standard deviation of the *ith* datum and γ_i is a realization of a gaussian random variable with zero mean and a standard deviation of 1.0. The l_1 norm of γ_i is given by,

$$\chi^1 = \sum_{i=1}^{N} | \gamma_i | .$$

Parker and McNutt (1980) have determined the expectation of χ^1 for N data,

$$E[\chi^1] = \sqrt{\frac{2}{\pi}} N$$

as well as the standard deviation,

$$s[\chi^1] = \sqrt{(1-\frac{2}{\pi})N}$$

Therefore the constraint on the errors becomes

$$\sqrt{\frac{2}{\pi}} N - \alpha \sqrt{(1-\frac{2}{\pi})N} \leq \chi^1 \leq \sqrt{\frac{2}{\pi}} N + \alpha \sqrt{(1-\frac{2}{\pi})N} .$$

α represents the significance level and is often taken as 1.0. This constraint allows a few data to have large misfits while bounding the error as a whole.

It is possible for a solution to satisfy the l_1 norm misfit criteria and violate an l_2 criteria such as the chi-squared test (Oldenburg, 1983). Closer agreement between the two criteria is possible by subtracting a positive constraint from each side of the above equation. The use of the chi-squared criteria as a constraint on finding the extremum of a linear functional is much more difficult. Unfortunately, general linear programming seems difficult to formulate under the l_1 constraint.

A third way to overcome errors in an inverse problem is to separate the over-determined parameters from the under-determined parameters. The over-determined variables are then determined in a least-squares sense while extremal inversion finds the under-determined parameters. The method used to decompose the problem into purely over and under-determined portions is singular value decomposition. Consider the set of linear equality constraints that the model satisfy the data

$$\mathbf{K}\Delta\theta = \mathbf{m} \tag{3.13}$$

The matrix $\mathbf{K}$ is known to have the following singular value decomposition,

$$\mathbf{K} = \mathbf{U}\Lambda\mathbf{V}^t . \tag{3.14}$$

The matrix Λ is a diagonal matrix containing the singular-values λ_i. $\mathbf{U}$ and $\mathbf{V}$ are matrices containing the eigenvectors of $\mathbf{K}\mathbf{K}^t$ and $\mathbf{K}^t\mathbf{K}$ respectively. Some singular-values are zero and the eigenvectors, $\mathbf{u}_i{}^0$,$\mathbf{v}_i{}^0$ are associated with these vanishing λ_i. Consider the partitioning of the matrix $\mathbf{U}$ into eigenvectors associated with non-zero λ_i, $\mathbf{U}_p$, and eigenvectors associated with vanishing λ_i, $\mathbf{U}_0$,

$$\mathbf{U} = [\mathbf{U}_p\, \mathbf{U}_0].$$

Similarly for the matrix $\mathbf{V}$ we can write

$$\mathbf{V} = [\mathbf{V}_p\, \mathbf{V}_0]. \tag{3.15}$$

Now examine the set of linear equations (3.10) in terms of the representation in equation (3.14) of $\mathbf{K}$,

$$\mathbf{U}\Lambda\mathbf{V}^t\,\Delta\theta = \mathbf{m}. \tag{3.16}$$

Let

$$\pi = \mathbf{V}^t\,\Delta\theta \tag{3.17}$$

or

$$\Delta\theta = \mathbf{V}\pi.$$

In terms of the regrouping in equation (3.20) and

$$\pi = \begin{bmatrix} \pi_p \\ \pi_0 \end{bmatrix}$$

$\Delta\theta$ has the decomposition

$$\Delta\theta = \begin{bmatrix} \mathbf{V}_p \mathbf{V}_0 \end{bmatrix} \begin{bmatrix} \pi_p \\ \pi_0 \end{bmatrix} \tag{3.18}$$

$$= \mathbf{V}_p \pi_p + \mathbf{V}_0 \pi_0.$$

The extremal inverse problem may now be written in terms of the singular value decomposition. This can be done by substituting the decomposition of $\mathbf{m}$ given in equation (3.18) into the extremal inverse problem of equation (3.10) and using the Lanczos solution for the over-determined parameters π_p ,

$$\mathbf{K}\mathbf{V}_p \pi_p = \mathbf{K}\mathbf{V}_p \Lambda_p^{-1} \mathbf{U}_p{}^t \mathbf{m} = \mathbf{U}_p \mathbf{U}_p{}^t \mathbf{m}$$

Realizing that the second equation in the extremal inverse problem of equation (3.10) need only be satisfied in the least-squares sense the requirement that the model satisfy the data can be replaced by the specification that the under-determined parameters lie in the null-space of $\mathbf{K}$,

$$\mathbf{K}\mathbf{V}_0 \pi_0 = 0.$$

Thus the problem becomes

$$\min z = \mathbf{a}^t \mathbf{b} + \mathbf{a}^t \mathbf{y}_0$$

with

$$\mathbf{K}\mathbf{y}_0 = 0$$

$$\mathbf{C}(\mathbf{y}_0 + \mathbf{b}) \leq \mathbf{h}$$

where

$$\mathbf{y}_0 = \mathbf{V}_0 \pi_0$$

and

$$\mathbf{b} = \mathbf{V}_p \pi_p .$$

Letting

$$\mathbf{w}_0 = \mathbf{y}_0 + \mathbf{b}$$

and using the fact that

$$\mathbf{K}\mathbf{b} = \mathbf{U}_p \mathbf{U}_p{}^t \mathbf{m}$$

then the above problem becomes

$$\min z = \mathbf{a}^t \mathbf{w}_0$$

with

$$\mathbf{K}\mathbf{w}_0 = \mathbf{U}_p \mathbf{U}_p{}^t \mathbf{m} \tag{3.19}$$

$$\mathbf{C}\mathbf{w}_0 \leq \mathbf{h}.$$

If the data resolution matrix $\mathbf{U}_p \mathbf{U}_p{}^t$ is the identity matrix $\mathbf{I}$ then the problem Equation (3.19) is identical to the original extremal inverse problem in equation (3.10).

Previous discussions (Wunsch and Minster, 1982; Menke, 1984) presented the extremal problem in terms of the null-space vectors $\mathbf{V}_0$. The above derivation makes no explicit use of the null-space vectors $\mathbf{U}_0$ and $\mathbf{V}_0$. This may be advantageous in that these vectors can be difficult to calculate accurately.

The above decomposition will prevent inconsistent constraints from arising due to errors in the data. However errors in the data can prevent a feasible solution, one satisfying the inequality constraints, from existing. For this reason the method of linear programming with error bounds, which takes this difficulty into account, may be preferable in certain situations.

While the above methods are suited to deal with measurement errors, those errors due to linearization and discretization are not considered. Linearization restricts the method to small perturbations about some reference model. The finite nature of computation limits the perturbations to those that can be described by a finite number of parameters. These limitations introduce errors in the inversion. These errors may be dealt with by blurring the distinction between

coefficients and parameters but this takes the problem out of the realm of linear programming.

Conclusions

For the inverse static displacement problem there are methods available by which one may derive unique bounds on model parameters. The ideal body method and the method of positivity constraints are closely related techniques. However, the two approaches are in some ways complementary. The derivation of the ideal body for the general N datum problem is unwieldy and expensive. In the full treatment of N data the discretized method of positivity constraints (linear programming) is called for. When just two or three data are examined and/or a three dimensional model is required the ideal body method can give a quick estimate of bounds on the fractional volume change or the depth. The versatility of the method of positivity constraints is an advantage as is the universal availability of computer codes for solving the linear programming problem (Cuer and Bayer 1980). Also the method can readily treat a layered halfspace. The bounds computed here by the method of positivity constraints will still stand for a model space restricted to homogeneous bodies. The limits are merely more pessimistic in that they include inhomogeneous distributions which may broaden the bounds. Work is in progress in applying the method of positivity constraints to the leveling data at Mammoth Lakes, California. Perhaps the method may be extended to the simultaneous inversion of all volume dependent properties. Such a joint extremal inversion for gravity and magnetics has been presented by Mottl and Mottlova' (1984).

Chapter 4

Extremal Inversion of Vertical Displacements, Long Valley Caldera, California 1975-1982,1983 and 1985

Introduction

Long Valley Caldera has been the site of recent permanent and seismic displacements. Repeated leveling surveys between 1975 and August 1985 within the caldera have measured up to 0.47 meters of vertical displacement. These displacements have contributed to the hypothesis that a magma chamber still exists beneath the caldera and that this chamber has reinflated to some extent. This notion is compatible with recent moment tensor inversions of seismic data (Julian 1983) and P wave delay time inversions (Steeples and Iyer 1976). Similarly, a study of seismic attenuation within the caldera (Sanders and Ryall 1983) suggests the presence of a "region of molten or partially molten magma".

If one accepts the possibility of a magma body at depth it is possible to invert the uplift data for parameters of the causative body such as the depth and the volume change. For example, Savage and Clark (1982) inverted the 1982 displacement data of the survey line along Highway 395. Assuming a point source these authors produced an estimate of the source depth as well as the volume change. Similarly Castle et al. (1984) inverted the 1983 vertical displacement data along this line for estimates of the same parameters. Recently other models have been proposed. Savage and Cockerham (1984) were able to reproduce observed horizontal and vertical surface deformation reasonably well using two separate dike injection models. The first model consists of a single dike that dips 30° northward beginning at a depth of 8 km and extending to about 12 km in depth. The second model is similar to the first with the addition of a dike extending vertically from the top of the dipping intrusion to within 3 km of the surface. Right lateral slip was

needed in both models in order to satisfy the horizontal displacement data. Recently, Rundle and Whitcomb (1984) proposed an additional model. In their model deformation is attributed to the inflation of two spherical magma chambers, one at a depth of 5 km located 1.5 km west of station Casa, the other 9 km deep about 5.5 km north-northwest of Casa. All of the above models fit the data reasonably well.

Given the deformation data alone there is no reason to prefer one model over another. Even when including other information such as gravity or magnetotelluric data in the inversion, some ambiguity will remain in the description of the source. Therefore any proposed model must be viewed critically . Answers to the question "What magma body has produced these displacements?" are seldom unequivocally found. Definite answers are more forthcoming if one asks "How do the data constrain the range of possible models?" One way to answer this is to examine all the models which fit the data and determine properties common to all these models. However, this is a laborious task. There is a method available which allows one to find bounds or limits on certain properties of the models. Limits are placed on model properties such that all models satisfying the data must have properties within these bounds. Such limits are important, allowing one to assess the ambiguity present in the data set. It is for this reason that I have chosen to examine the bounds which the the 1975-1982, 1975-1983 and 1975-1985 leveling data place on the vertical and lateral extent of a proposed magma body under Long Valley Caldera. Using the method of extremal inversion (Parker 1975, Sabatier 1977a,b,c) I derive unique bounds on certain properties of the assumed source. Specifically, the bounds constrain the depth and horizontal extent of the perturbing body. Upper bounds on the possible fractional volume change at depth between 1975 and 1985 are also derived. Full nonsymmetric, three dimensional bodies are allowed and random leveling errors are incorporated into the inversion procedure.

The 1982, 1983 and 1985 Leveling Surveys

Leveling surveys within Long Valley Caldera were run along Highway 395 in 1932, 1954, 1975, 1980, 1982, 1983 and 1985. In addition, surveys were run along various access roads in the area. Figure 4.1 shows the stations used in the inversion. Two survey lines are shown in the figure. Line 1, along Highway 395, runs diagonally along the figure from the north-west to the south-east. Line 2 was measured along an access road from a point on line 1 almost due east then approximately due south. Movement along the Hilton Creek fault occurred in May 1980 and displacements, not associated with volume change, could adversely affect the inversion. This must be taken into account in the inversions. Trilateration data measuring horizontal length changes of survey lines within the caldera were not examined. These data would provide additional constraints on the model parameters.

The early surveys prior to and including the 1975 leveling line detected little or no uplift, however, between 1975 and 1982, up to .25 m of uplift occurred. Subsequent surveys in August 1982 and August 1983 detected .35 m and .40 m of maximum uplift respectively. The most recent survey in 1985 found about .47 meters of vertical change since 1975. This suggests that one may take the 1975 elevation as a baseline with which to measure the changes occurring in the 1975/1982, 1975/1983 and 1975/1985 intervals. These elevation changes along line 1 are shown in Figure 4.2. The horizontal distance, measured in kilometers, is the line length starting from the north-westernmost end of line 1. Also show in the figure are the standard deviations due to survey error. In addition, a second line of data extending approximately east-west and then north-south was included in the inversion. The vertical displacement along this line is shown in Figure 4.3. One assumption made in the production of these uplift profiles is that the southern end of leveling line 1 has remained stable with respect to Lee Vining in the north (Castle et al. 1984), which permitted one to treat the Long Valley system as if it were isolated from the surrounding region. Furthermore, Castle et al. (1984) also argue that only random errors are significant in the data, i.e. systematic deviations were shown to be negligible.

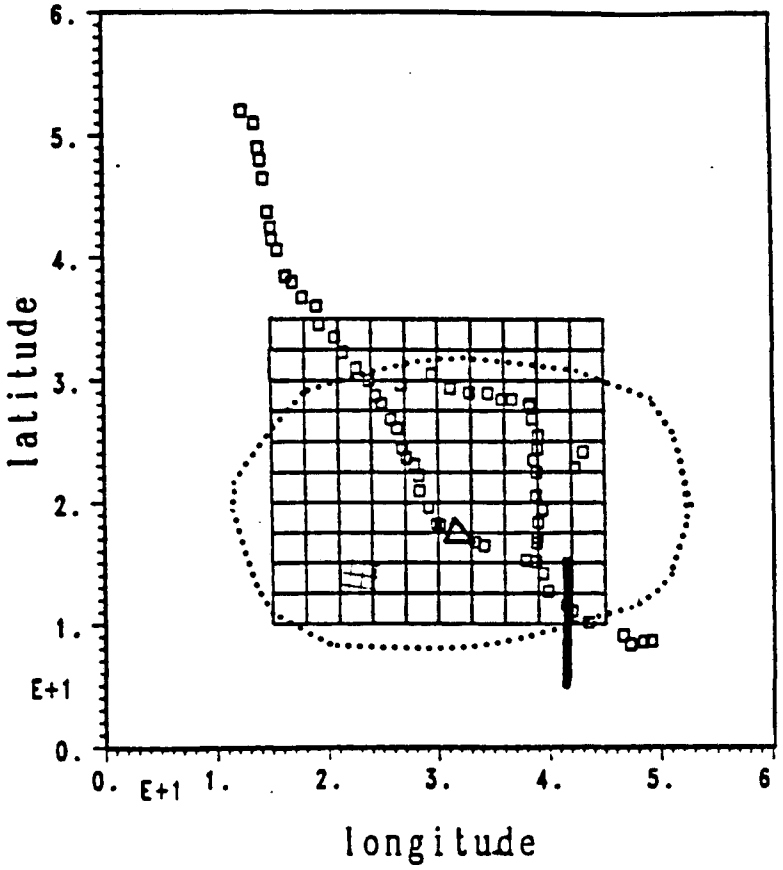

Figure 4.1 Map of the Long Valley Caldera region. The caldera is denoted by the dotted line. The town of Mammoth Lakes is shown by cross hatching. The Hilton Creek fault is denoted by the heavy black line. Boxes represent the leveling stations used in the study. Station Casa is the labeled triangle. Lee Vining is off the upper left hand corner of the map. The discretization of the region used in the inversion is shown.

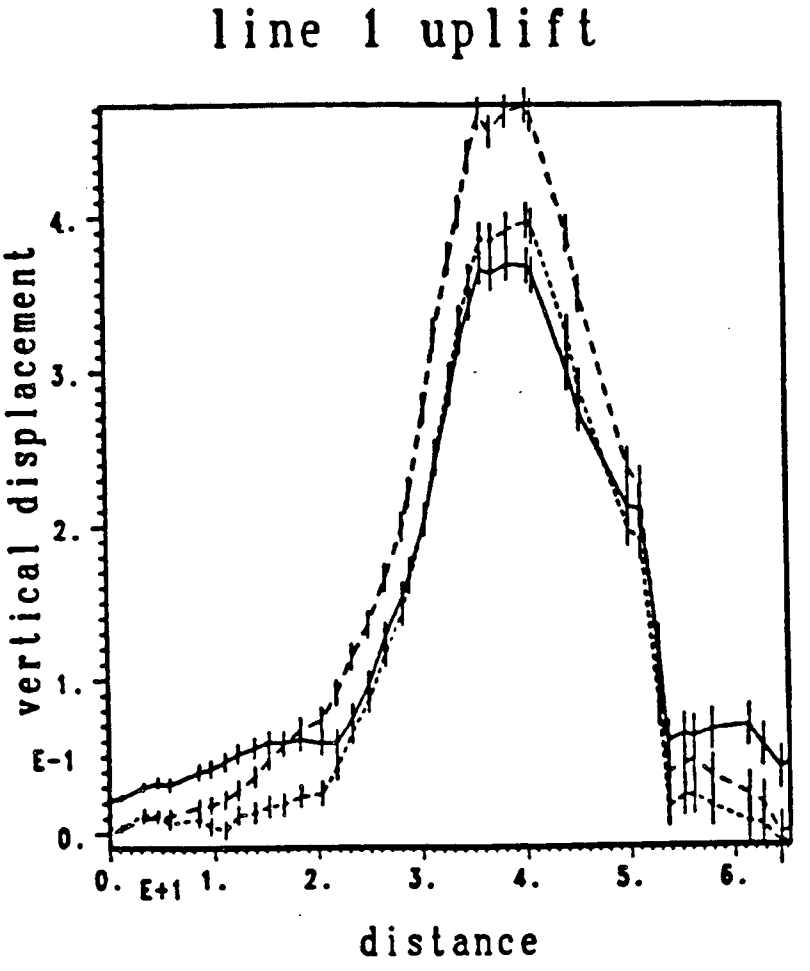

Figure 4.2 The vertical displacement data from the August 1982 survey (solid line), the 1983 survey (dashed line) and the 1985 survey for line 1 which ran along Highway 395 from Tom's Place to Lee Vining. Error bounds of two standard deviations are denoted by vertical lines. The data are shown relative to a 1975 baseline.

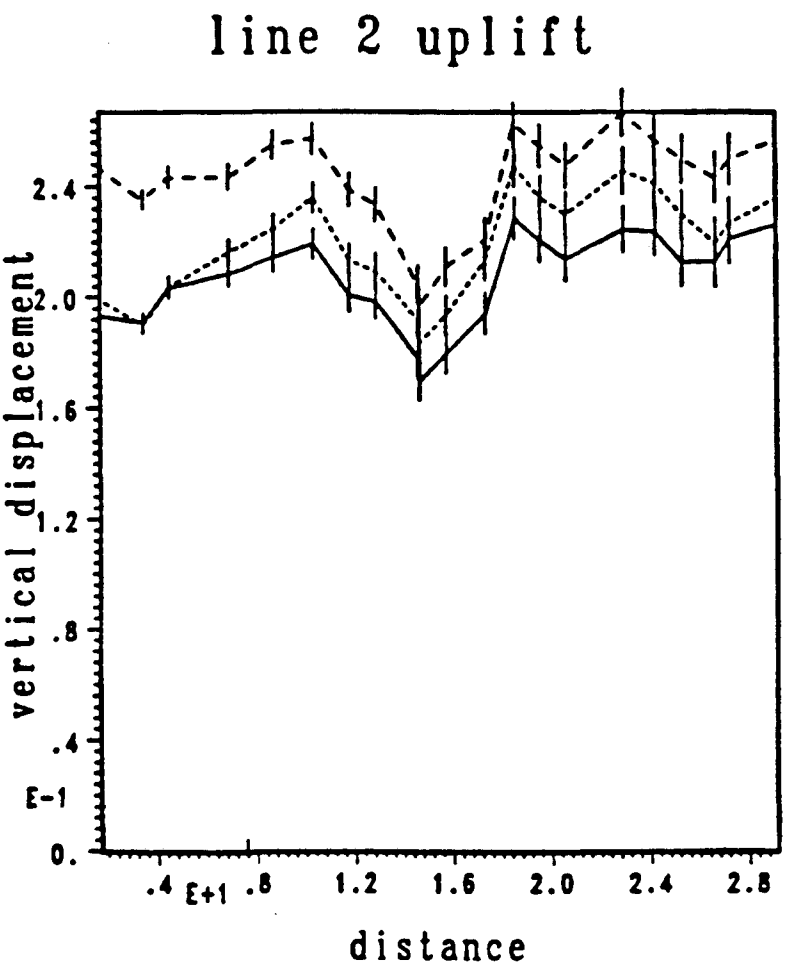

Figure 4.3 The vertical displacement data from the August 1982 survey (solid line), the 1983 survey (dashed line) and the 1985 survey for line 2 which ran along an access road shown in Figure 12. Error bounds of two standard deviations are denoted by vertical lines. The data are also shown relative to a 1975 baseline.

Application of Extremal Inversion to the Leveling Data of Long Valley Caldera

As mentioned previously, a variety of models have been proposed for the magma body giving rise to the observed displacements. Unfortunately, the data do not allow for discrimination among the various models. For this reason an alternative approach was taken. Properties common to all models fitting the data were searched for. For example, bounds on the depth and the horizontal location of the source were found. The method of extremal inversion was used to derive these bounds. This is a versatile technique and one that enables the inversion of all static displacement data, horizontal as well as vertical, to give unique bounds on properties of the source model. The only assumptions made are that the fractional volume change is of one sign (expansion) and that the region is homogeneous and may be characterized by a single Poisson's ratio. The technique is discussed by Parker (1975), Sabatier (1977a,b), Safon et al. (1977) and Reitsch (1978). The adaptation of this method to the inversion of static earth displacements was given in Chapters 2 and 3.

Recapitulating, one is interested in minimizing the moment, minimum or maximum, of a generalized moment

$$A = \sum_{n=1}^{N} \alpha_n \Delta\theta_n \tag{4.1}$$

subject to the constraint that equations (1) are satisfied within a specified error ϵ,

$$m_i - \epsilon_i \leq \sum_{n=1}^{N} k_{i,n} \Delta\theta_n \leq m_i + \epsilon_i \qquad i = 1,2,3,....,M \tag{4.2}$$

$$\Delta\theta_n \geq 0 \qquad n = 1,2,3,....,N.$$

The α_n in the above equation are constants. The generalized moment A may represent some physically significant property depending on the possible choices of the constants α_n . A possible choice of α_n and the one used in the following application to the Long Valley uplift data is that given in equation (2.11) in chapter 2,

$$\alpha_n(\vec{\xi}) = \begin{cases} 1 & \vec{\xi} \text{ in } U \\ 0 & \vec{\xi} \text{ not in } U \end{cases} \tag{4.3}$$

where U is a region of interest, that is some subset of the N blocks. Using such α_n, A represents the total fractional volume change in the region U.

The values of ϵ_i can be estimated for the above surveys. It has been argued (Castle et al. 1984) that the errors in the leveling survey are principally random errors described by the standard deviation

$$\sigma_i = \gamma L_i^{\frac{1}{2}}$$

where γ is a constant and L_i is the distance between the i th station and the base bench mark. For the single-run first order leveling surveys of 1982 ,1983 and 1985 $\gamma = 2.0mm/km^{\frac{1}{2}}$. For the double-run first order leveling survey of 1975 $\gamma = 1.5mm/km^{\frac{1}{2}}$. The lower precision value $\gamma = 2.0mm/km^{\frac{1}{2}}$ was considered as a measure of the error in the 1975-1982, 1975-1983 and 1975-1985 data. Assuming a gaussian distribution of errors, the 99.7% confidence intervals for $m_i (\pm 3\sigma_i)$ were incorporated into the inversion.

As mentioned above, movement along the Hilton Creek Fault occurred between the initial survey in 1975 and the subsequent surveys. It appears in the data shown in Figure 4.2 by sudden large changes in the vertical displacement. The effects were taken into account by modeling the fault giving rise to such changes. The fault model of Castle et. al. (1984), dip slip fault dipping 60° to the east with .12 meters of slip, was used. The dip, location, and slip were varied somewhat to attempt an improved fit. It was found that their model leads to the smallest discontinuity in the vertical displacement. The effect of the fault along line 1 is shown in Figure 4.4. The way in which this disturbance was incorporated into the inversion was through the error bounds. The displacement due to faulting at each station was considered part of the data errors. therefore, it was added to the errors given above. The data and resultant error bounds are shown in Figure 4.5. Similarly, for line 2, Figures 4.6 and 4.7 show the displacement caused by the faulting and the new resulting error bounds respectively.

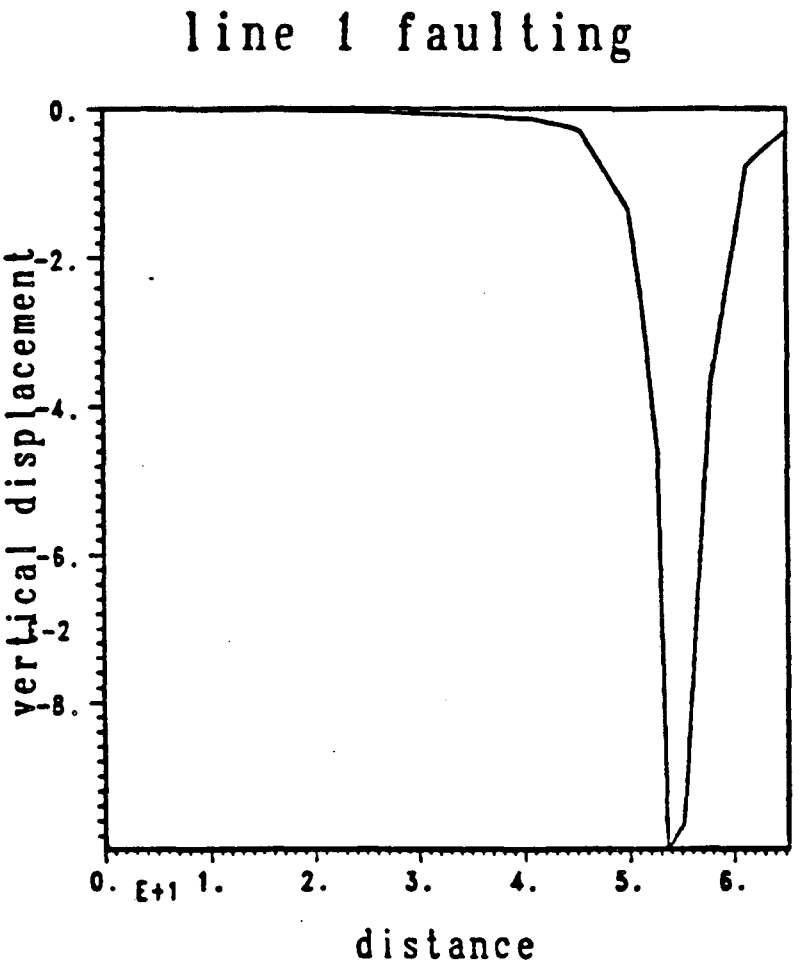

Figure 4.4 Vertical displacement along line 1 caused by a dip-slip fault located on the Hilton Creek fault trace. The fault dips 60° to the east with .12 meters of slip

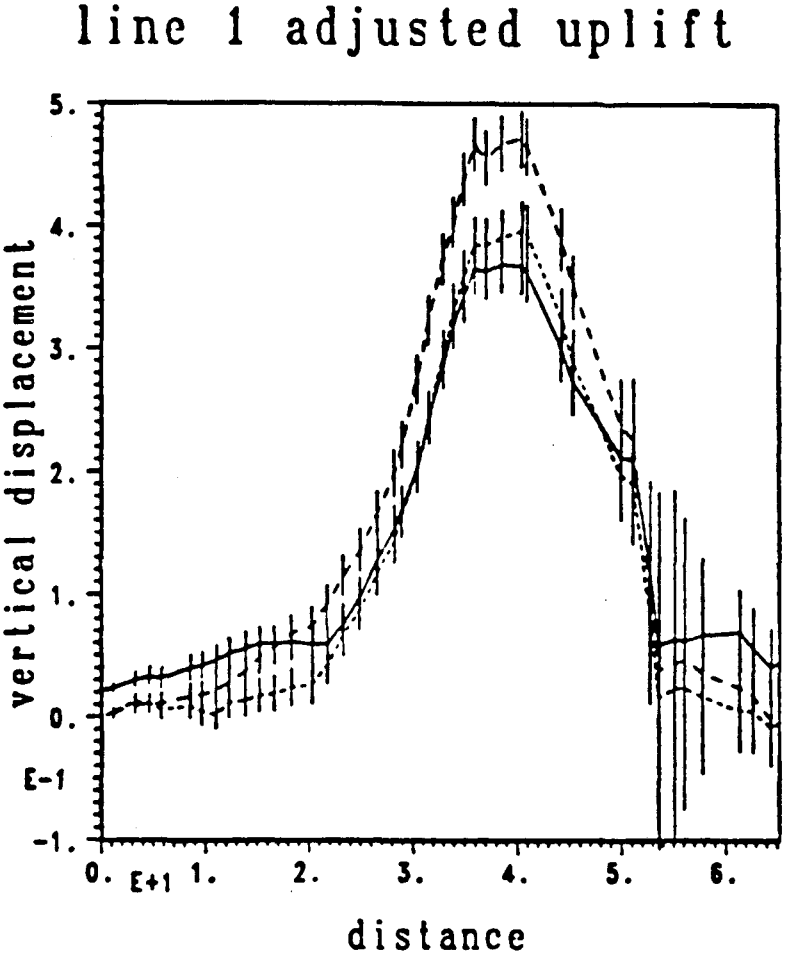

Figure 4.5 Vertical displacement along line with error bounds of two standard errors adjusted by the amount of displacement due to the faulting which was shown in Figure 4.4.

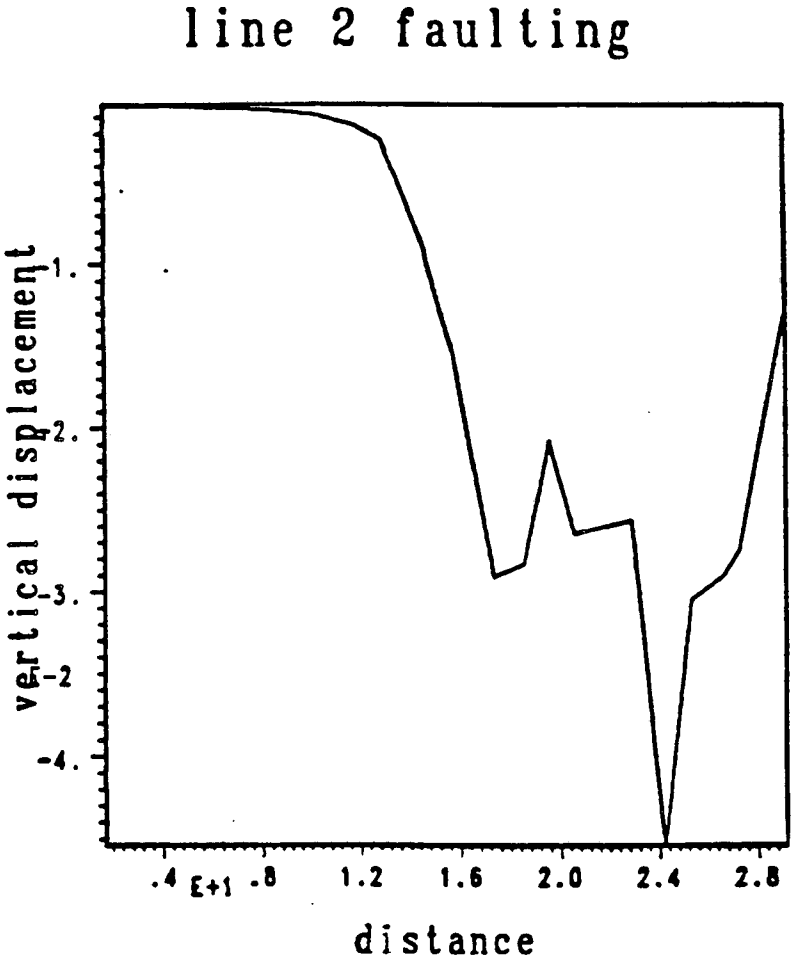

Figure 4.6 Vertical displacement along line 2 caused by the dip-slip fault described in Figure 4.4.

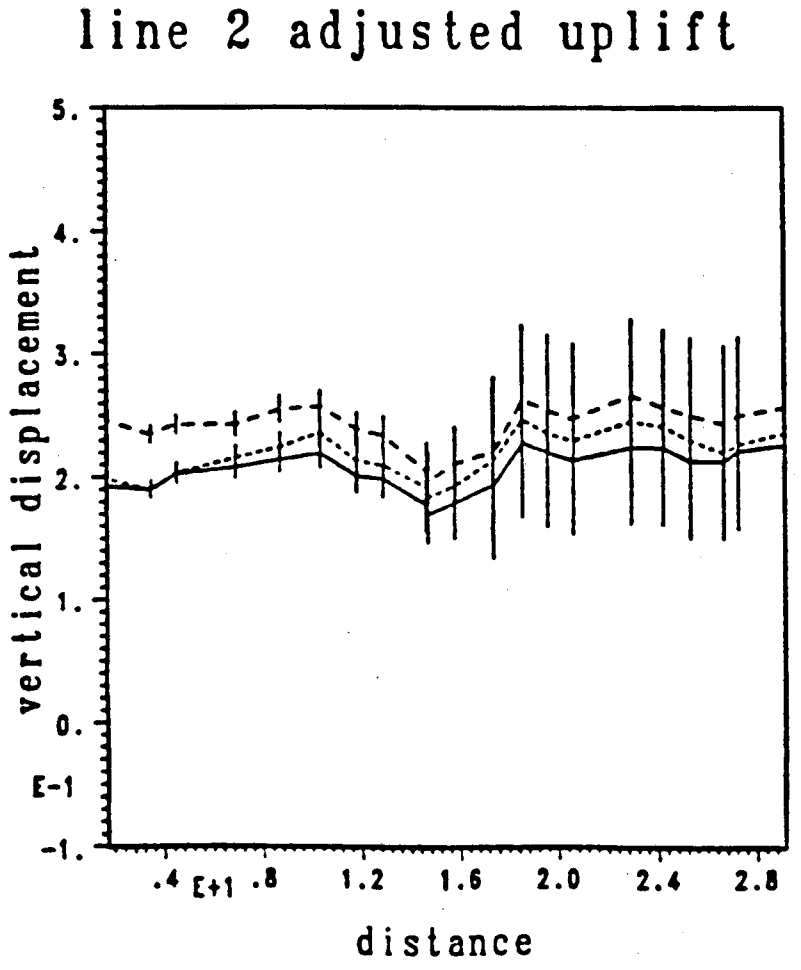

Figure 4.7 Vertical displacement along line with error bounds of two standard errors adjusted by the amount of displacement due to the faulting which was shown in Figure 4.4. Stations lying within one pixel of the fault were given bounds of plus or minus the maximum displacement of the uplift due to the fault. This was because the location of the fault was not known exactly.

The method of extremal inversion was applied to the data set discussed above. The aim was to determine bounds on the depth to the top of the body and on the location of the east-west and north-south boundaries of all possible magma bodies fitting the data. First the region of interest was divided into 20 layers and each layer was divided into 100 horizontal blocks shown if Figure 4.1. This resulted in 2000 blocks, each of 1 km height, 3.0 km east-west length, and 2.5 km north-south length. The initial volume of each block was 7.5 cubic kilometers. The range of possible models then is represented by all the possible combinations of fractional volume changes within the blocks. Given this space of possible models and a desire to produce bounds on the depth and horizontal boundaries of acceptable models, it is necessary to define an appropriate generalized moment. I have chosen to use α_n as defined in (4.3).

First examine the bound on the depth to the top of the magma body. Consider a horizontal plane which lies at a depth h_1. Define U to be the region between h_1 and the free surface and find the solution $\Delta\theta_n$, $n = 1,2,....,N$ which minimizes the total fractional volume change in the region U given by the functional A while still satisfying the constraints (4.2). Now move to a greater depth h_2 and repeat the process. For each depth $(h_1,h_2,\cdots)$ one has a particular minimum value of A . Plotting these particular minimum values of A derived for the various regions with lower boundaries given by h_i against the depth h_i results in the curves in Figure 4.8 and 4.9. The least upper bound on the depth of the body is given by the depth of the first point where the volume change is non zero, for this is the shallowest depth above which some volume change is required in order to satisfy the data. If the lower boundary of the region U extends down to or deeper than this point, then some volume change is required in U. The lower bound on the required volume change is given by the ordinate. Figure 4.8 presents bounds when two standard errors are used. The difficulties associated with requiring all the data to lie within rigid error bounds was discussed in the previous chapter. The probability the no data points are outside of these bounds is only 15% when calculated as in chapter 3. Hence it is felt that these bounds are unrealistic. Figure 4.9 presents the three standard error inversion. The probability that all the data lie within these bounds is much higher, about 82%. As can be seen in Figure

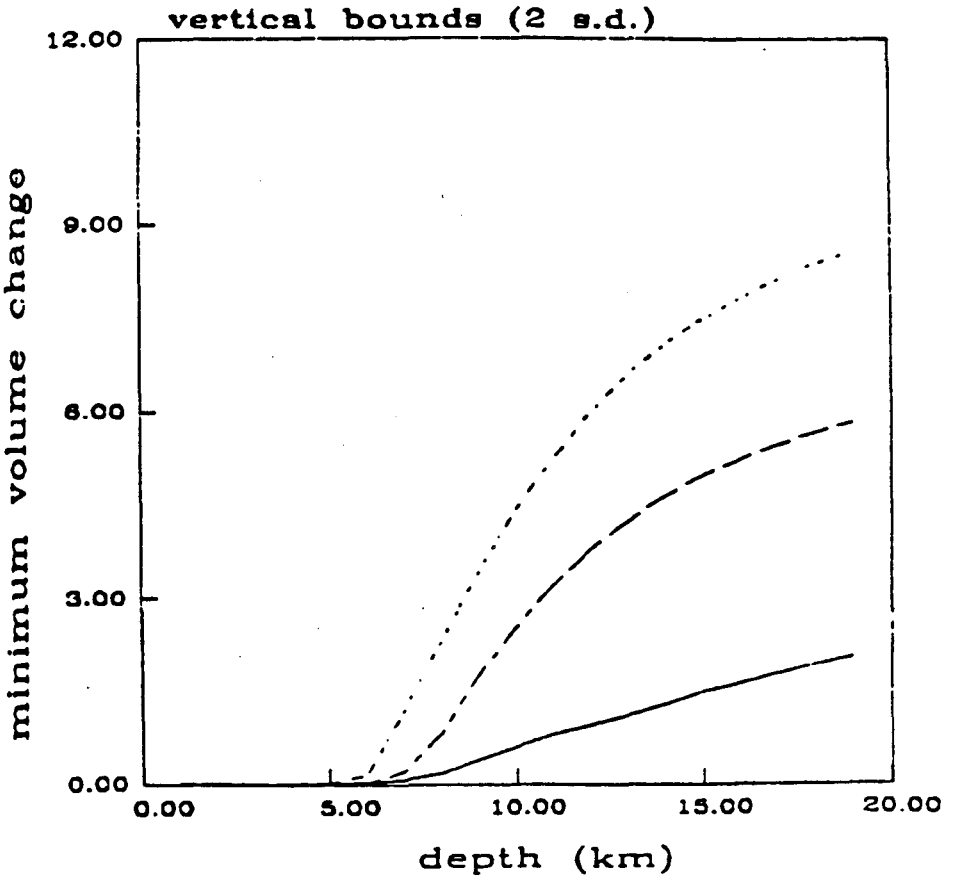

Figure 4.8 Vertical depth bounds derived from the leveling data in Figures 4.2 and 4.3 using error bounds of two standard errors. Shown here is the minimum volume change which must occur above the given depth. The bounds derived from the 1982 data are denoted by a solid line, the 1983 bounds are denoted by a dotted line while the 1985 bounds are denoted by a dashed line.

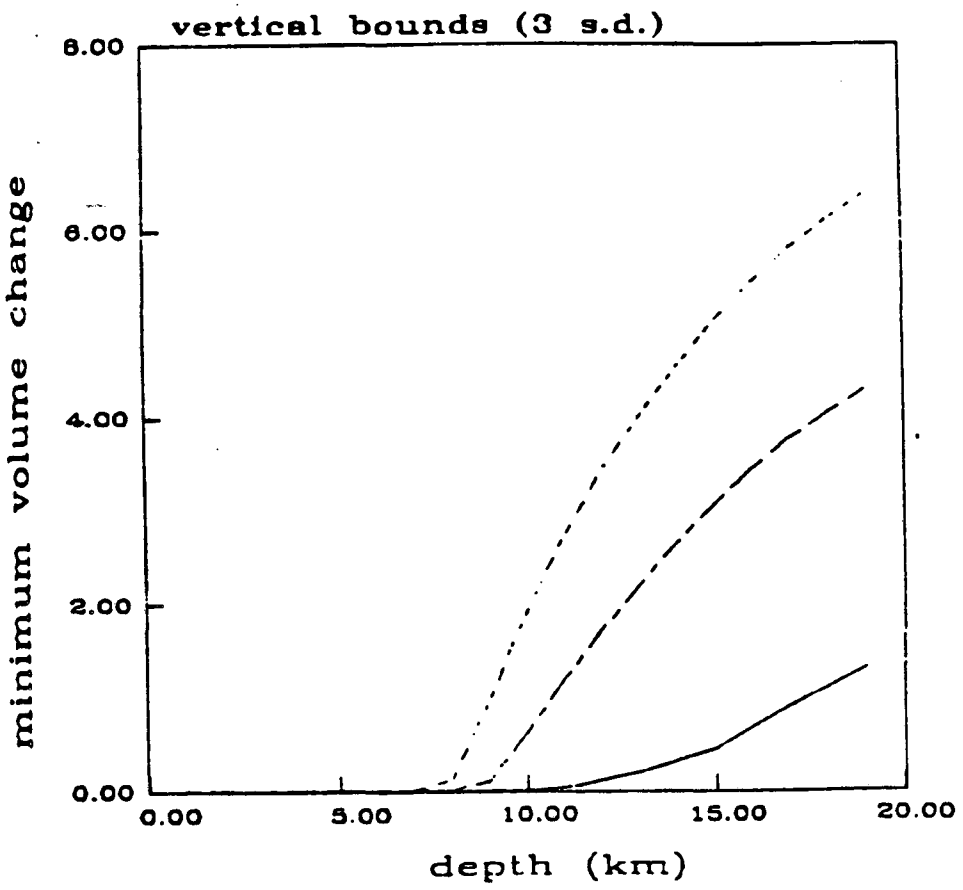

Figure 4.9 Vertical depth bounds derived from the leveling data in Figures 4.2 and 4.3 using error bounds of three standard errors. Shown here is the minimum volume change which must occur above the given depth. The bounds derived from the 1982 data are denoted by a solid line, the 1983 bounds are denoted by a dotted line while the 1985 bounds are denoted by a dashed line.

4.9, in order to satisfy the 1982 leveling data some volume change must have occurred above 11.0 km. For the 1983 survey the bound is 9.0 km. Finally, for 1985 vertical displacement, some magma intrusion must have occurred above 8.0 km.

The method of extremal inversion was also used to produce horizontal bounds on the body. This was done in the same way as for the vertical bounds. Again, three standard errors were used along with the calculated fault displacement to compute the ϵ_i in equation (4.2). A plane perpendicular to a specified direction defines a region U to the right or to the left of the plane. The minimum volume change in region U is sought and the plane is then shifted to a new position. The results are shown in Figures 4.10 and 4.11 for east-west and north-south directions respectively. Here, both right and left bounds are shown. In Figure 4.10 one can see that there has been essentially no change in the east-west or north-south bounds between August 1982 and August 1985.

A final property of the fractional volume change model which was derived was the upper bound on the changes occurring within any given cell or pixel. This was done by defining the region U in equation (4.3) to be a single pixel. The results are shown in Figures 4.12a through 4.12j. The region was discretized into ten layers, each two kilometers thick, consisting of 100 blocks of the same horizontal dimensions as before. The greatest fractional volume change that can occur in each pixel and still satisfy the data within three standard errors is shown in each pixel. It is seen that for the first 6.0 kilometers (layers 1, 2 and 3) the most highly constrained pixels lie under the two lines of stations. This is due to the fact that uplift from small shallow cells falls off sharply away from the cell. So the cells farthest away from any stations have the weakest constraints. The deeper the cell however, the broader the effect. Therefore, for cells below six kilometers the restrictions begin to tighten for cells far from any station. The most highly constrained pixels are those on the boundary of the model. These pixels are bounded by the stations far away from the region of possible volume change. Therefore, stations on the north-west and south-east corners of the region are constrained by the ends of line 1 which extend beyond the discretized region.

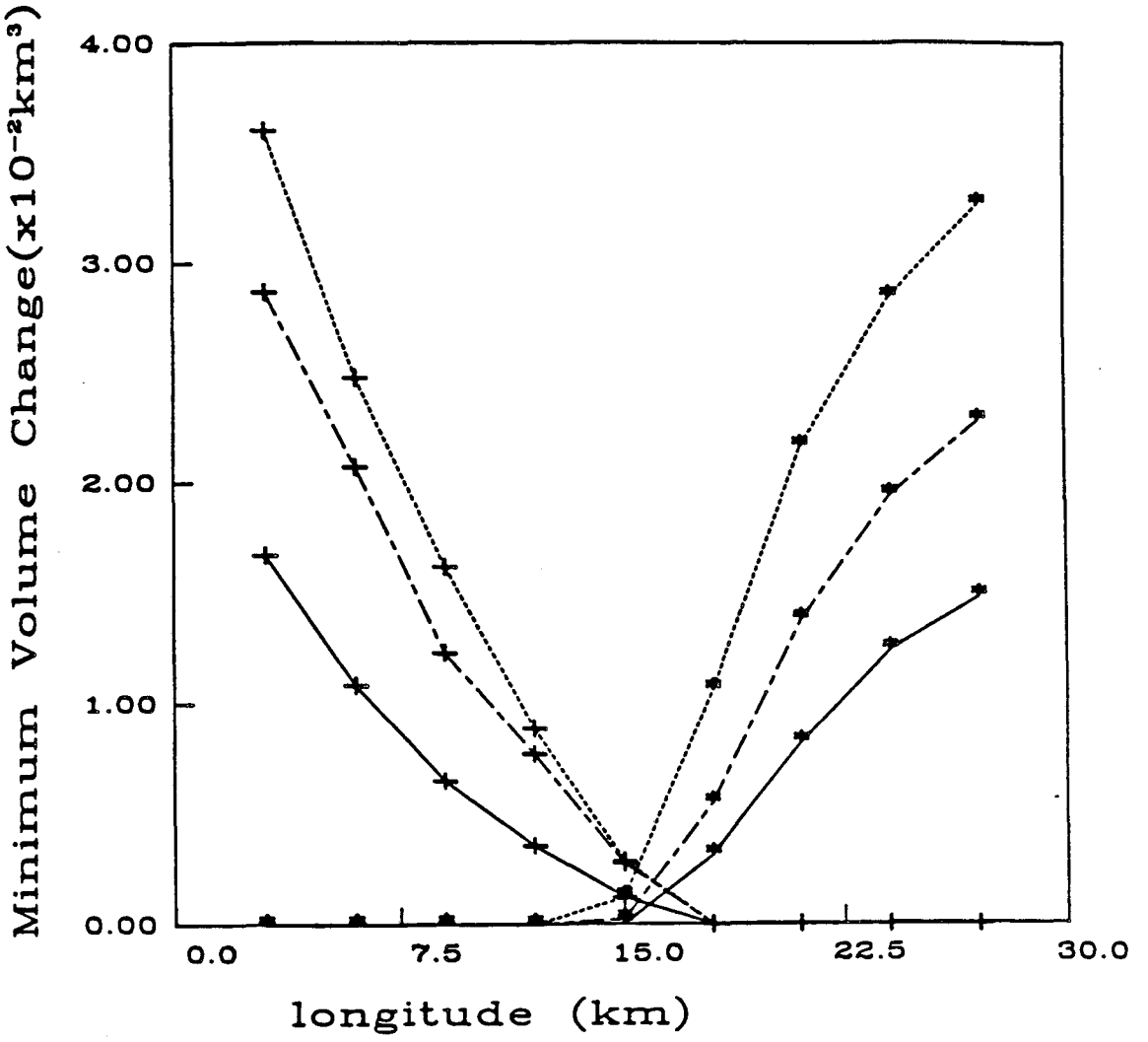

Figure 4.10 East-west (longitudinal) bounds derived from the leveling data for error bounds of three standard errors. This displays the minimum volume change which must occur to the east of the points * and to the west of the points +. The bounds on the 1982 data are indicated by solid lines while the 1983 bounds are given by dashed lines.

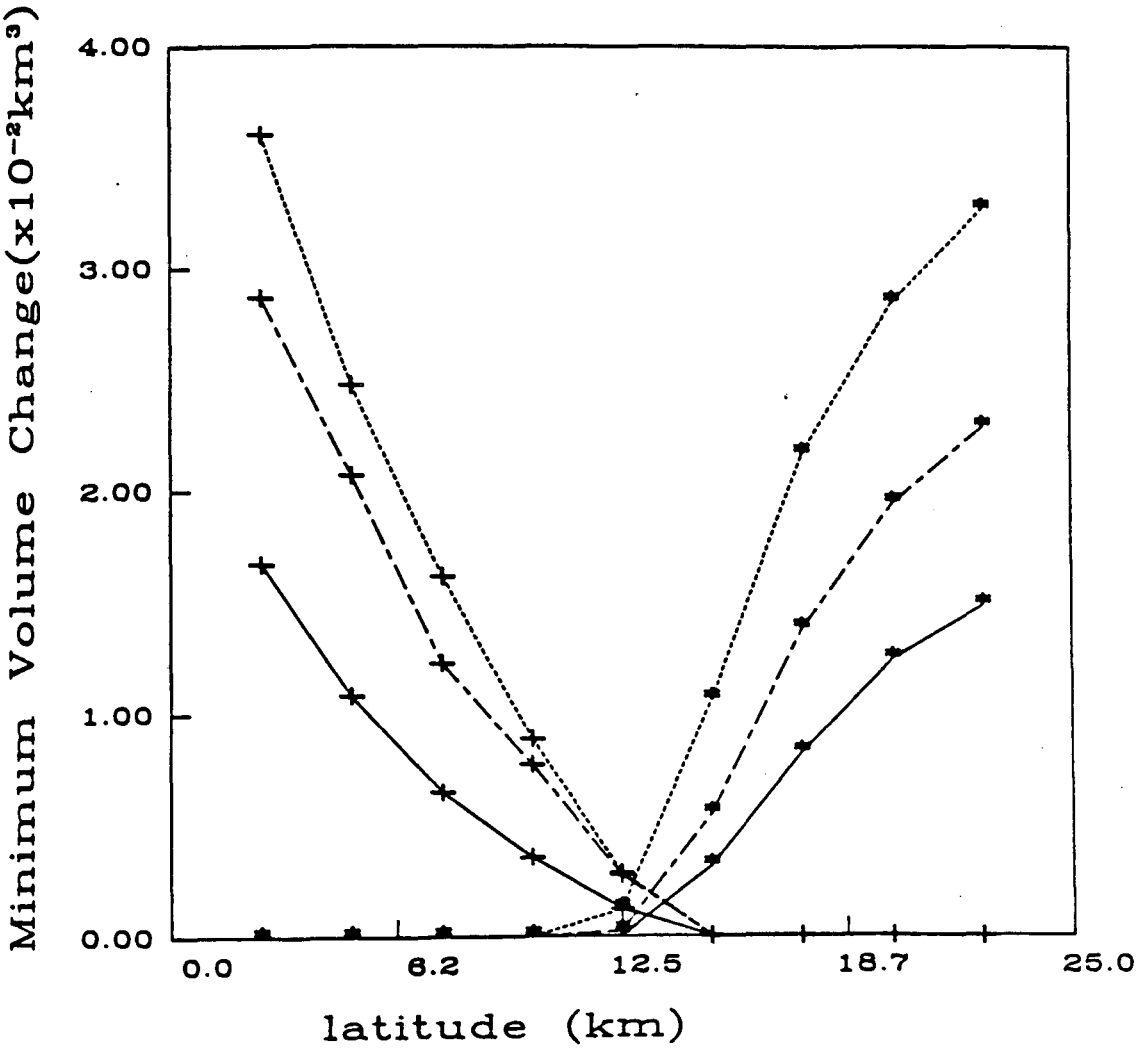

Figure 4.11 North-south bounds (latitudinal) derived from the leveling data for three standard error bounds on the data. This displays the minimum volume change which must occur to the north of the points * and to the south of the points +. The bounds on the 1982 data are indicated by solid lines while the 1983 bounds are given by dashed lines.

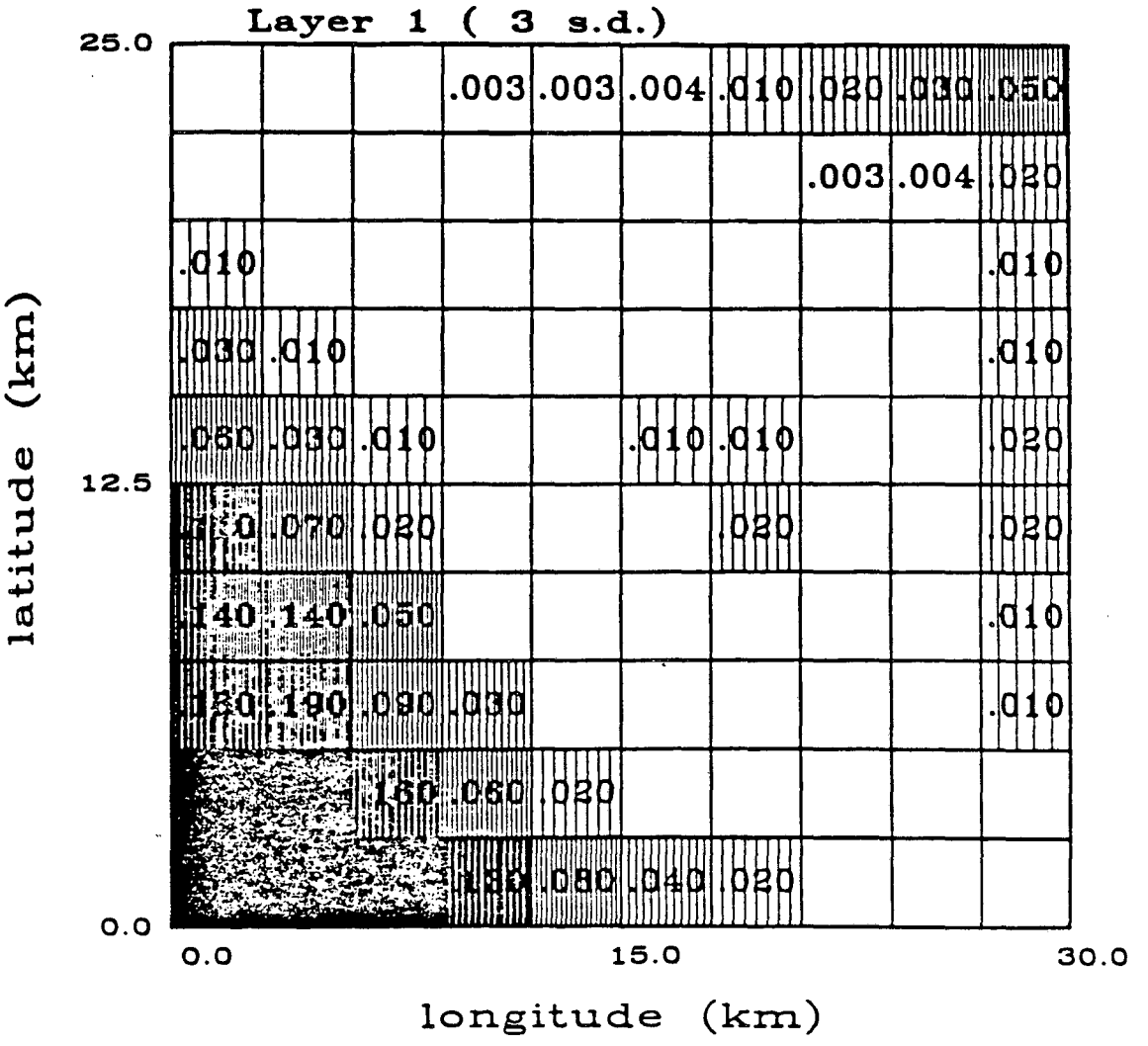

Figures 4.12a-4.12j Pixel upper bounds for each the ten layers which the region was divided. Three standard errors were incorporated into the computation of these upper bounds. Each layer is two kilometers thick.

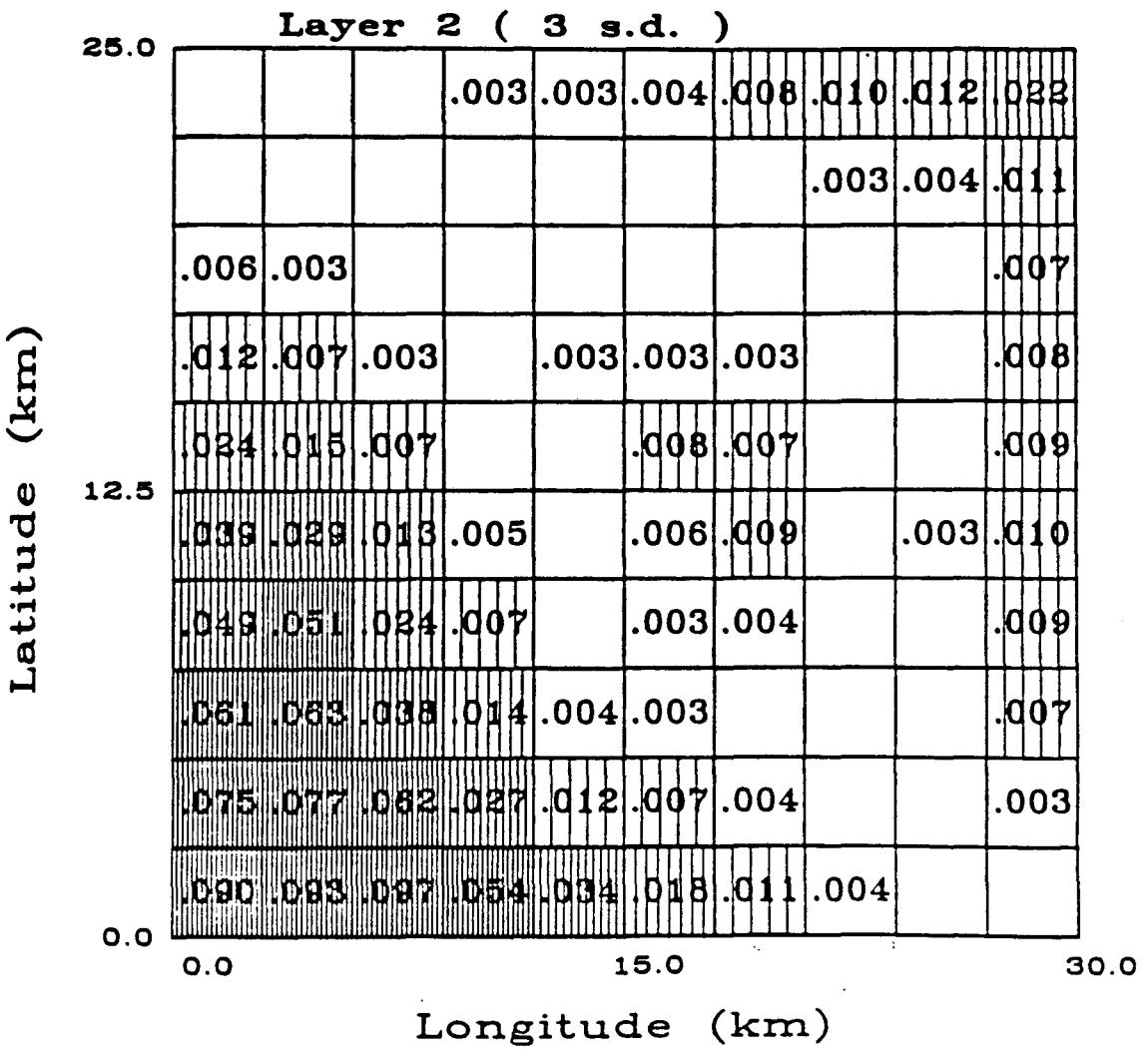
Layer 2 (3 s.d.)
25.0
12.5
0.0
Latitude (km)
.003 .003 .004 .008 .010 .012 .022
.003 .004 .011
.006 .003 .007
.012 .007 .003 .003 .003 .003 .008
.024 .015 .007 .008 .007 .009
.039 .029 .013 .005 .006 .009 .003 .010
.049 .051 .024 .007 .003 .004 .009
.061 .063 .038 .014 .004 .003 .007
.075 .077 .062 .027 .012 .007 .004 .003
.090 .093 .087 .054 .034 .018 .011 .004
0.0
15.0
30.0
Longitude (km)

Figure 4.12b

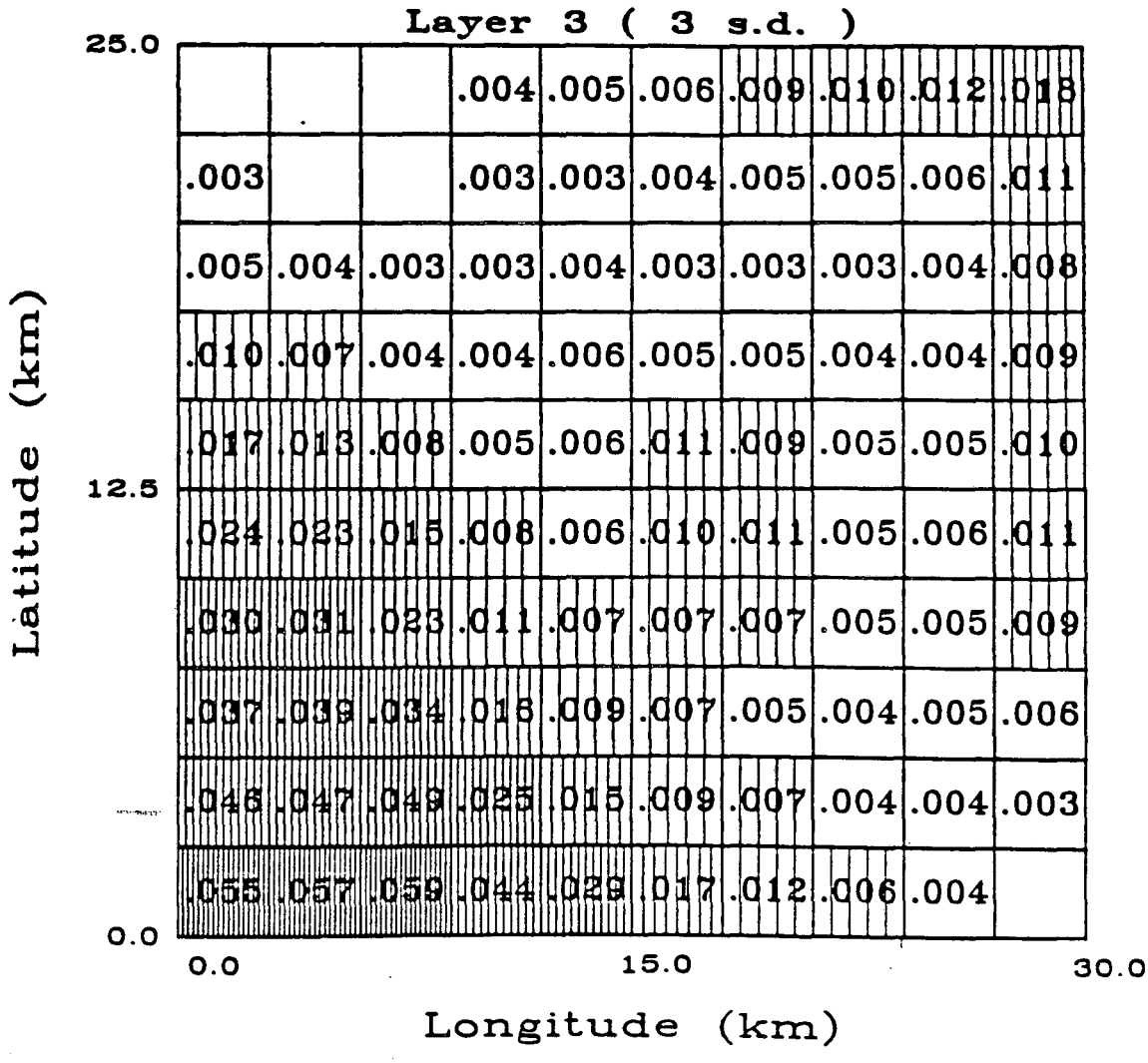
Layer 3 (3 s.d.)
25.0
12.5
0.0
Latitude (km)
.004 .005 .006 .009 .010 .012 .018
.003 .003 .003 .004 .005 .005 .006 .011
.005 .004 .003 .003 .004 .003 .003 .003 .004 .008
.010 .007 .004 .004 .006 .005 .005 .004 .004 .009
.017 .013 .008 .005 .006 .011 .009 .005 .005 .010
.024 .023 .015 .008 .006 .010 .011 .005 .006 .011
.030 .031 .023 .011 .007 .007 .007 .005 .005 .009
.037 .039 .034 .018 .009 .007 .005 .004 .005 .006
.046 .047 .049 .025 .015 .009 .007 .004 .004 .003
.055 .057 .059 .044 .029 .017 .012 .006 .004
0.0
15.0
30.0
Longitude (km)

Figure 4.12c

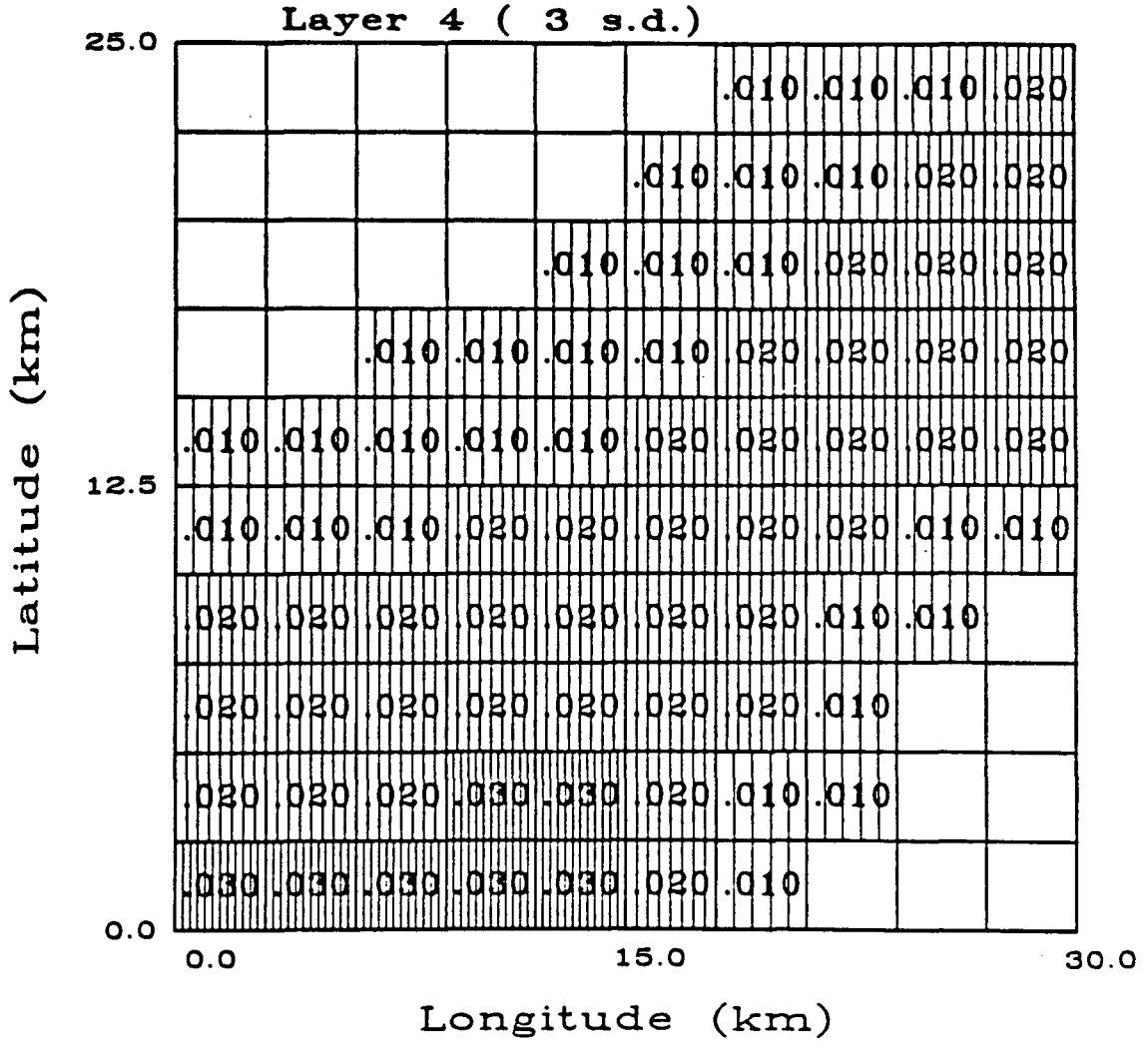
Layer 4 (3 s.d.)
25.0
12.5
0.0
Latitude (km)
.010 .010 .010 .020
.010 .010 .010 .020 .020
.010 .010 .010 .020 .020 .020
.010 .010 .010 .010 .020 .020 .020 .020
.010 .010 .010 .010 .010 .020 .020 .020 .020 .020
.010 .010 .010 .020 .020 .020 .020 .020 .010 .010
.020 .020 .020 .020 .020 .020 .020 .010 .010
.020 .020 .020 .020 .020 .020 .020 .010
.020 .020 .020 .030 .030 .020 .010 .010
.030 .030 .030 .030 .030 .020 .010
0.0
15.0
30.0
Longitude (km)

Figure 4.12d

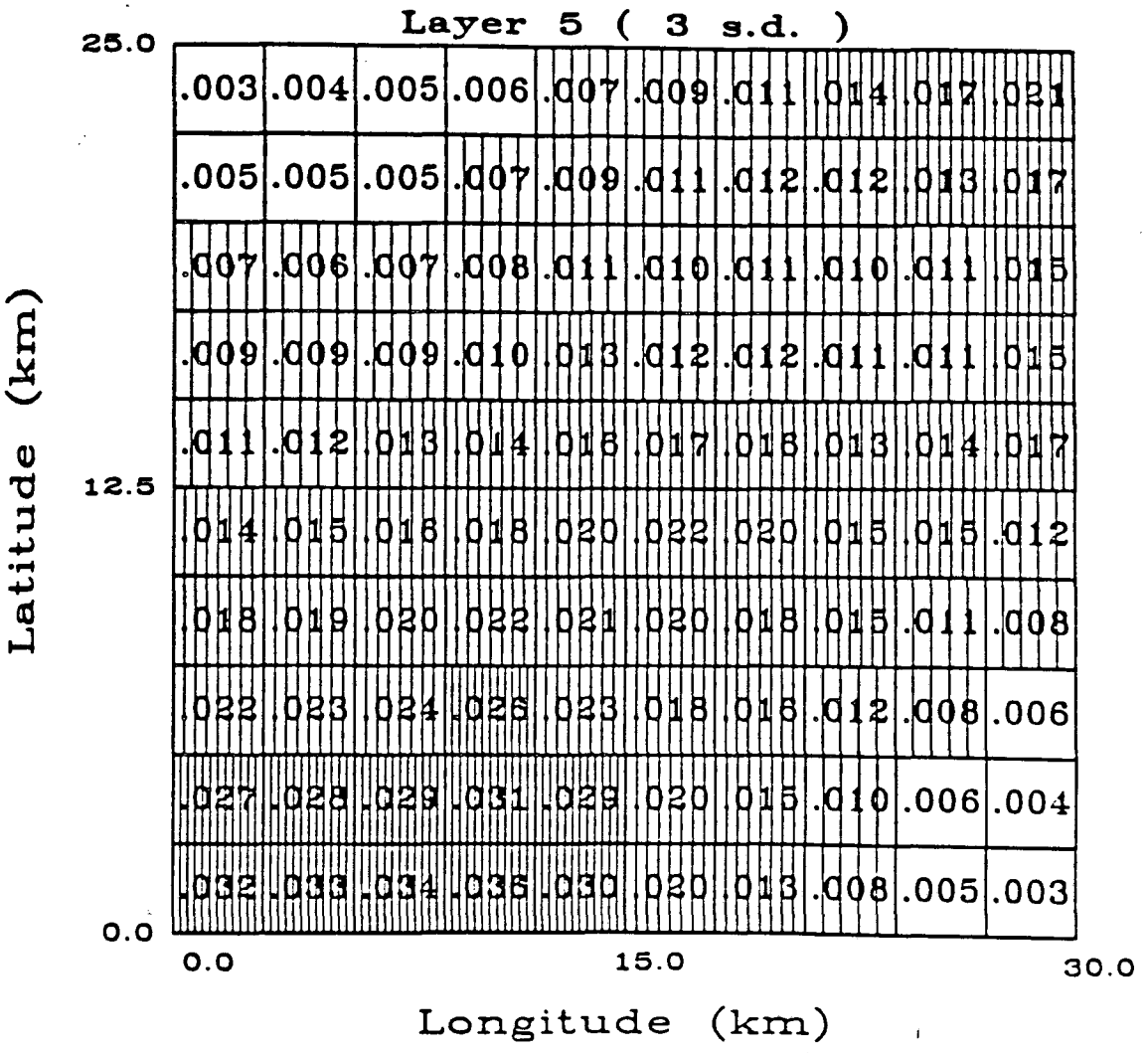
Layer 5 (3 s.d.)
25.0
12.5
0.0
.003 .004 .005 .006 .007 .009 .011 .014 .017 .021
.005 .005 .005 .007 .009 .011 .012 .012 .013 .017
.007 .006 .007 .008 .011 .010 .011 .010 .011 .015
.009 .009 .009 .010 .013 .012 .012 .011 .011 .015
.011 .012 .013 .014 .016 .017 .016 .013 .014 .017
.014 .015 .016 .018 .020 .022 .020 .015 .015 .012
.018 .019 .020 .022 .021 .020 .018 .015 .011 .008
.022 .023 .024 .026 .023 .018 .016 .012 .008 .006
.027 .028 .029 .031 .029 .020 .015 .010 .006 .004
.032 .033 .034 .036 .030 .020 .013 .008 .005 .003
0.0
15.0
30.0
Latitude (km)
Longitude (km)

Figure 4.12e

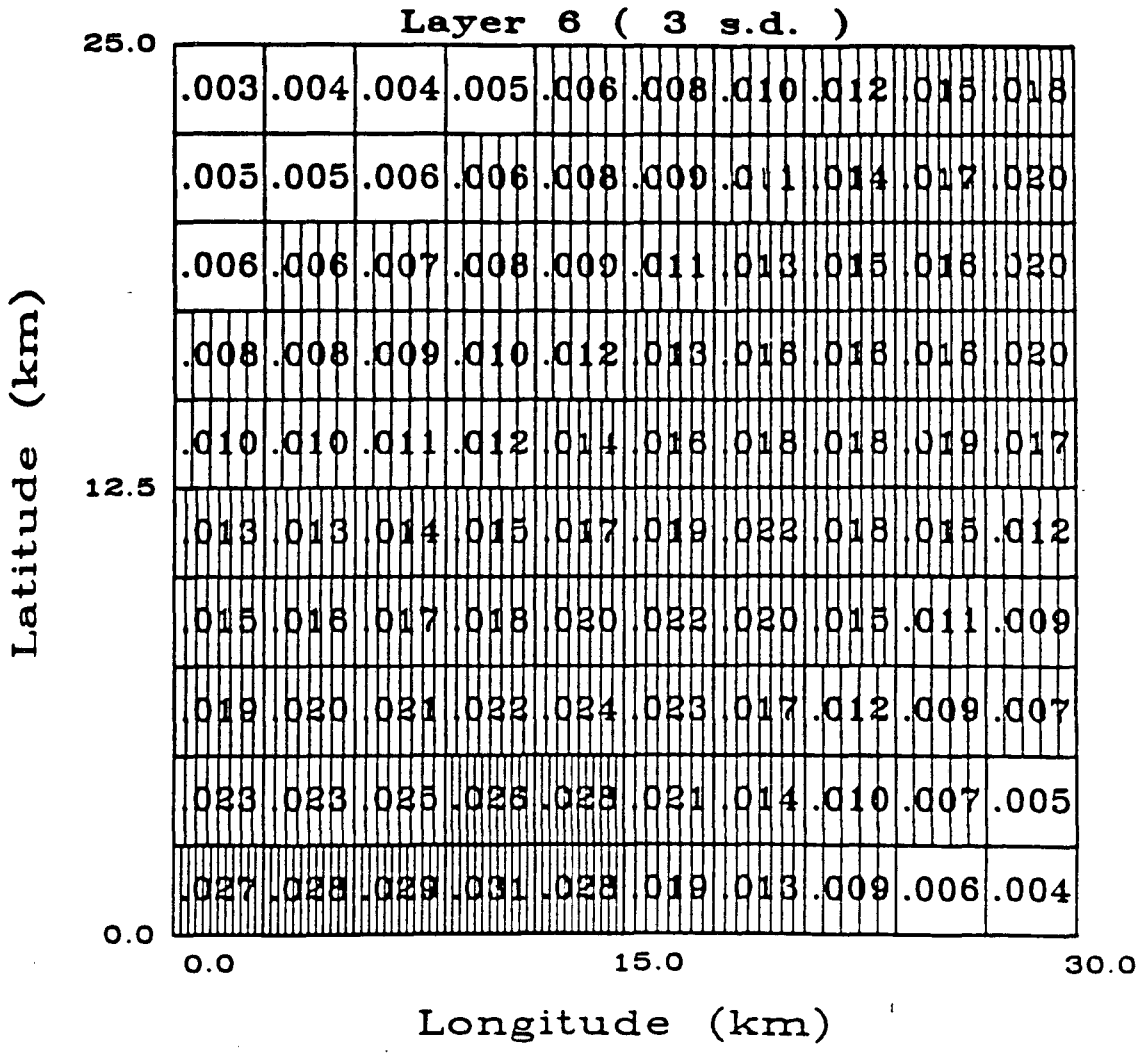
Layer 6 (3 s.d.)
25.0
12.5
0.0
.003 .004 .004 .005 .006 .008 .010 .012 .015 .018
.005 .005 .006 .006 .008 .009 .011 .014 .017 .020
.006 .006 .007 .008 .009 .011 .013 .015 .016 .020
.008 .008 .009 .010 .012 .013 .016 .016 .016 .020
.010 .010 .011 .012 .014 .016 .018 .018 .019 .017
.013 .013 .014 .015 .017 .019 .022 .018 .015 .012
.015 .016 .017 .018 .020 .022 .020 .015 .011 .009
.019 .020 .021 .022 .024 .023 .017 .012 .009 .007
.023 .023 .025 .026 .028 .021 .014 .010 .007 .005
.027 .028 .029 .031 .028 .019 .013 .009 .006 .004
0.0
15.0
30.0
Latitude (km)
Longitude (km)

Figure 4.12f

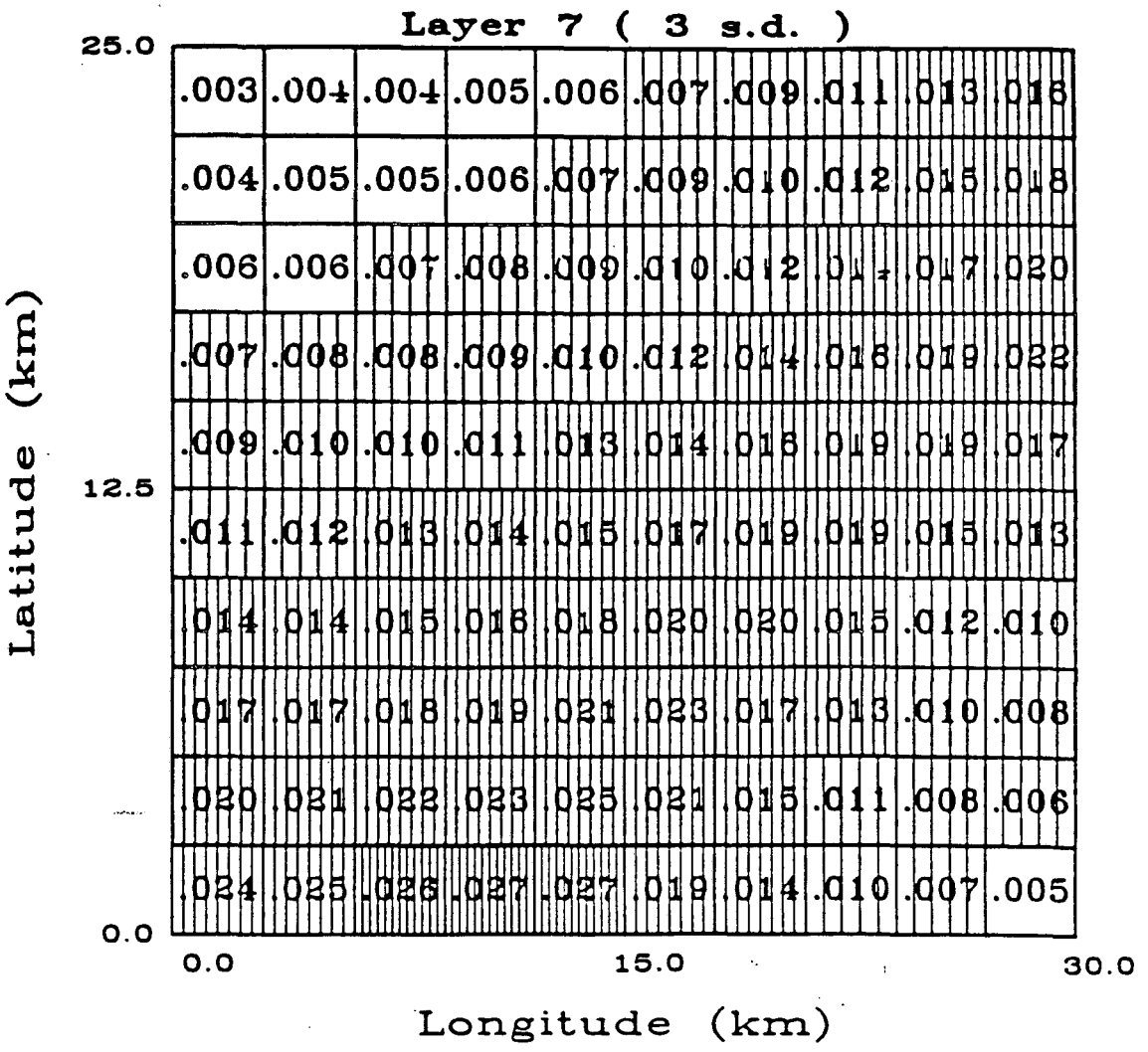
Layer 7 (3 s.d.)
25.0
12.5
0.0
Latitude (km)
.003 .004 .004 .005 .006 .007 .009 .011 .013 .016
.004 .005 .005 .006 .007 .009 .010 .012 .015 .018
.006 .006 .007 .008 .009 .010 .012 .014 .017 .020
.007 .008 .008 .009 .010 .012 .014 .016 .019 .022
.009 .010 .010 .011 .013 .014 .016 .018 .019 .017
.011 .012 .013 .014 .015 .017 .019 .019 .015 .013
.014 .014 .015 .016 .018 .020 .020 .015 .012 .010
.017 .017 .018 .019 .021 .023 .017 .013 .010 .008
.020 .021 .022 .023 .025 .021 .015 .011 .008 .006
.024 .025 .026 .027 .027 .019 .014 .010 .007 .005
0.0
15.0
30.0
Longitude (km)

Figure 4.12g

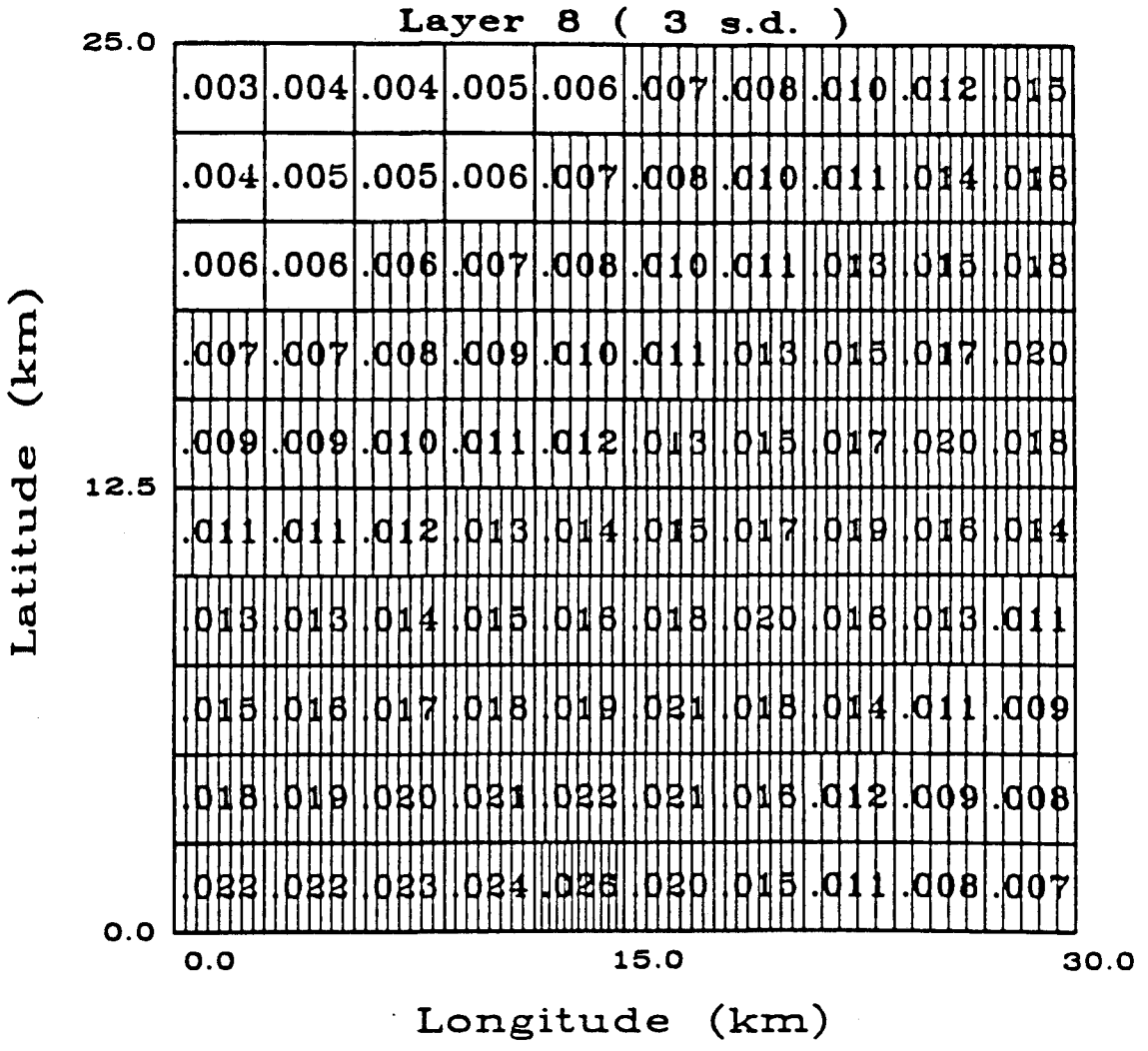
Layer 8 (3 s.d.)
25.0
12.5
0.0
.003 .004 .004 .005 .006 .007 .008 .010 .012 .015
.004 .005 .005 .006 .007 .008 .010 .011 .014 .016
.006 .006 .006 .007 .008 .010 .011 .013 .015 .018
.007 .007 .008 .009 .010 .011 .013 .015 .017 .020
.009 .009 .010 .011 .012 .013 .015 .017 .020 .018
.011 .011 .012 .013 .014 .015 .017 .019 .016 .014
.013 .013 .014 .015 .016 .018 .020 .016 .013 .011
.015 .016 .017 .018 .019 .021 .018 .014 .011 .009
.018 .019 .020 .021 .022 .021 .016 .012 .009 .008
.022 .022 .023 .024 .026 .020 .015 .011 .008 .007
0.0
15.0
30.0
Latitude (km)
Longitude (km)

Figure 4.12h

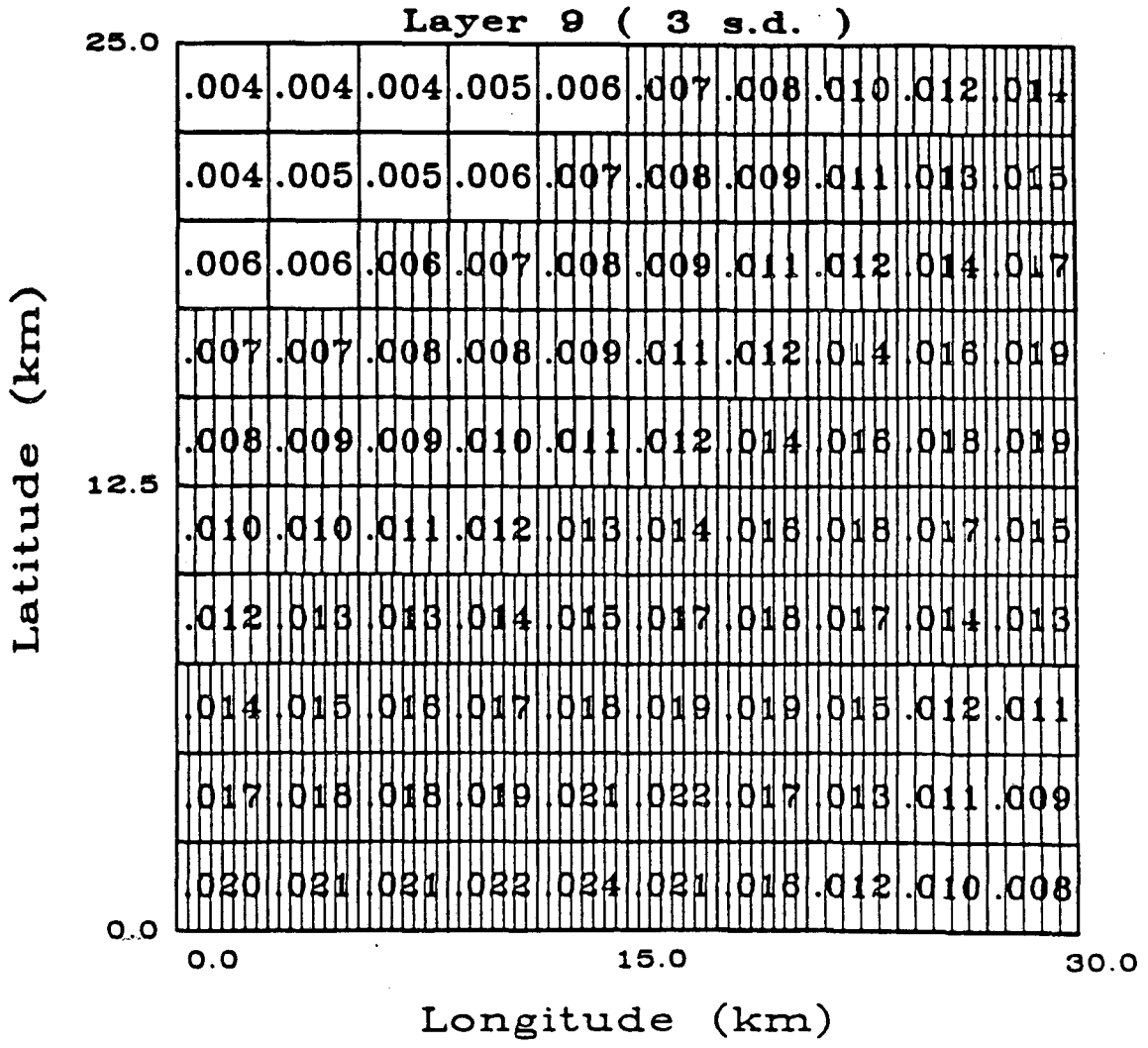
Layer 9 (3 s.d.)
25.0
12.5
0.0
.004 .004 .004 .005 .006 .007 .008 .010 .012 .014
.004 .005 .005 .006 .007 .008 .009 .011 .013 .015
.006 .006 .006 .007 .008 .009 .011 .012 .014 .017
.007 .007 .008 .008 .009 .011 .012 .014 .016 .019
.008 .009 .009 .010 .011 .012 .014 .016 .018 .019
.010 .010 .011 .012 .013 .014 .016 .018 .017 .015
.012 .013 .013 .014 .015 .017 .018 .017 .014 .013
.014 .015 .016 .017 .018 .019 .019 .015 .012 .011
.017 .018 .018 .019 .021 .022 .017 .013 .011 .009
.020 .021 .021 .022 .024 .021 .016 .012 .010 .008
0.0
15.0
30.0
Latitude (km)
Longitude (km)

Figure 4.12i

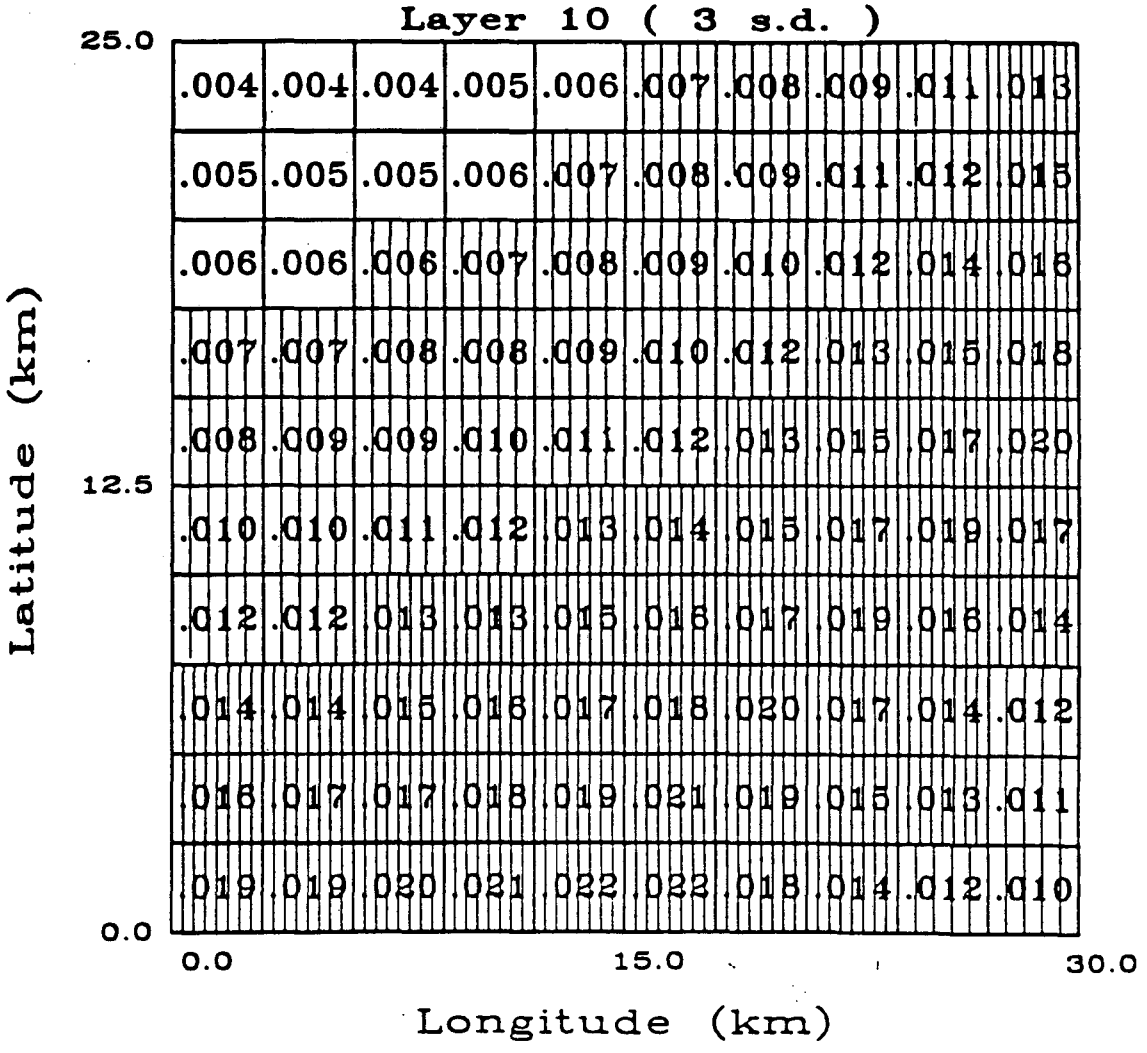
Layer 10 (3 s.d.)
25.0
12.5
0.0
.004 .004 .004 .005 .006 .007 .008 .009 .011 .013
.005 .005 .005 .006 .007 .008 .009 .011 .012 .015
.006 .006 .006 .007 .008 .009 .010 .012 .014 .016
.007 .007 .008 .008 .009 .010 .012 .013 .015 .018
.008 .009 .009 .010 .011 .012 .013 .015 .017 .020
.010 .010 .011 .012 .013 .014 .015 .017 .019 .017
.012 .012 .013 .013 .015 .016 .017 .019 .016 .014
.014 .014 .015 .016 .017 .018 .020 .017 .014 .012
.016 .017 .017 .018 .019 .021 .019 .015 .013 .011
.019 .019 .020 .021 .022 .022 .018 .014 .012 .010
Latitude (km)
0.0
15.0
30.0
Longitude (km)

Figure 4.12j

Discussion and Conclusions

Extremal inversion techniques were able to produce depth bounds on a proposed magma body within Long Valley Caldera. The August 1982 leveling data require a volume change above a depth of 11.0 km. The August 1983 data require volume change above a depth of 9.0 km, while the 1985 data require some volume change above 8.0 km. The horizontal bounds are for the most part unchanged, the only difference is the northward extension of the north-south bounds by one grid element. The significance of these results lies in what they indicate about the range of models that may fit the vertical leveling data. The sole conclusion one may make about the depth to the top of any supposed magma chamber is that it must be less than or equal to 11.0 km in 1982, less than or equal to 9.0 km in 1983 and less than or equal to 8.0 km in 1985. As for the horizontal bounds (Figures 4.10 and 4.11), for the discretization given it is not possible to constrain the width of the source body. So the geometrical constraints on possible models satisfying the data have been clearly laid out. It should be noted that these are necessary and not sufficient constraints: any model satisfying the data must include some volume change in the region described above but a model with volume change in the region does not necessarily satisfy the data. Finally, the bounds derived are not merely the properties of a point source in the given model space (discretization). This is because it is the requirement that the models fit the data within three standard deviations which determines the bounds.

A number of models have been proposed to explain the vertical and horizontal deformation (Rundle and Whitcomb 1984, Savage and Cockerham 1984, Castle et al. 1984). Though the models do differ in detail they seem to share some common properties. All models require inflation of a magma reservoir beneath the resurgent dome to fit the vertical displacement data. It is interesting to compare the above models with the bounds placed on the range of possible models by the method of extremal inversion. First consider the point source model of Castle et al. (1984). For the 1975-1983 vertical deformation data their model lies within the specified extremal bounds. Similarly Savage and Cockerham's (1984) models of dipping dike intrusions satisfy the horizontal bounds. Finally consider the model of Rundle and Whitcomb (1984) which

involves the inflation of two spherical magma chambers, one at a depth of 5 km located 1.5 km west of leveling station Casa, the other 9 km deep about 5.5 km north-northwest of Casa. Their two magma chambers taken separately do not satisfy the horizontal bounds derived above. However, because the body is not a single body it is not required to lie in the intersection of the horizontal bounds. Non-convex or multiply connected bodies can satisfy the bounds without having volume change occur within the intersection. The depths to the model of Rundle and Whitcomb of 5 and 9 km also satisfy the restriction that some or all of the magma intrusion occur at or above 11 km in the 1975-1982 interval and at or above 9 km in the 1975-1983 interval. However, the models of Castle et al. (1984) and Savage and Cockerham (1984) do not satisfy the depth bounds derived. This may be due to the differing treatment of errors and the differing criteria of fit used. As has been said, the use of rigid bounds may be more restrictive than least squares criteria for fit. It is felt that the use of three standard errors in the derivation of the bounds is sufficient to account for any outlying data points. The presence of model errors is difficult to evaluate however. It would be interesting to use the method of Oldenburg (1983) to derive a model fitting the data with the smallest l^1 norm as discussed in chapter 3.

The importance of the extremal bounds is not in judging proposed models. The importance lies in what the method states about the limits of the vertical displacement data in determining the location and shape of a model. The best one can say with the given data set, for the chosen parameters, is that volume change must have occurred somewhere in the rectangle defined by the latitude, longitude, and depth bounds if the body is assumed to be a single convex body. If multiple or non-convex bodies are allowed then one can merely say that the bodies must be distributed such that all of the individual bounds are satisfied.

In addition to the vertical and horizontal displacement data the models are constrained by gravitational and magnetic field changes, teleseismic P wave residuals (Steeples and Iyer 1976), and S wave attenuation data (Sanders 1984). One might hope that comparisons could be made among the various data sets. Extremal inversion can provide one model independent way to accomplish this. Extremal inversion techniques have been developed for gravity and magnetic

(Safon et al. 1977), temperature (Huestis 1979) and electro-magnetic induction (Weidelt 1981) problems as well as for static displacements. The bounds derived from each of the above data sets can be compared. The data set which most tightly constrains some model property such as the depth to the top of the magma body can be determined. So the effectiveness of each data set in constraining the range of possible models becomes clear. This allows a more realistic assessment of the constraints on the body giving rise to the data sets.

It must be pointed out that the analysis was somewhat simplified. It was assumed that all fractional volume changes were positive. This excludes local deflation and assumes that the source of the material causing the expansion was sufficiently removed from the stations. Also, the interpretation of the bounds depends on assumptions of the form of the body i.e. if it is convex or non-convex. A Poisson's ratio of .25 was assumed for the whole caldera. But, as can be shown, Poisson's ratio does not effect the depth estimate itself, though it does effect the minimum volume change estimates. Also, although it passed nearby, the survey did not traverse the region of maximum uplift. Hence the depth bounds are slightly deeper than necessary but are still valid and unique for the given data set. A homogeneous halfspace was assumed in the calculations. Jovanovich et al. (1974) noted the effects of layering upon displacements. He also presented integral relationships between displacement and volume change which would allow one to invert the leveling data while accounting for overlying structure. Layers of high rigidity, such as thick lava flows, tend to reduce and broaden surface flexure resulting in an overly cautious depth bound and a greater minimum width estimate. Finally, the volume change was assumed to have taken place in a specified region. That region was then discretized. By changing the boundaries of the volume considered, it was found that the extremal bounds are insensitive to the exact extent of the region. For example, vertical bounds were calculated for regions with total depth extents of 15, 20 and 25 km. The minimum volume changes at depth were identical for each of the regions. In order to estimate the depth or width bounds correctly it is only necessary for the region considered to encompass the boundary between the area of zero volume change and the area of nonzero volume change. However, the exact location of the bounds depends on the

discretization, finer divisions of the region will give better bounds. One is only limited by computational expense in deciding on a discretization. Given these caveats, I believe that this is a robust technique which has produced meaningful bounds on the source volume in Long Valley Caldera.

Chapter 5

Assessment of non-uniqueness for non-linear problems: The homotopy method

Introduction

For linear inverse problems the question of uniqueness has been extensively investigated. Unfortunately, for non-linear inverse problems other solutions are possible solely due to the nature of the problem. This chapter examines an alternative approach to linearizing the problem. A technique is described which solves the full non-linear optimization problem as given in equations (1.3) and (1.4). The method is essentially a local search method which does not simply find one solution and then stop. Once a solution has been computed the method searches for additional solutions.

The homotopy approach can be used to determine fault parameters in an iterative manner as an extension of methods described in Jovanovich (1975) and Matsu'ura (1977). Another use, one examined in this chapter, is to use the method to find a polyhedral body undergoing volume expansion which fits a set of vertical displacement observations. A method to rapidly compute vertical uplift due to an expanding polyhedron is derived. It is based on a well known method for the gravitational problem (Talwani et al. 1959).

The Homotopy method

The underlying concept behind the homotopy method for solving non-linear equations is simple. Consider a problem which is to be solved, write it in the form $\mathbf{F(x)=0}$. Consider a simpler related system written in the same form $\mathbf{E(x)=0}$. The homotopy technique embeds the problem in a space of one higher dimension which may be characterized by a parameter t . A

new function $\mathbf{H}(\mathbf{x},t)$ is formed in this higher dimensional space such that when the parameter $t=0$ the simple problem is obtained and when $t=1$ the original problem of interest is obtained. The idea then is to deform the problem from the solved to the unsolved by varying t and at the same time deforming the solution to that of the original problem. Thus a path parameterized by t is followed from the known solution to the unknown solution.

Stated more precisely, consider a mapping between n dimensional Euclidean spaces R^n i.e. $\mathbf{F}:R^n \rightarrow R^n$

$$\mathbf{F}(\mathbf{x}) = (F_1(\mathbf{x}), \cdots, F_n(\mathbf{x})) \qquad \mathbf{x} = (x_1, \cdots, x_n).$$

The object is to solve the $n \times n$ system of nonlinear equations

$$\mathbf{F}(\mathbf{x}) = 0 \tag{5.1}$$

in detail, solving

$$F_1(x_1, \cdots, x_n)=0$$

$$F_2(x_1, \cdots, x_n)=0$$

$$\cdots$$

$$F_n(x_1, \cdots, x_n)=0$$

for a solution $\mathbf{x}^*=(x_1^*, \cdots, x_n^*)$. To obtain $\mathbf{x}^*$ set up a system of solvable equations

$$E_1(x_1, \cdots, x_n)=0$$

$$E_2(x_1, \cdots, x_n)=0$$

$$\cdots$$

$$E_n(x_1, \cdots, x_n)=0$$

with solution $\mathbf{x}^0$. The above system of equations may be written

$$\mathbf{E}(\mathbf{x}) = 0. \tag{5.2}$$

Now define a **homotopy function** $\mathbf{H}(\mathbf{x},t)$ which is a mapping from R^{n+1} to R^n, where $\mathbf{x}$ are

the original variables and t is an additional parameter. The homotopy function is constructed so that

$$\mathbf{H(x,0) = E(x)}$$

$$\mathbf{H(x,1) = F(x)}$$

Therefore $\mathbf{H(x,0)=0}$ has the solution $\mathbf{x}^0$ and $\mathbf{H(x,1)=0}$ is satisfied at $\mathbf{x=x}^*$. In general, for arbitrary t , $\mathbf{x}(t)$ solves

$$\mathbf{H(x}(t),t) = 0 \tag{5.3}$$

In summary the idea is to begin at $t=0, \mathbf{x}(0)=\mathbf{x}^0$ and increase t , thereby generating a path $\mathbf{x}(t)$ to $\mathbf{x}(1)=\mathbf{x}^*$ when $t=1$, the solution to the original system.

Consider now some specific forms for $\mathbf{H(x}(t),t)$, in particular, consider three common homotopies. The first follows from the work of Isaac Newton and hence the label Newtons method. It is of the form

$$\mathbf{H(x}(t),t) = \mathbf{F(x)} - (1-t)\mathbf{F(x}^0) \tag{5.4}$$

For $t=0$

$$\mathbf{H(x,0) = F(x)} - \mathbf{F(x}_0) = \mathbf{E(x)}$$

This vanishes when $\mathbf{x=x}^0$. Because $\mathbf{x}^0$ may be arbitrarily chosen this homotopy allows the path to begin at any point. Another homotopy, the fixed point homotopy, also allows the path to begin arbitrarily. The form of the homotopy is given by

$$\mathbf{H(x},t) = (1-t)(\mathbf{x}-\mathbf{x}^0) + t\,\mathbf{F(x)} \tag{5.5}$$

The third approach, the linear homotopy, has the other two methods as special cases. The homotopy function is given by a linear combination of the two functions $\mathbf{E(x)}$ and $\mathbf{F(x)}$,

$$\mathbf{H(x},t) = (1-t)\mathbf{E(x)} + t\,\mathbf{F(x)} \tag{5.6}$$

The homotopy differential equation

It will be shown how a system of differential equations can be solved to yield a path $\mathbf{x}(t)$ from $\mathbf{x}(0)$ to $\mathbf{x}^*$. Before continuing it will be convenient to define the matrix of partial derivatives of the homotopy matrix, an $n+1 \times n+1$ matrix denoted by $\mathbf{H}'$. Furthermore, let $\mathbf{H}'_{\mathbf{x}}$ be the matrix formed by deleting the column of $\mathbf{H}'$ containing the partial derivatives of $\mathbf{H}$ with respect to t. Similarly, let $\mathbf{H}'_{t}$ be the column of $\mathbf{H}'$ containing only the partial derivatives of $\mathbf{H}$ with respect to t, $\frac{\partial \mathbf{H}}{\partial t}$.

To derive the system, the homotopy differential equations, consider the homotopy function again depending on $(\mathbf{x},t)$,

$$\mathbf{H}(\mathbf{x}(t),t) = 0$$

The homotopy differential equation is obtained by differentiating this with respect to t,

$$\mathbf{H}'_{\mathbf{x}} \frac{d\,\mathbf{x}}{dt} + \mathbf{H}'_{t} = 0 \tag{5.7}$$

If $\mathbf{H}'_{\mathbf{x}}$ is non-singular this may be written

$$\frac{d\,\mathbf{x}}{dt} = -[\mathbf{H}'_{\mathbf{x}}]^{-1}\mathbf{H}'_{t} \tag{5.8}$$

Solving this will give the path $\mathbf{x}(t)$. Uniqueness and existence of the path follow from the theory of differential equations and the non-singularity of $\mathbf{H}'_{\mathbf{x}}$. It is apparent that this system of equations is not valid at points in which $\mathbf{H}'_{\mathbf{x}}$ is not of full rank. Fortunately this problem is alleviated through a change of variables at such points.

Newtons solution and the Newton homotopy

Consider now the specific homotopy, the Newton homotopy (5.4),

$$\mathbf{H}(\mathbf{x},t) = \mathbf{F}(\mathbf{x}) - (1-t)\mathbf{F}(\mathbf{x}^0)$$

For this homotopy

$$\mathbf{H}'_{\mathbf{x}} = \mathbf{F}'(\mathbf{x})$$

and

$$\mathbf{H'}_{t} = \mathbf{F}(\mathbf{x}^0)$$

So the homotopy differential equation becomes

$$\frac{d\,\mathbf{x}}{dt} = -\mathbf{F'}\ (\mathbf{x})^{-1}\mathbf{F}(\mathbf{x}^0). \tag{5.9}$$

This equation was introduced in numerical analysis by Broyden (1969) as a method for solving nonlinear optimization problems. In this case $\mathbf{F}(\mathbf{x})$ represents the gradient of a scalar function to be optimized. Hence (5.9) represents a method of nonlinear optimization.

One problem with the practical use of equation (5.9) is that numerical methods for solving this equation such as Euler's method will, after a number of iterations, drift off the path $\mathbf{H}(\mathbf{x}(t),t)=0$. There is a technique which remedies this, not by eliminating the drift but by restarting the method at the point to which it has drifted. Specifically it does not follow a path to the solution, it follows one path for a number of iterations, and then generates a new path which is followed toward the solution. This periodic rejuvination has come to be known as the restart method. As an example consider a point arrived at after a number of iterations $\mathbf{y}^k=(\mathbf{x}^k,t^k)$. A restart homotopy can be defined

$$\overline{\mathbf{H}}(\mathbf{y},\mathbf{y}^k) = \mathbf{H}(\mathbf{y}) - \frac{(1-t)\mathbf{H}(\mathbf{y}^k)}{1-t^k} \tag{5.10}$$

At $t=1$

$$\overline{\mathbf{H}}((\mathbf{x},1);\mathbf{y}^k) = \mathbf{H}(\mathbf{x},1)$$

At $t=t^k$

$$\overline{\mathbf{H}}(\mathbf{y}^k;\mathbf{y}^k) = 0$$

The restart homotopy creates a new path which leads from $\mathbf{y}=\mathbf{y}^k$ to $\mathbf{x}(1)=(x^*)$. It may be noted that at $t^k=1$ the method breaks down. One approach is to set $t^k=0$ when this occurs. Equation (5.10) becomes

$$\overline{\mathbf{H}}(\mathbf{y};\mathbf{y}^k) = \mathbf{H}(\mathbf{y}) - (1-t)\mathbf{H}(\mathbf{x}^k,0) \tag{5.11}$$

And so a new path may be followed from $(\mathbf{x}^k,0)$ to $(\mathbf{x}^*,1)$. Note that this restart homotopy can be used for any value of $0 \leq t^k \leq 1$, it is not necessary for $t^k = 1$. Consider now the restart method applied to Newton's homotopy. In this case formula (5.11) will be used at each iteration. For the Newton homotopy this becomes

$$\overline{\mathbf{H}}(\mathbf{y};\mathbf{y}^1) = \mathbf{F}(\mathbf{x})-(1-t)\mathbf{F}(\mathbf{x}^0)-(1-t)(\mathbf{F}(\mathbf{x}^1)-\mathbf{F}(\mathbf{x}^0)) \tag{5.12}$$

$$= \mathbf{F}(\mathbf{x}) - (1-t)\mathbf{F}(\mathbf{x}^1)$$

where $\mathbf{x}^1$ is the point arrived at after one iteration. The homotopy differential equation associated with this homotopy is

$$\frac{d\,\mathbf{x}}{dt} = -\mathbf{F}'\,(\mathbf{x})^{-1}\mathbf{F}(\mathbf{x}^1). \tag{5.13}$$

If at each step the homotopy is restarted (5.13) becomes

$$\frac{d\,\mathbf{x}}{dt} = -\mathbf{F}'\,(\mathbf{x})^{-1}\mathbf{F}(\mathbf{x}). \tag{5.14}$$

This differential equation was presented as a method of global nonlinear optimization by Branin (1972).

Multiple solutions in nonlinear optimization problems

Branin (1972) began with the differential equation

$$\frac{d\,\mathbf{F}(\mathbf{x})}{dt} + \mathbf{F}(\mathbf{x}) = 0 \tag{5.15}$$

where $\mathbf{F}(\mathbf{x})$ is the gradient of a scalar function of say n variables. Using the chain rule for the derivative of $\mathbf{F}(\mathbf{x})$ with respect to t

$$\frac{d\,\mathbf{F}(\mathbf{x})}{dt} = \frac{\partial \mathbf{F}(\mathbf{x})}{\partial \mathbf{x}}\,\frac{d\,\mathbf{x}}{dt}$$

Equation (5.15) becomes

$$\frac{d\,\mathbf{x}}{dt} = -\,\mathbf{F}'\,(\mathbf{x})^{-1}\mathbf{F}(\mathbf{x}) \tag{5.16}$$

What has been obtained then is a means of generating a path from a starting point to an extremum. However, it is not necessary to end the path at the extremum found. It is possible to project through the point to search for another extremum. In detail, having found an extreme point, say $\mathbf{x}^*_1$, the path is projected through $\mathbf{x}^*_1$ in the direction of the tangent vector to the path $\mathbf{F}$. That is, the path is continued from $\mathbf{x}^*_1$ to $\mathbf{x}_p = \mathbf{x}^*_1 + \alpha\mathbf{F}$ where α is some positive constant modifying the step size of the projection. Having projected through the extremum the use of equation (5.14) would lead back to $\mathbf{x}^*_1$. This is because, for α such that $\mathbf{x}_p$ is in a small enough neighborhood of $\mathbf{x}^*_1$, $\mathbf{x}^*_1$ will be the extremum throughout the region. For example, in trying to find the minimum of a scalar function $\omega(\mathbf{x})$ say that the path has lead to a local minimum $\mathbf{x}^*_1$. Then for any small perturbation $\Delta\mathbf{x}$ about $\mathbf{x}^*_1$

$$\omega(\mathbf{x}^*_1) < \omega(\mathbf{x}^*_1+\Delta\mathbf{x}).$$

Therefore from any projected point $\mathbf{x}_p$ the path will lead back to $\mathbf{x}^*_1$. The remedy for this problem is to create a path which repels from $\mathbf{x}^*_1$ to a new stationary point. This is done by changing the sign of the right hand side of (5.25), the velocity vector. Then the path is repelled from $\mathbf{x}^*_1$ until a new stationary point $\mathbf{x}^*_2$ is encountered or the boundary of the region is reached. Note that the new extremum will be of the opposite sense i.e. if $\mathbf{x}^*_1$ is a minimum then $\mathbf{x}^*_2$ is a maximum and vice-versa. The process is repeated from $\mathbf{x}^*_2$ until one is satisfied that most extrema have been found. Hence a modified form of equation (5.16),

$$\frac{d\,\mathbf{x}}{dt} = (-1)^k \; \mathbf{F}'^{\,-1}\mathbf{F} \tag{5.17}$$

where $k = 1,2,\ldots,n$ denotes the number of stationary points encountered, can be used to find multiple stationary points.

Problems may occur when points are encountered at which the determinant of the Hessian matrix $\mathbf{F}'(\mathbf{x})$ changes sign. Using Cramers rule to expand $\mathbf{F}'^{\,-1}$ equation (5.17) may be written

$$\frac{d\,\mathbf{x}}{dt} = (-1)^k \; \frac{adj\,\mathbf{F}'}{\det\mathbf{F}'}\mathbf{F} \tag{5.18}$$

An obvious problem occurs when $\det\mathbf{F}'(\mathbf{x})$ changes sign. Hardy (1975) suggests projecting the

path through such points with an accompanying sign change. Including this in equation (5.18) results in

$$\frac{d\,\mathbf{x}}{dt} = (-1)^k \, sgn\,[\det \mathbf{F}'\,(\mathbf{x})]\mathbf{F}'^{\,-1}\mathbf{F} \tag{5.19}$$

The strategy associated with (5.19) is thus: Begin with $k=1$ and generate a path to the first stationary point. Once the point has been approximated project the path vector $\mathbf{x}$ through the stationary point and change the sign of the right hand side of (5.30). The vector $\mathbf{x}$ is then repelled from that stationary point to another stationary point. If at some location along the path $\det \mathbf{F}'\,(\mathbf{x})$ vanishes then $\mathbf{x}$ is projected through this point and the sign of the right hand side of (5.19) is again changed. The above procedure is continued until the trajectory cycles or diverges towards infinity. The homotopy path is shown in Figure 5.1 for the Treccani function which is given by,

$$g\,(\mathbf{x}) = x_1^4+4x_1^3+4x_1^2+x_2^2.$$

The minima for this function lie on the homotopy path at (0,0) and (–2,0).

Consider, in detail, the projection strategy. A simple way to accomplish this is to take a large step along the coordinate axis from which the stationary point was last approached. The method is liable to be inaccurate however. Instead consider a step across the stationary point which is some multiple of the iteration immediately preceeding the stationary point. Hence a step $\mathbf{s}$ is taken

$$s^i = k_s \mid x_k{}^i - x_{k-1}{}^i \mid$$

where k_s is some constant and $x_k{}^i$ is the ith component of the kth iterate. Unfortunately some components of $\mathbf{x}_k$ may have vanishingly small values, not allowing the projection beyond the stationary point. Therefore it is necessary to introduce a minimum step size resulting in the following step choice

$$s^i = k_1 \mid x_k{}^i - x_{k-1}{}^i \mid \tag{5.20}$$

or

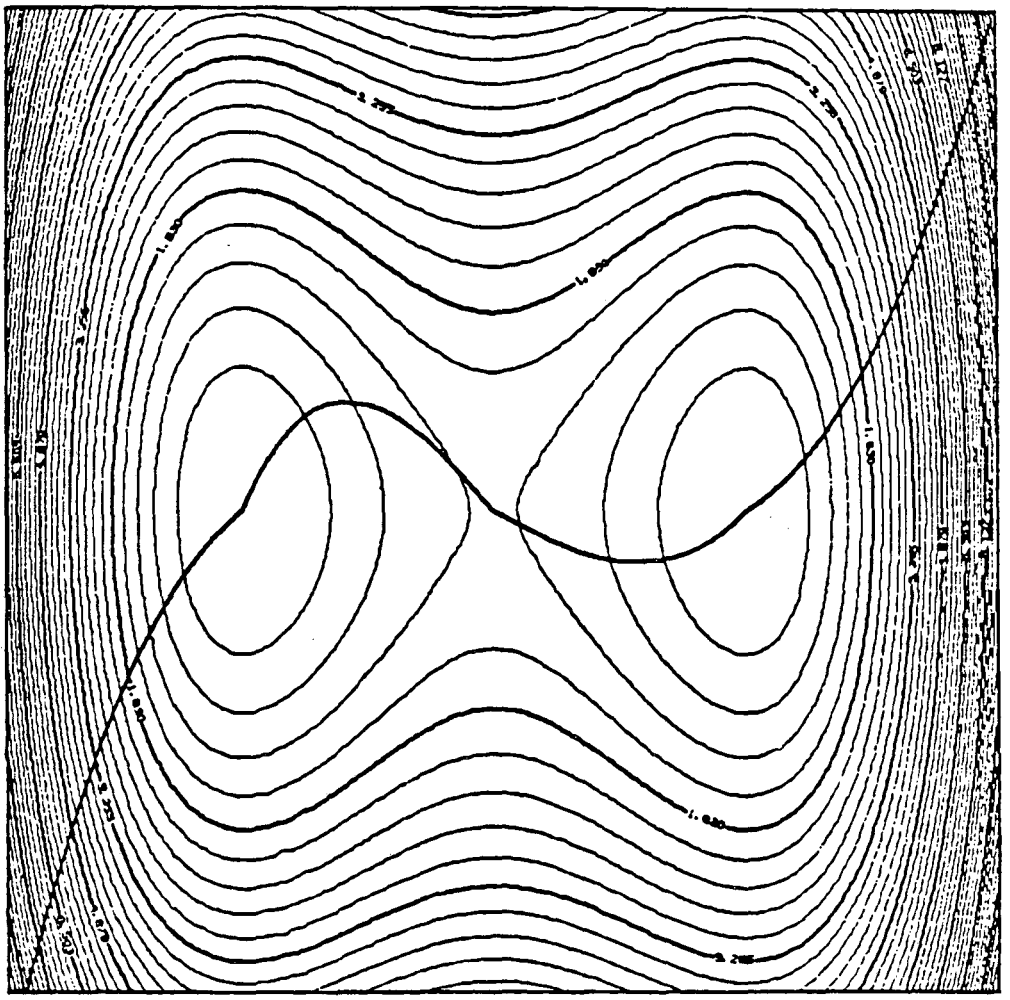

Figure 5.1 Contour map of the Treccani function with minima at (0,0) and (-2,0). The homotopy pathway is indicated by the curve. Both minima were found in this case. The contours rise from a low of 0.67 in increments of 0.3.

$$s^i = k_2$$

which ever is greater.

Though Branin's method is capable of finding all extremum it cannot guarantee that all will be found. The trajectory may be diverted toward infinity by a saddle point or may simply cycle around the same extrema. The cycling phenomena is shown in Figure 5.2, here the contours of the six-humped camel back function are displayed. Therefore extensions to the method were introduced by Hardy (1975) in order to increase the number of extrema found. It should be noted that these modifications, while improving the technique, do not guarantee global convergence to global extrema. The first extension deals with trajectories that diverge towards infinity. In Hardy's implementation, when preassigned bounds are exceeded the point at which they were violated is reflected through the origin. Then the sign of the path following equation (5.19) is adjusted so that the trajectory proceeds away from the boundary. The other extension of Branin's method is a secondary exploration from extrema already found. There are two primary means of accomplishing this. The first involves creating new trajectories eminating from found extrema along the coordinate axes. The second approach directs the secondary trajectories along the axes of an orthogonal coordinate system of which the tangent vector to the original path is taken as one axis. The above extension of Branin's method have been show by Hardy (1975) to increase the number of extrema located. However, it must again be emphasized that there is no guarantee that the global extrema will be found.

Geophysical Application: Fitting Polyhedra to Vertical Displacement Observations

A problem in geophysical studies of magma bodies is the determination of an expanding volume source best fitting a given set of uplift measurements. Except under very restrictive conditions it is not possible to have a unique solution to this problem. Ambiguity is present in the form of local extrema of the nonlinear functional representing the degree of misfit between the anomaly caused by the model and the anomaly actually measured. The commonly used nonlinear optimization techniques find the local extremum generated by a steepest descent path from a

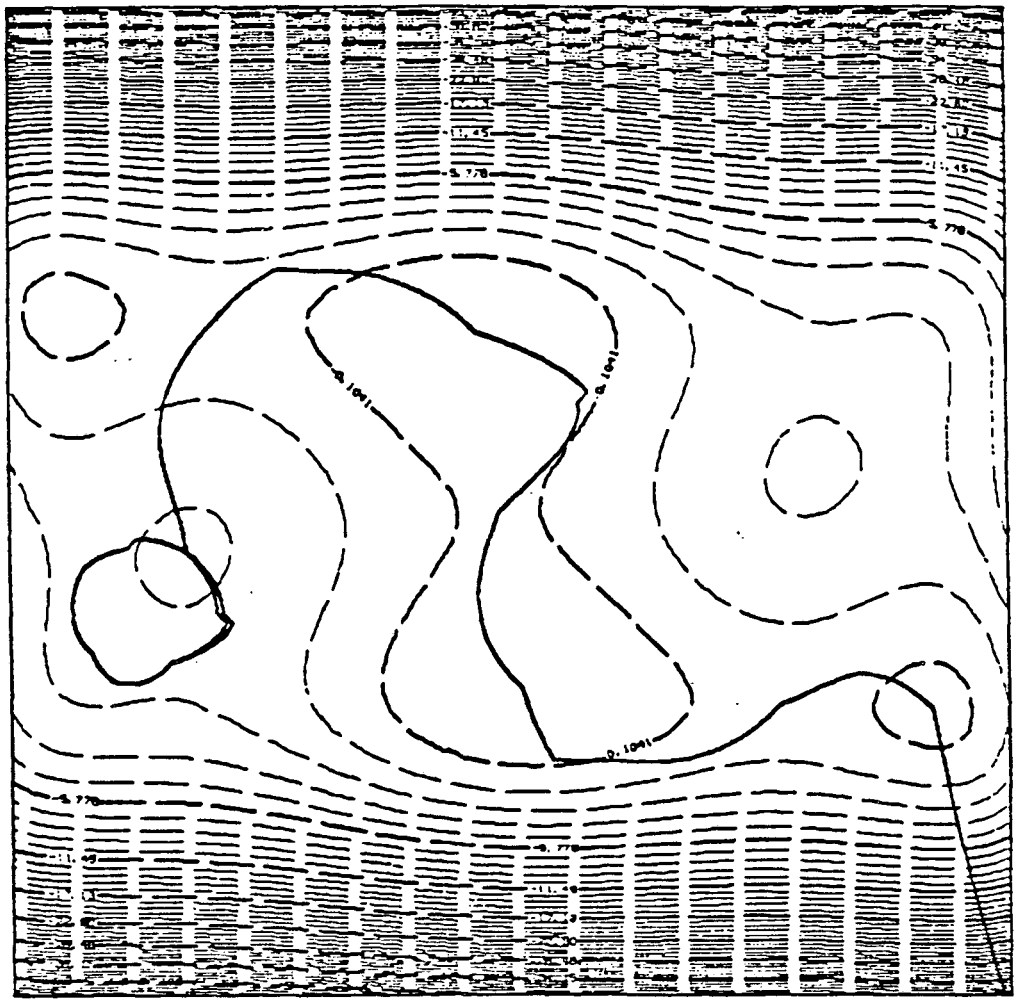

Figure 5.2 Contour map of the six hump camel-back function. The homotopy path is shown. Four of the six minima were found before cycling occurred. The lowest contour represents a value of 0.1 increasing in steps of 1.14.

given starting model. For most realistic situations this is not the only extremum present, others exist due to to incomplete knowledge of the full length of the anomaly, representation of the source by models which are much simpler than it is, the presence of observational errors, and lack of resolving power. Furthermore, there is a fundamental ambiguity in the interpretation of surface displacement: theory dictates that a given anomaly on some plane may be produced by an infinite number of possible solutions below this plane, down to a certain depth. It is possible to limit this nonuniqueness by restricting the class of models. In the following work the model space is restricted in the following sense: both the true source and the model are polyhedra bounded by a finite number of sides. The bodies have a uniform, possibly unknown, fractional volume change within a homogeneous surrounding medium. Finally, any vertical line through the body will not intersect the bounding surface more than twice, thus ruling out cavities within the body. The above conditions exclude the nonuniqueness inherent in the problem. Consider an N-sided polygon with fractional volume change ρ. The anomaly at the *kth* station may be written (appendix A),

$$u = 2(\nu+1)\rho \sum_{i=1}^{N} u_i \tag{5.21}$$

where

$$u_i = a_i \sin\phi_i \cos\phi_i \left[\theta_i - \theta_{i+1} + \tan\phi_i \ln \frac{\cos\theta_i (\tan\theta_i - \tan\phi_i)}{\cos\theta_{i+1}(\tan\theta_{i+1} - \tan\phi_i)} \right] \tag{5.22}$$

where

$$\theta_i = \tan^{-1}\frac{z_i}{x_i},$$

$$\phi_i = \tan^{-1}\frac{z_{i+1}-z_i}{x_{i+1}-x_i},$$

and

$$a_i = x_{i+1} + z_{i+1}\frac{x_{i+1}-x_i}{z_i - z_{i+1}}.$$

It may be shown that another N' -sided polygon producing exactly the same external field will necessarily have all its corners coincident with those of any other N-sided polygon if $N' \geq N$. If $N' < N$ then it is not possible to reproduce the vertical displacement caused by the N sided polygon. Therefore given $N' \geq N$, complete and exact knowledge of the displacement, and sufficient resolving power, uniqueness is assured.

Consider a measure of misfit between the uplift at station k, A_k and the calculated vertical displacement at k due to a particular model, C_k,

$$O(\mathbf{x}) = \sum_{k=1}^{n} (A_k - C_k)^2 \tag{5.23}$$

The set of minima of this objective functional in parameter space delineates the solution of the inverse problem, that is, the set of models which produces the smallest discrepancy between the calculated and observed displacements. Unfortunately, due to the factors mentioned above, many local minima exist in most practical situations. Standard steepest descent methods will find at most one local minimum. Instead, one may use the homotopy method described above to find the multiple minima of the objective functional (5.23).

Consider the following simplified illustration: determining the location of a rectangular shaped body which minimizes the misfit between the calculated uplift and the uplift anomaly shown in Figure 5.3. The rectangle is of fixed dimension, four units of height and five units of width. The horizontal and vertical position of the body is allowed to vary from 0 to 120 horizontaly and from 0 to 20 in depth. A portion of the objective functional is shown in Figure 5.4. Also shown in this figure is the homotopy path generated by equation (5.19). The starting path was under one peak of the uplift anomaly in Figure 5.3. The algorithm successfuly found the first minima of the objective and then continued to find the other minima caused by the second peak.

This application was admittedly simplistic but much more difficult problems exist. Al-Chalabi (1971) notes that finite data length, errors and insufficient sampling can cause nonuniqueness in the fitting of polygonial bodies to potential anomalies. He presents many examples in which multiple solutions exist due to these factors.

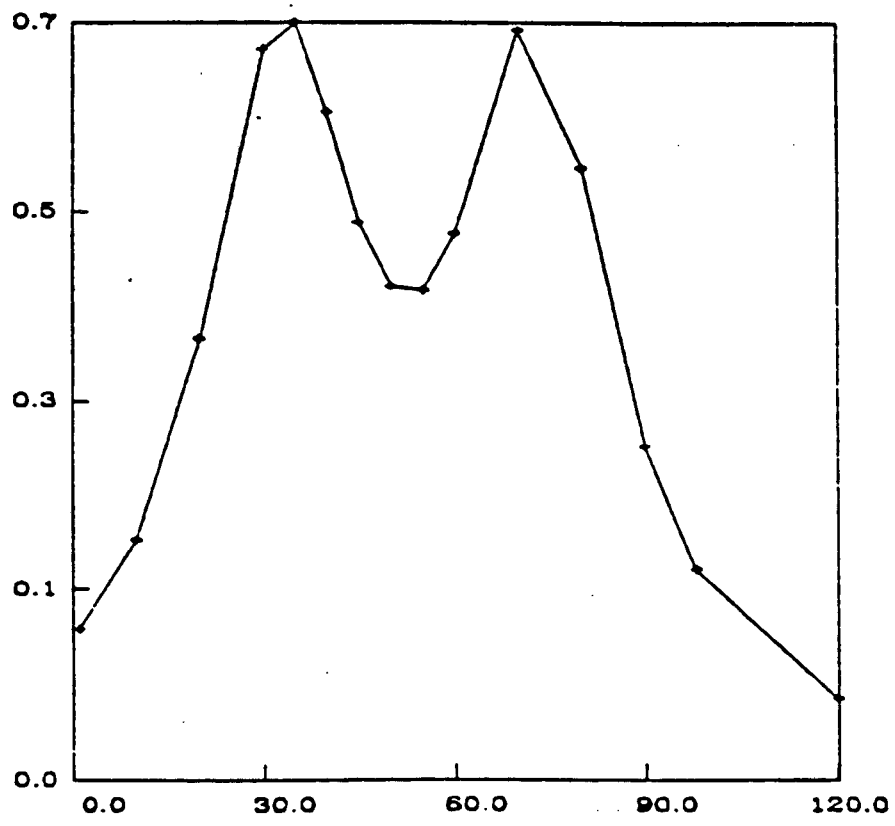

Figure 5.3 Vertical displacement caused by volume expansion at depth.

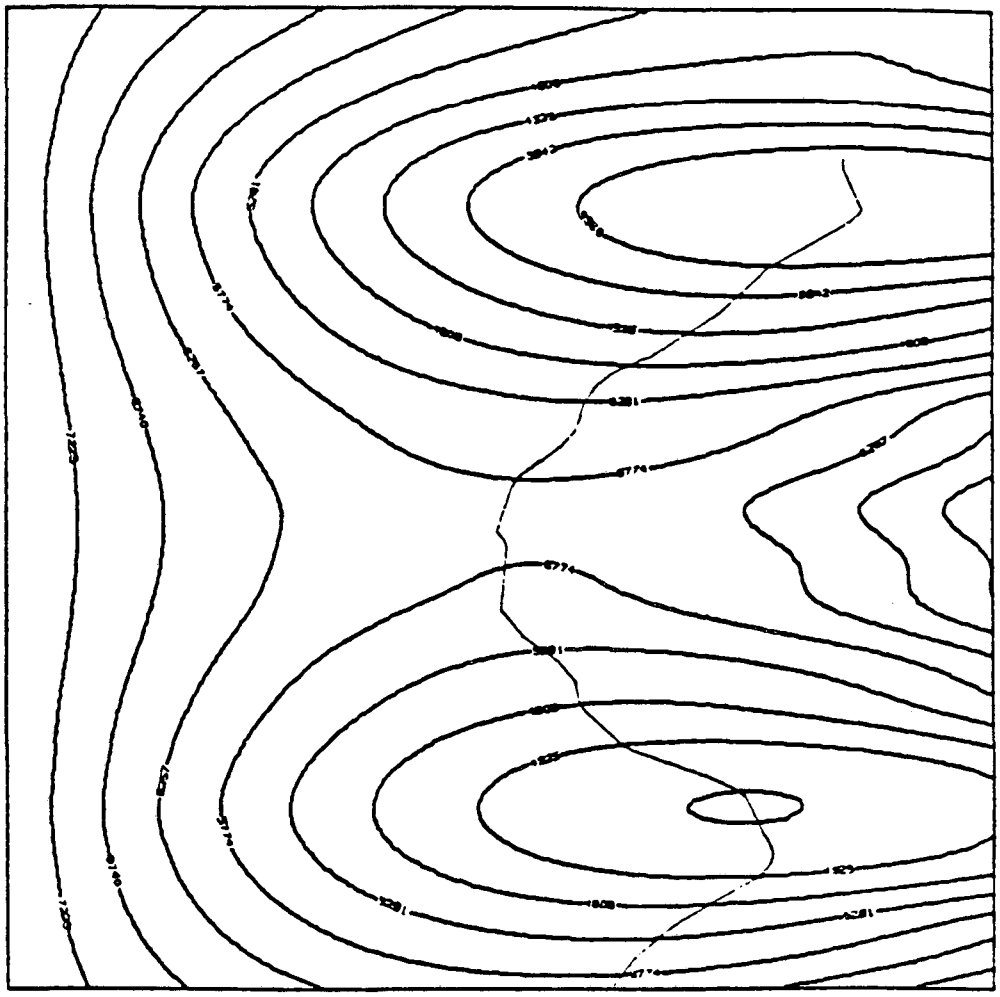

Figure 5.4 Contour map of the objective functional determined by the horizontal and vertical location of an initial model. The homotopy path shown found both minima. The lowest contour is the residual value 3358. The interval is 483.

Conclusions

Multiples solutions to geophysical inverse problems are common. Much has been done to deal with this difficulty in linear inverse problems. Unfortunately, for non-linear problems the trouble has not been treated as effectively. For multi-dimensional problems of high dimension, extensive computation is required to find multiple solutions for most available techniques. The homotopy method is an alternative to the previous methods. It suffers little from additional dimensionality. Furthermore, it is easy to implement and versatile.

The homotopy method can be applied to other problems in geophysics. It is applicable to potential problems involving fitting polyhedrons to a given anomaly. It is also applicable to the non-linear earthquake location problem. It has been successfully applied to raytracing in piecewise homogeneous media (Perozzi 1980). The future may see more uses for this technique in such applications as automated potential anomaly interpretation.

Appendix A

Here, techniques are developed for the efficient computation of vertical displacement due to the expansion of a polygonal volume. The method is a variation of Talwani's method (Talwani et al. 1959) for the computation of the vertical gravitation attraction due to polygonal bodies.

Computation of uplift due to volume expansion in a half-space

Begin with the volume integral form of the Volterra integral,

$$u(\vec{x}) = \int\int\int_V \rho(\vec{\xi}) K(\vec{\xi}) dV(\xi). \tag{A.1}$$

ρ represents the fractional volume change which is defined by $\frac{\delta V}{V_0}$. δV denotes the change in volume and V_0 is the initial volume of the fluid body. The kernel $K(\vec{\xi})$ appearing in equation (1) has been derived by an extension of Maruyama's (1964) study of the response of a homogenous half space to point forces and couples.

For the full three dimensional treatment for a station at $\vec{x}=(x_1,x_2,0)$,

$$K(\vec{\xi}) = \frac{1}{3\pi}(\nu+1)\frac{\xi_3}{r^3} \tag{A.2}$$

where

$$r = \sqrt{(x_1-\xi_1)^2 + (x_2-\xi_2)^2 + \xi_3^2}.$$

ν is Poisson's ratio for the half space and ξ_3 is the vertical coordinate of the source point and

Consider first the calculation of the surface displacement due to a body which does not vary in shape along one axis. The formulas above imply that

$$\Delta u = \frac{1}{3\pi}(\nu+1)\frac{\xi_3}{r^3}\Delta V \rho. \tag{A.3}$$

Δu is the uplift caused by a change in volume at depth ξ_3. The volume ΔV undergoes a fractional volume change ρ at source point $\vec{\xi}$. The vertical displacement Δu is observed at a point $\vec{x}$ on the surface. Noting that $\frac{\xi_3}{r} = \cos\theta$ where θ is the angle between the vertical and a radial line

between the source and the station. Therefore,

$$\Delta u = \frac{1}{3\pi}(\nu+1)\frac{\cos\theta}{r^2}\Delta V \rho \tag{A.4}$$

ΔV may be written in terms of a increment in depth Δz and a small element of surface area ΔS. Then equation (4) becomes

$$\Delta u = \frac{1}{3\pi}(\nu+1)\frac{\cos\theta}{r^2}\Delta z\, \Delta S\, \rho. \tag{A.5}$$

But $\frac{\Delta S \cos\theta}{r^2} = \Delta\Omega$ where $\Delta\Omega$ is the solid angle subtended by the surface element ΔS from the station. Therefore, in two dimensions,

$$u = \frac{2}{3\pi}(\nu+1)\rho \int\int_S dz d\,\theta \tag{A.6}$$

The line integral

$$\int_\epsilon z d\,\theta = 0+(z+dz)\,d\,\theta+0-z d\,\theta$$

$$= dz d\,\theta.$$

Integrating over the cross-sectional area of the body,

$$\int\int_S dz d\,\theta = \int\int_\theta \int_\epsilon z d\,\theta$$

$$= \int_\theta z d\,\theta$$

a line integral over the boundary of the body. Hence

$$u = \frac{2}{3\pi}(\nu+1)\rho \int_S z d\,\theta \tag{A.7}$$

For a polygonal volume this is just the sum of the line integrals from vertex to vertex.

Consider an N-sided polygon with fractional volume change ρ. Similarly to Talwani et al. (1959) treatment of gravity. The uplift at station $\vec{x}$ given by equation (7) may be written as a sum of the line integrals over the sides of the polygon.

$$u = 2(\nu+1)\rho \sum_{i=1}^{N} u_i \tag{A.8}$$

where

$$u_i = \int_{(z_i, z_i)}^{(z_{i+1}, z_{i+1})} z\, d\theta \tag{A.9}$$

$$= \int_{(z_i, z_i)}^{(z_{i+1}, z_{i+1})} \frac{a_i \tan\theta \tan\phi_i}{\tan\phi_i - \tan\theta} d\theta$$

$$= a_i \sin\phi_i \cos\phi_i \left[\theta_i - \theta_{i+1} + \tan\phi_i \ln \frac{\cos\theta_i (\tan\theta_i - \tan\phi_i)}{\cos\theta_{i+1} (\tan\theta_{i+1} - \tan\phi_i)} \right]$$

where

$$\theta_i = \tan^{-1} \frac{z_i}{x_i},$$

$$\phi_i = \tan^{-1} \frac{z_{i+1} - z_i}{x_{i+1} - x_i},$$

and

$$a_i = x_{i+1} + z_{i+1} \frac{x_{i+1} - x_i}{z_i - z_{i+1}}.$$

The application of this formulation is illustrated by the computation of vertical displacement due to the expansion of the square volume shown in Figure A.1. The application of the summation method of equation (A.8) results in the vertical displacement as seen in Figure A.2. The uplift has been normalized by $\frac{2(\nu+1)\rho}{3\pi}$. In this figure summation over the three rectangles defined by the portions of the cross in each layer gives the surface movement without integration over a surface. The results are identical to the integration of Maruyama's equations over the volume which is shown in Figure A.3. The summation method uses less than one third of the cpu time required for the integration over the volume. Also the coding of the problem was simpler for the summation over the vertices.

Another two-dimensional problem of interest is the computation of the uplift due to the expansion of a thin horizontal lamina of thickness Δz. As will be seen, this has an important role in the calculation of vertical displacement due to three dimensional. Begin with equation (A.5),

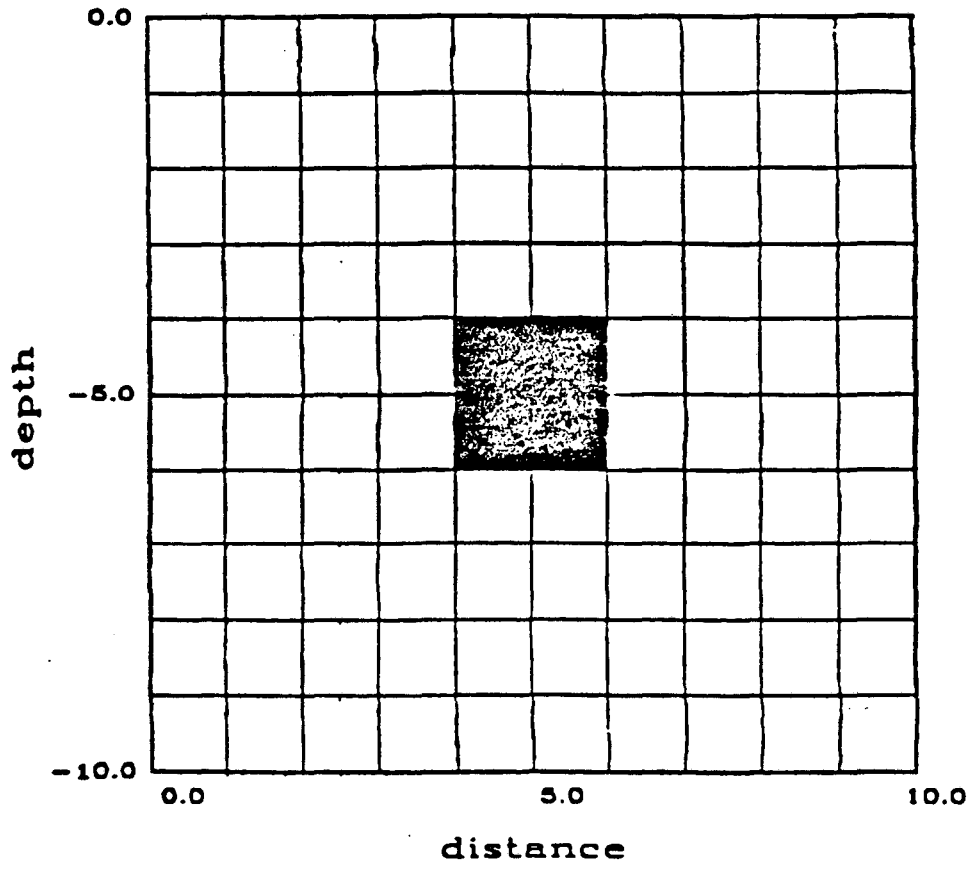

Figure A.1 Source model of volume expansion. The black square has undergone a volume expansion of 1.0.

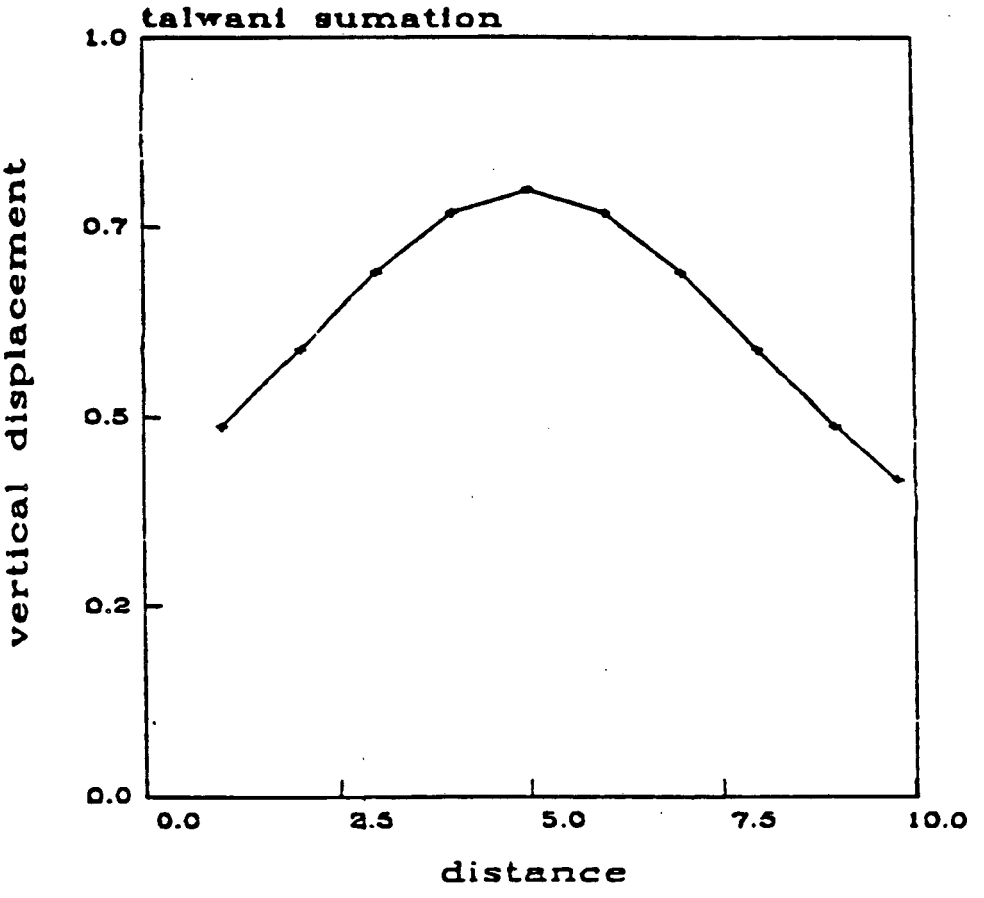

Figure A.2 Vertical displacement calculated by the summation of the vertices of the polygon in Figure A.1.

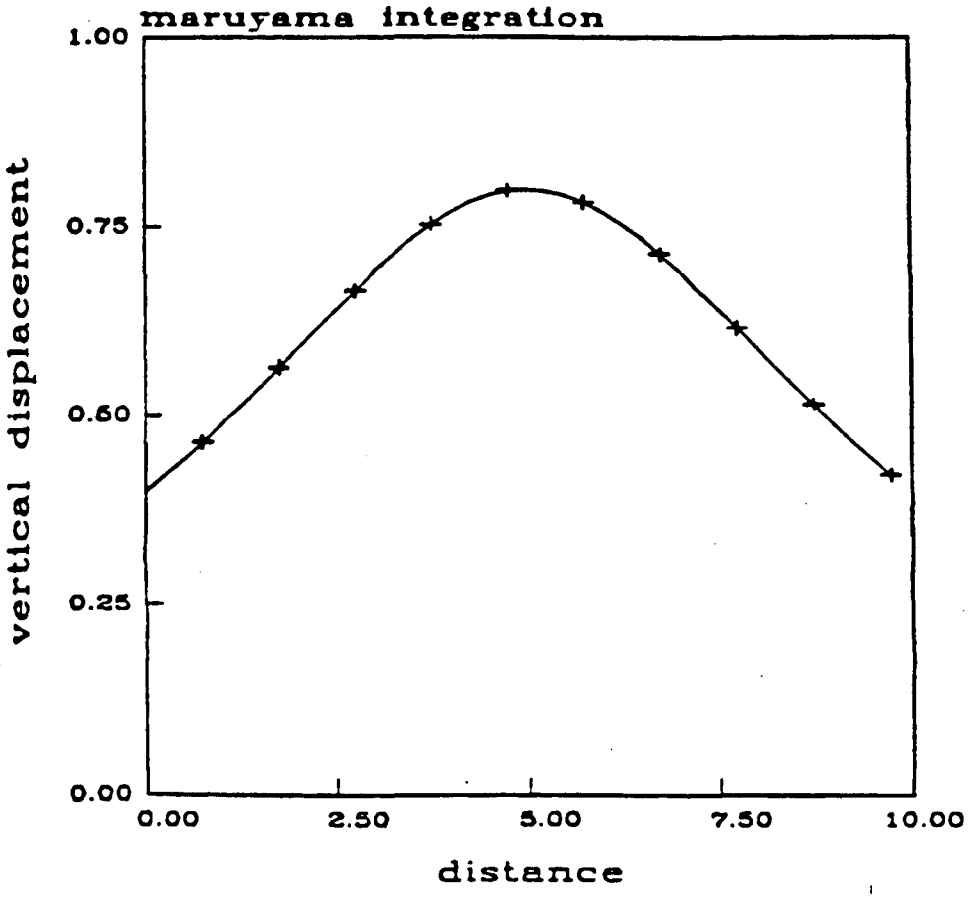

Figure A.3 Vertical displacement calculated by integrating Maruyama equations.

integrating over the surface element ΔS. In cylindrical coordinates with the station at the origin and a horizontal lamina at depth z,

$$\Delta u = \frac{1}{3\pi}(\nu+1)\rho \int_{\psi_i}^{\psi_{i+1}} \int_0^R \frac{\cos\theta}{r^2} R dR d\psi \tag{A.10}$$

where R is the radius of the cylindrical coordinates. ψ is the angular coordinate in this system. The integration over R may be computed analytically, arriving at the line integral

$$\Delta u = \frac{1}{3\pi}(\nu+1)\rho \int_{\psi_i}^{\psi_{i+1}} (1-\frac{z}{\sqrt{R^2+z^2}}) d\psi. \tag{A.11}$$

This integral may also be evaluated analytically (Talwani and Ewing 1960) over the side of a polygon. The uplift due to the lamina then is the sum of the integrals over the sides. This results in

$$\Delta u = \frac{1}{3\pi}(\nu+1)\rho \sum_{i=1}^{N} [\psi_{i+1}-\psi_i - arcsin\frac{z\cos\theta_i}{\sqrt{p_i{}^2+z^2}} + arcsin\frac{z\cos\phi_i}{\sqrt{p_i{}^2+z^2}}]\Delta z \tag{A.12}$$

expressing the uplift due to an N-sided horizontal polygonal lamina. The summation within the above integral may be written in terms of the coordinates of successive vertices (Talwani and Ewing 1960),

$$\sum_{i+1}^{N} W \arccos\left(\frac{x_i x_{i+1}+y_i y_{i+1}}{r_i r_{i+1}}\right) - \arcsin\frac{z q_i S}{(p_i{}^2+z^2)^{\frac{1}{2}}} + arcsin\frac{z f_i S}{(p_i{}^2+z^2)^{\frac{1}{2}}} \tag{A.13}$$

where

$$S = \begin{cases} +1 & p_i \geq 0 \\ -1 & p_i < 0 \end{cases}$$

$$W = \begin{cases} +1 & m_i \geq 0 \\ -1 & m_i < 0 \end{cases}$$

$$p_i = \frac{x_i y_i - x_i y_{i+1}}{r_{i,i+1}}$$

$$q_i = \frac{(x_i - x_{i+1})x_i + (x_i - x_{i+1})y_{i+1}}{r_{i,i+1} r_{i+1}} .$$

$$f_i = \frac{(x_i - x_{i+1})x_{i+1} + (y_i - y_{i+1})y_{i+1}}{r_{i,i+1} r_{i+1}}$$

$$m_i = \frac{x_{i+1} y_i - x_i y_{i+1}}{r_i r_{i+1}}$$

$$r_i = (x_i^2 + y_i^2)^{\frac{1}{2}}$$

$$r_i = ((x_i - x_{i+1})^2 + (y_i - y_{i+1})^2)^{\frac{1}{2}}$$

Many geologically significant bodies can be described by the above shapes. For example, often intrusive dikes can be approximated by an infinitely long body. Similarly, the effect of intruding sills may be treated using the above equation for a thin horizontal lamina. In the next section an approximate method for computing the effects of three dimensional bodies is presented.

The surface uplift due to the expansion of an irregular three dimensional body at depth follows directly from equation (A.12). By integration over the depth dependence the uplift may be calculated. The basic idea is to approximate the body by a stack of thin lamina which outline a series of contours describing the body. The sum of the effect of each lamina then produces the desired uplift.

Generalization to bodies in a spherical or ellipsoidal Earth

The displacement components in cartesian coordinates are

$$u_1 = \frac{1}{3\pi}(\nu+1)\rho \frac{x_1 - \xi_1}{r^3}$$

$$u_2 = \frac{1}{3\pi}(\nu+1)\rho \frac{x_2 - \xi_2}{r^3} \qquad (14)$$

$$u_3 = -\frac{1}{3\pi}(\nu+1)\rho \frac{\xi_3}{r^3}$$

where u_i is the displacement in the x_i direction. Thus the displacement vector $\vec{u}$ may be written as the gradient of a potential $U(\vec{x})$ where

$$U(\vec{x}) = \frac{(\nu+1)\rho}{3\pi r} \qquad (A.15)$$

This potential is the basis for the computation of uplift in a spherical of ellipsoidal earth. The derivation mirrors that for the computation of gravitational attraction given in Johnson and Litehiser (1972).

The Earth is treated as an ellipsoid of eccentricity

$$e^2 = \frac{(a^2-c^2)}{c^2}$$

where a is the semimajor (equatorial) axis and c is the semiminor (polar) axis. The point of observation O is located with respect to the reference ellipsoid at latitude θ_0, longitude ϕ_0 and height above the ellipsoid h_0. The reference ellipsoid that approximates the ellipsoid has semimajor axis a_0. A three dimensional volume within the Earth undergoing expansion is described by it's intersection with successive concentric ellipsoids. The surface defined by this intersection is denoted by Σ, the curve bounding the intersection surface is given by Γ. The concentric ellipsoids that bound the top and bottom of the volume have semimajor axes a_t and a_b respectively. The uplift potential at an observation point O can be represented as

$$U(\theta_0,\phi_0,h_0) = \frac{(\nu+1)}{3\pi}\int_{a_b}^{a_t}\int\int_{\Sigma}\frac{\rho(a)}{R(\theta_0,\phi_0,h_0,\theta,\phi,a)}dV(\theta,\phi,a). \qquad (A.16)$$

$R(\theta_0,\phi_0,h_0,\theta,\phi,a)$ represents the distance between the source and a reciever at O. The integral is expanded in terms of the eccentricities of the ellipsoid and all terms of order greater than 2 are neglected. The resulting analysis, which is identical to that presented in Johnson and Litehauser (1972) and will not be given here, results in the double integral

$$U(\theta_0,\phi_0,h_0) = \frac{(\nu+1)}{3\pi}\int_{a_b}^{a_t}\rho(a)\int_{\Gamma}U_{\Phi}'(\theta_0,\phi_0,h_0,\varsigma,a)\,d\varsigma da \qquad (A.17)$$

where ς is a new variable representing the azimuth in a set of spherical coordinates with the polar axis passing through the observation point O. U_{Φ}' is a known algebraic expression,

$$U_{\Phi}'(\theta_0,\phi_0,h_0,\varsigma,a) = H_0' + \frac{e^2}{2}(\sin^2\theta_0 H_3' + 2\sin\theta_0\cos\theta_0\cos\varsigma H_6')$$

$$-\frac{e^2}{2}\left(2+\frac{a}{e^2}\frac{de^2}{da}\right)[\sin^2\theta_0 H_2' + \cos^2\theta_0\cos^2\varsigma(H_0' - H_2') - 2\sin\theta_0\cos\theta_0\cos\varsigma H_1'] \qquad (A.18)$$

$$-\frac{e^2}{2}[\sin^2\theta_0 H_5' + \cos^2\theta_0\cos^2\varsigma(H_4' - H_5') + 2\sin\theta_0\cos\theta_0\cos\varsigma H_7']$$

The terms H_i' are given below.

The expressions for H_i' were first presented in Johnson and Litehiser.

$$H_0' = q^2[t^{-1}(1-q-u) - sgn(1-q)]$$

$$H_1' = \frac{1}{15}\Big\{ t^{-1}[(1-q)(1+q)^{-1}(2-5q-29q^2-2q^3+4q^4)$$

$$+qu(2-6q-3q^2)+3q^2u^2]\sin\Phi$$

$$-(1+q)^{-2}[(7+7q+87q^2-57q^3-30q^3-14q^5)F_e(\frac{\Phi}{2},K)$$

$$-(7+21q+183q^2-131q^3-58q^4-14q^5)E_e(\frac{\Phi}{2},K)]$$

$$H_2' = \frac{1}{15q}\Big\{ t^{-1}[(1-q)(4+5q^3+6q^5)+qu(4+4q-11q^2-6q^3-6q^4)-q^2u^2(2-9q-3q^2)-3q^3u^3]-(4+5q^3+6q^5)sgn(1-q\Big\}$$

$$H_3' = \frac{a_0}{s_0}q^2\Big\{ t^{-3}[2(1-q)^3-2u(1-3q+3q^2)-3q^2]-2sqn(1-q)\Big\}$$

$$H_4' = q^2\Big\{ t^{-3}[(1-q)^3-u(1-2q+3q^2)-qu^2]-sgn(1-q)\Big\}$$

$$H_5' = \frac{-1}{15q}\Big\{ t^{-3}[(1-q)^3(8-5q^3-18q^5)+3qu(8-5q^2+5q^5+18q^6)$$

$$+3q^2u^2(4-q+4q^2+9q^3+9q^4)+q^3u^3(1-12q-9q^2)+3q^4u^4]$$

$$-(8-5q^3-18q^5)sgn(1-q)$$

$$H_6' = -q\Big\{[t^{-1}q - t^{-3}\frac{h_0}{s_0}q(1+q)^{-1}((1-q)^2(1+2q)+qu(1-5q^2)(1-q)^{-1})]\sin\Phi$$

$$+(1+q)^{-1}[1+q^2-\frac{h_0}{s_0}(1+2q^2)]F_c(\frac{\Phi}{2},K)$$

$$-[1+q-\frac{h_0}{s_0}(1-2q^2)(1-q)^{-1}]E_c(\frac{\Phi}{2},K)$$

$$H_7' = \frac{1}{15}\Big\{t^{-3}[(1-q)^2(1+q)^{-1}(14+31q+67q^2-76q^3-18q^4+12q^5)$$

$$+qu(1+q)^{-1}(32+76q+151q^2-145q^3-27q^4+33q^5)-q^2u^2(1-9q-9q^2)-3q^3u^3]\sin\Phi$$

$$+q^{-1}(1+q)^{-2}[(20+41q+26q^2+266q^3-166q^4-85q^5-42q^6)F_c(\frac{\Phi}{2},K)-(20+81q+128q^2+584q^3$$

$$-378q^4-169q^5-42q^6)E_c(\frac{\Phi}{2},K)]$$

The following definitions have been made,

$$q = \frac{a}{s_0}$$

$$u = 2\sin^2(\frac{\Phi}{2})$$

$$t^2 = (1-q)^2+2qu$$

$$K^2 = 4q(1+q)^{-2}$$

$$F^c(\frac{\Phi}{2,}K) = F(\frac{\pi-\Phi}{2},K)-F(\frac{\pi}{2},K)$$

$$E_c(\frac{\Phi}{2},K) = E(\frac{\pi-\Phi}{2},K)-E(\frac{\pi}{2},K)$$

here F and E are the incomplete elliptic integrals of the first and second kind, respectively.

The integration over the azimuthal ς is seldom analytically possible and numerical methods must be resorted to. As in the previous section, this is done by approximating the boundary by a polygonal closed curve. The successive vertices are connected by arcs of great circles. A

relationship, given in Johnson and Litehiser (1972), enables U_Φ' to be expressed totally in terms of the variable ς. Consider two adjacent vertices with distance-azimuth pairs (Φ_1,ς_1) and (Φ_2,ς_2). Along the great circle path between the vertices Φ is related to ς by

$$ctn\ \Phi = [ctn\ \Phi_1 \sin(\varsigma_2-\varsigma)+ctn\ \Phi_2 \sin(\varsigma-\varsigma_1)][\sin(\varsigma_2-\varsigma_1]^{-1}.$$

As before, the integration over the semimajor axis is evaluated numerically. Because the depth to a lamina varies with latitude it is necessary to specify an average latitude for the body $<\theta>$. Then the semimajor axis a is related the the depth of the lamina h by

$$a = a_0 - h\,[1+\frac{e^2}{2}\sin^2<\theta>(1+\frac{a_0}{e^2}\frac{de^2}{da}.$$

Examples of the application of this algorithm are presented in Johnson and Litehiser (1972) as is a comparison between calculations for a flat, spherical and an elliptical earth. As a final note, for a spherical Earth equation (A.18) becomes

$$U_\Phi'\ (\theta_0,\phi_0,h_0,\varsigma,a) = \frac{a^2}{s^2}\left\{[(s-a)-2s\sin^2\frac{\Phi}{2}][(s-a)^2+4s\sin^2\frac{\Phi}{2}]^{-\frac{1}{2}}-sgn\,(s-a)\right\}.$$

References

Al-Chalabi, M., 1971. Some studies relating to nonuniqueness in gravity and magnetic inverse problems, Geophysics, 36, 835-855.

Alewine, R. W., Jordan, T. H., 1973. Generalized inversion of earthquake static displacement fields, Geophys. J. R. astr. Soc., 35, 357.

Backus, G., 1970. Inference from inadequate and inaccurate data I, Proc. Nat. Academy Sci., 65, 1.

Backus, G. E., Gilbert, J. F., 1967. Numerical applications of a formalism for geophysical inverse problems, Geophys. J. R. astr. Soc., 13, 247-276.

Backus, G. E., Gilbert, J. F., 1968. The resolving power of gross earth data, Geophys. J. R. astr. Soc., 16, 169-205.

Branin, F. H., 1972. Widely convergent method for finding multiple solutions of simultaneous nonlinear equations, IBM J. Res. Develop., 505-522.

Broyden, C. G., 1969. A new method of solving nonlinear simultaneous equations, Comp. J., 12, 94-99.

Canitez, N., Toksoz, N. M., 1972. Static and dynamic study of earthquake source mechanism: San Fernando earthquake, J. Geophys. Res., 77, 2583-2594.

Castle, R. O., Estrem, J. E., Savage, J. C., 1984. Uplift across Long Valley caldera, California, J. geophys. Res. 89, 11507-11515.

Cuer, M., Bayer, R., 1980. Fortran routines for linear inverse problems, Geophysics 45, 1706.

Dantzig, G. B., 1963. Linear Programming and Extensions, Princeton Univ. Press.

Dieterich, J. H., Decker, R. W., 1975. Finite element modeling of surface deformation associated with volcanism, J. geophys. Res., 80, 4094.

Franklin, J. N., Well-posed stochastic extensions of ill-posed linear problems, J. Math. Anal. Appl., 31, 682-716.

Garfinkel, R., Nemhauser, G., 1972. Integer Programming, John Wiley & Sons, New York.

Hadley, G., 1962. Linear Programming, Addison-Wesley,Reading, Massachusetts.

Hardy, J. M., 1975. An implemented extension of Branin's Method, in Towards Global Optimization, L. C. W. Dixon and G. P. Szego Eds., American Elsevier Publishing Co. inc., New York.

Huestis, S. P., 1979. Extremal temperature bounds from surface gradient measurements. Geophys J. R. Astron. Soc. 58, 249-260.

Huestis, S. P., 1982. A geometrical interpretation of ideal body problems, Geophys. J. R. astr. Soc., 69, 253-263.

Ikeda, K., 1983. Inverse problem for stress in the Earth based on geodetic data, Master's thesis.

Johnson, L. R. and Joe J. Litehiser, A method for computing the gravitational attraction of three-dimensional bodies in a spherical of ellipsoidal earth, J. of Geophys. Res., 77, 6999-7009, 1972.

Jordan, T. H., Franklin, J. N., 1971. Optimal solutions to a linear inverse problem in geophysics, Proc. Natl. Acad. Sci. U. S., 68, 291-293.

Jovanovich, D. B., Husseini, M. I. and Chinnery, M. A., 1974. Elastic Dislocations in a layered half-space I. Basic theory and numerical methods. Geophys J. R. Astron. Soc. 39, 205-217.

Jovanovich, D. B., 1975. An inversion method for estimating the source parameters of seismic and aseismic events from static strain data, Geophys. J. R. astr. Soc., 43, 347.

Julian, B. R., 1983. Evidence for dyke intrusion earthquake mechanisms near Long Valley caldera, California. Nature 303, 323-324.

Karmarkar, N., 1985. Proceedings of the 16th annual ACM symposium on the Theory of Computing, 302-311.

Langbein, J. O., 1981. An interpretation of episodic slip on the Calaveras fault near Hollister, California, J. Geophys. Res., 86, 1981.

Luenberger, D. G., 1969. Optimization by Vector Space Methods, Wiley, New York.

McCowan, D. W., Glover, P. and Alexander, S. S., 1977. Geophys. J. R. astr. Soc., 48, 163-185.

Manshina, L., Smylie, D. E., 1971. The displacement fields of inclined faults, Bull. Seis. Soc. Am., 61, 1433-1440.

Maruyama, T., 1964. Statical elastic dislocations in an infinite and semi- infinite medium, Bulletin of the Eqk Res Institute U. of Tokyo 42, 289.

Matsu'ura, M., 1977. Inversion of geodetic data Part I. mathematical formulation, J. of Physics Earth 25, 69.

Menke, W., 1984. Geophysical Data Analysis: Discrete Inverse Theory, Academic Press, Orlando, Florida.

Mottl, J., Mottlova', L., 1984. The simultaneous solution of the inverse problem of gravity and magnetics by means of non-linear programming, Geophys. J. R. astr. Soc., 76, 563-579.

Oldenburg, D. W., 1983. Funnel functions in linear and nonlinear appraisal, J. Geophys. Res., 88, 7387-7398.

Parker, R. L., 1972. Inverse theory with Grossly inadequate data, Geophys. J. R. astr. Soc., 29, 123.

Parker, R. L., 1974. Best bounds on density and depth from gravity data, Geophysics 39, 644.

Parker, R. L., 1975. The theory of ideal bodies for gravity interpretation, Geophys. J. R. astr. Soc., 42, 315.

Perozzi, D. J., 1980. I. Seismic Ray-Tracing in Piecewise Homogeneous Media II. Analysis of Optimal Step Size Selection in Homotopy and Continuation Methods , Ph. D. thesis, California Institute of Technology.

Reitsch, E., 1978. Extreme models from the maximum entropy formulation of inverse problems. J. Geophys. 44, 273-275.

Rundle, J. B., Whitcomb, J. H., 1984. A model for deformation in Long Valley, California, 1980-1983. J. Geophys. Res. 89, 9371-9380.

Sabatier, P. C., 1977a. Positivity constraints in linear inverse problems: I. General Theory, Geophys. J. R. astr. Soc. 48, 415.

Sabatier, P. C., 1977b. Positivity constraints in linear inverse problems: II. applications, Geophys. J. R. astr. Soc., 48, 443.

Sabatier, P. C., 1977c. On geophysical inverse problems and constraints. J. Geophys. 43, 115-137.

Safon, C., Vasseur, G., Cuer, M., 1977. Some applications of linear programming to the inverse gravity problem, Geophysics 42, 1215.

Sanders, C. O., 1984. Location and configuration of magma bodies beneath Long Valley, California, determined from anomalous earthquake signals. J. Geophys. Res. 89, 8287-8302.

Sanders, C. O., Ryall, F., 1983. Geometry of magma bodies beneath Long Valley, determined from anomalous earthquake signals. Geophys. Res. Lett. 10, 690-692.

Savage, J. C., Clark, M. M., 1982. Magmatic resurgence in Long Valley caldera, California: Possible cause of the 1980 Mammoth Lakes earthquakes. Science 217, 531-533.

Savage, J. C., Cockerham, R. S., 1984. Earthquake swarm in Long Valley Caldera, California, January 1983: Evidence for dike inflation. J. Geophys. Res., 89, 8315-8324.

Savage, J. C., Hastie, L. M., 1966. Surface deformation associated with dip-slip faulting, J. Geophys. Res., 71, 4897-4904.

Sezawa, K., 1929. The tilting of the surface of a semi-infinite solid due to internal nuclei of strain. Bull. of Earthqk. Res. Inst., 7, 1-14.

Steeples, D. W., Iyer, H. M., 1976. Low-velocity zone under Long Valley as determined from teleseismic events. J. Geophys. Res., 81, 849-860.

Talwani, M., J. Lamar Worzel and M. Landisman, 1959. Rapid gravity computations for two dimensional bodies with application to the Mendocino submarine fractional zone, J. Geophys. Res., 64, 49-59.

Talwani, M., and M. Ewing, 1960. Rapid computation of gravitational attraction of three-dimensional bodies of arbitrary shape, Geophysics, 25, 203-225.

Tarantola, A., Valette, B., 1982. Generalized nonlinear inverse problems solved using the least squares criterion, Rev. of Geophys. and Space Phys., 20, 219-232.

Volterra, V., 1907. Sur l'equilibre des corps elastiques multiplement connexes, Ann. sci. ecole norm. superieure, Paris, 24, 401-517.

Weidelt, P., 1981. Extremal models for electromagnetic induction in two-dimensional perfect conductors, J. Geophys. 49, 217-225.

Whipple, F. J. W., 1936. On the theory of the strain in an elastic solid bounded by a plane where there is a nucleous of strain at an internal point, and on the relation of the theory to seismology. Mon. Not. Royal Astron. Soc. Geophys. Suppl., 3, 380-388.

Wiggins, R. A., 1972. The general linear inverse problem: Implication of surface waves and free oscillations for earth structure, Rev. Geophys. Space Phys., 10, 251-285.

Wunsch, C., Minster, J-F., 1982. Methods for box models and ocean circulation tracers: mathematical programming and nonlinear inverse theory, J. Geophys. Res., 87, 5647-5662.

LAWRENCE BERKELEY LABORATORY
TECHNICAL INFORMATION DEPARTMENT
UNIVERSITY OF CALIFORNIA
BERKELEY, CALIFORNIA 94720